Universidade Federal do Rio Grande – FURG

Instituto de Oceanografia

Programa de Pós-Graduação em Oceanologia

O Papel das Substâncias Húmicas no Ciclo Biogeoquímico do Ferro Dissolvido: Descobertas e Perspectivas

Camila Fiaux Sukekava

Tese apresentada ao Programa de Pós-Graduação em Oceanologia, como parte dos requisitos para a obtenção do Título de Doutor.

Orientador: *Prof. Dr.*Carlos Francisco Ferreira de Andrade

Universidade Federal do Rio Grande (FURG), Brasil.

Co-orientador: *Prof. Dr.* Luis Felipe Hax Niencheski

Universidade Federal do Rio Grande (FURG), Brasil.

Rio Grande, RS, Brasil

Setembro 2023

Substâncias húmicas, uma das principais formas de manutenção do ferro dissolvido na água do mar

Tese apresentada ao Programa de Pós-Graduação em Oceanologia, como parte dos requisitos para a obtenção do Título de Doutor Por

Camila Fiaux Sukekava

Rio Grande, RS, Brasil

Setembro, 2023

Ficha Catalográfica

S948p Sukekava, Camila Fiaux.
O papel das substâncias húmicas no ciclo biogeoquímico do ferro dissolvido: descobertas e perspectivas / Camila Fiaux Sukekava. – 2023.
123 f.

Tese (doutorado) – Universidade Federal do Rio Grande – FURG, Programa de Pós-Graduação em Oceanologia, Rio Grande/RS, 2023.
Orientador: Dr. Carlos Francisco Ferreira de Andrade.
Coorientador: Dr. Luis Felipe Hax Niencheski.

1. Ferro 2. Substâncias húmica 3. Especiação orgânica 4. Complexos de ferro nos oceanos I. Andrade, Carlos Francisco Ferreira de II. Nienchesk, Luis Felipe Hax III. Título.

CDU 551.46

Catalogação na Fonte: Bibliotecário José Paulo dos Santos CRB 10/2344

UNIVERSIDADE FEDERAL DO RIO GRANDE - FURG
IO – INSTITUTO DE OCEANOGRAFIA
PROGRAMA DE PÓS-GRADUAÇÃ0 EM OCEANOLOGIA
E-mail: ccpofqg@furg.br – home-page: www.ppgo.furg.br

ATA ESPECIAL DE DEFESA DE TESE DE DOUTORADO – 04/2023

Às nove horas do dia doze de setembro do ano de dois mil e vinte e três , no Auditório João Rocha-IO/FURG, presencial e https://conferenciaweb.rnp.br/sala/carlos-francisco-ferreira-de-andrade-carlos, virtual, reuniu-se a Comissão Examinadora da Tese de **DOUTORADO** intitulada: **"O papel das substâncias húmicas no ciclo biogeoquímico do ferro dissolvido: Descobertas e perspectivas "**, da **Acad. Camila Fiaux Sukekava .** A Comissão Examinadora foi composta pelos seguintes membros: Prof. Dr. Carlos Francisco Ferreira de Andrade – Orientador – (IO/FURG); Prof. Dr. Luis Felipe Hax Niencheski – Co-orientador – (IO/FURG); Profa. Dra. Mônica Wallner-Kersanach – (IO/FURG); Dra. Cacinele Mariana da Rocha – (UFRGS) e Dra. Juliana Villela Maciel – (EQA/FURG). Dando início à reunião, a Coordenadora do Programa de Pós-Graduação em Oceanologia-PPGO, Profa. Dra. Grasiela Lopes L. Pinho, agradeceu a presença de todos e fez a apresentação da Comissão Examinadora. Logo após esclareceu que a Candidata teria um tempo de 45 a 60 min para explanação do tema, e cada membro da Comissão Examinadora, um tempo máximo de 30 min para perguntas. A seguir, passou à palavra a Candidata que apresentou o tema e respondeu às perguntas formuladas. Após ampla explanação, a Comissão Examinadora reuniu-se em reservado para discussão do conceito a ser atribuído a Candidata. Foi estabelecido que as sugestões de todos os membros da Comissão Examinadora, que seguem em pareceres em anexo, foram aceitas pela Orientador/Candidata para incorporação na versão final da Tese. Finalmente, a Comissão Examinadora considerou a candidata **APROVADA,** por unanimidade. Nada mais havendo a tratar, foi lavrada a presente ATA que após lida e aprovada, será assinada pela Comissão Examinadora, pela Candidata e pela Coordenadora do Programa de Pós-Graduação em Oceanologia.

gov.br Documento assinado digitalmente
CARLOS FRANCISCO FERREIRA DE ANDRADE
Data: 13/09/2023 12:34:18-0300
Verifique em https://validar.iti.gov.br

Prof. Dr. Carlos Francisco Ferreira de Andrade

gov.br Documento assinado digitalmente
LUIS FELIPE HAX NIENCHESKI
Data: 28/09/2023 09:47:51-0300
Verifique em https://validar.iti.gov.br

Prof. Dr. Luis Felipe Hax Niencheski

gov.br Documento assinado digitalmente
MONICA WALLNER KERSANACH
Data: 28/09/2023 09:36:44-0300
Verifique em https://validar.iti.gov.br

Profa. Dra. Mônica Wallner-Kersanach

gov.br Documento assinado digitalmente
CACINELE MARIANA DA ROCHA
Data: 21/09/2023 14:00:55-0300
Verifique em https://validar.iti.gov.br

Dra. Cacinele Mariana da Rocha

gov.br Documento assinado digitalmente
JULIANA VILLELA MACIEL
Data: 27/09/2023 17:12:23-0300
Verifique em https://validar.iti.gov.br

Dra. Juliana Villela Maciel

gov.br Documento assinado digitalmente
CAMILA FIAUX SUKEKAVA
Data: 28/09/2023 18:02:52-0300
Verifique em https://validar.iti.gov.br

Acad. Camila Fiaux Sukekava

gov.br Documento assinado digitalmente
GRASIELA LOPES LEAES PINHO
Data: 04/10/2023 15:03:07-0300
Verifique em https://validar.iti.gov.br

Profa. Dra. Grasiela Lopes L. Pinho
Coordenadora PPGO

Agradecimentos

Essa tese foi escrita com a ajuda de muitas pessoas, dentre elas eu agradeço:

Gostaria de agradecer ao Luis Miguel , acho que minha trajetória acadêmica não seria nem metade do que é hoje de não fosse seus muitos puxões de orelha e mil conversas e discussões. E ao meu companheiro de Laboratório Javier por estar comigo durante essas análises.

Gostaria de agradecer aos meus orientadores Carlos e Felipe pelo aprendizado e apoio ao longo desses 13 anos de Hidroquímica, acho que foi muito mais que somente meu período de doutorado, foi toda a minha vida acadêmica. A minha banca Mônica, Cacinele e Juliana por terem aceitado fazerem parte desse momento e estarem comigo nessa trajetória.

Gostaria de agradecer a todos os alunos antigos e novos desse processo: Carlos, Alessandra, Gabriel, Mariele, Karina, Kayla, Rafaela, Thayane, Iarema, Leonardo, Yasmym, Elis, Bruna, Maria Alice e Ingrid pelas conversas e ensinamentos.

Gostaria de agradecer a minha família: Jun, Eli e Isadora por estarem presentes em todos esses momentos e, apesar de sofrerem comigo, sempre me apoiarem e dizendo que iria dar certo. Ao meu marido por me aguentar em cada reclamação e a Naomi que sem ela acho que não teria terminado este doutorado tão tranquila.

Sumário

Agradecimentos ---- 4

Sumário ---- 6

Lista de Figuras ---- 8

Lista de Tabelas ---- 11

Lista de Acrônimos e Abreviações ---- 12

Resumo ---- 13

Abstract ---- 14

Capítulo I: Introdução ---- 15

Capítulo II Hipótese ---- 20

Capítulo III Objetivos ---- 21

3. 1 Objetivo geral ---- 21

3.2 Objetivos específicos ---- 21

Cápitulo IV-Material e Métodos ---- 22

4.1 Reagentes ---- 22

4.2 Equipamentos ---- 24

4.3 Parâmetros eletroquímicos ---- 25

4.5 Determinações de ferro dissolvido total ---- 25

4.6 Determinação de especiação orgânica do ferro ---- 26

4.7 Determinação de substâncias húmicas ---- 27

4.8 Capacidades de complexação de substâncias húmicas ---- 29

4.9. Reversibilidade: separação do ferro ligado a FOB e PPIX por HS ---- 30

4.10. Estudos da formação de adutos de HS e DFOB ---- 30

Capítulo V: Artigos Científicos ---- 32

5.1 "Macronutrients, iron and humic substances summer cycling over the extended continental shelf of the South Brazil Bight" ---- 33

5.1.1 Introduction ---- 34

5.1.2. Material and Methods ---- 36

5.1.3. Results and discussion ---- 40

5.1.4. Conclusions ---- 53

5.2 Ligand exchange provides new insight into the role of humic substances in the marine iron cycle. ---- 55

Abstract ---- 55

5.2.2. Introduction. ---- 56

5.2.2. Conceptual framework ---- 58

5.2.3. Material and methods ---- 61

5.2.4. Results and discussion. ---- 69

5.2.5. Implications for the study of iron cycling in seawater ---- 93

5.2.6. Conclusions ---- 96

5.2. 7. Supplementary Material ---- 97

Capítulo VI- Síntese dos resultados e conclusões ---- 107

Capítulo VII – Referências bibliográficas ---- 109

Lista de Figuras

***Figura 1**. Etapas de para análise de especiação orgânica de ferro. A) separação de 120 ml de amostra e adição do tampão e ligante artificial. B) Separação da amostra em 12 alíquotas e adição de ferro dissolvido, seguida de uma espera overnight de equilíbrio. C) Análise de AdCSV D) Tratamento da curva de titulação. 27*

***Figura 2.** Esquema do método determinação de HS e como ficariam os resultados de uma amostra ambiental. A) Período de condicionamento da amostra. B) Primeiras medidas com tamanho de pico constante (ip0). (C) Duas adições de ferro de 60 nM para saturar SH, resultado final indica $ip_{final.}$ (D) Adições de SRFA para determinação de HS 28*

***Figura 3.** Gráfico de capacidade de complexação da solução padrão de SRF. Corrente (ip em nano amperes) por adições de Fe em nanomolar. 29*

***Figure 4.** (A) Map of the Southeast coast of Brazil showing the location of the transect sampled in this study, and name of each station. (B) Surface chlorophyll map of the studied area showing the sampled transect. The arrows point to two important features of the Brazilian Current, the intermediate area of lower biomass, and to the outer string of high biomass. 41*

***Figure 5**. Wind speed and direction measured 15 days before sampling, 3 days during the cruise (in rectangle). Positive values indicate S/SW winds. 42*

***Figure 6.** Spatial distribution of temperature (ºC) (A), salinity (PSU) (B), oxygen saturation (%) (C), and turbidity (NTU) (D) in the transect off the Santa Marta Grande cape. The arrows remark the dome shape of the 18.5 ºC isotherm and the 35.3 ºC isohel, upper limit of the South Atlantic Central Water (SACW), indicative of upwelling in the transition from shelf to slope. 44*

***Figure 7**. Distribution of nitrogen and phosphorus ratio (N:P) in the transect off the Santa Marta Grande cape. 45*

***Figure 8.** Spatial distribution of nitrate (µM) (A), phosphate (µM), (B) and silicate (µM) (C) in the transect off Santa Marta Grande cape. Yellow arrows indicate location of the downwelling and red arrow's location of upwelling. 46*

***Figure 9.** Spatial Distribution of DFe (nM) (A), ligand (nM) (B), constant of stability (C), HS (µg SRFA L^{-1}) (D), Fe-HS (nM) (E) and overall ligands without the contribution of humic (F) in the transect off Santa Marta Grande cape. Yellow arrows indicate downwelling and red in the slope upwelling. The DFe plot had red arrow that show aerial deposition in surface and sediment resuspension. 48*

***Figure 10.** Modelling of the time course of the iron ligand exchange of 14 nM Fe-SRFA complexes after the addition of 15 nM L_{ad} using the following rate constants: $k_{a,FeDFOB}=2x10^{6}\ M^{-1}s^{-1}$, $kd_{,Fe-DFOB}=2x10^{-6}\ M^{-1}s^{-1}$, $k_{a,Fe-SRFA}=2x10^{6}\ M^{-1}s^{-1}$ and two different $k_{d,Fe-SRFA}=1x10^{-5}\ M^{-1}s^{-1}$ (strong ligand)*

and 1x10^{-4} M^{-1}s^{-1} (weak ligand). Red line: same experiment when the SRFA binding groups are divided into 8 nM of the weak ligand and 6 nM of the strong ligand. 60

***Figure 11.** Effect of pH shifting on the analytical response of 1 mg L^{-1} SRFA dissolved in UV-digested seawater in the presence of 19 nM Fe. The solution was 20 mM in BrO_3 and 5 mM in POPSO buffer. The first pH value was increased by NH_4OH additions and, immediate afterwards, decreased by HCl additions. 64*

***Figure 12.** Time course of the concentration of Fe-SRFA complexes in UV-digested seawater in response to different additions of iron-free DFOB. Prior to DFOB addition, SRFA solutions (1 mg L-1, BCSRFA of 14.5 ± 0.7 nM Fe) were spiked with iron to nearly saturate the binding sites. Solid red lines mark the BCSRFA. The red arrows on the left indicate the first measured concentration, approximately 2 minutes after DFOB addition. The lines are the result of fitting the concentration kinetics to the reaction model shown in Section 5.2.4.10**.** 71*

***Figure 13.** Modelling of the time course of the iron ligand exchange of 14 nM Fe-SRFA complexes in response to different additions of iron-free DFOB. The formation and dissociation constants were approximately those found in (Rose and Waite, 2003; Witter et al., 2000). 72*

***Figure 14**. Time course of the concentration of Fe-SRFA complexes (1 mg SRFA L^{-1}) after addition of 10, and 15 nM DFOB. The red line represents the BCSRFA. The red thick arrows indicate the first concentration obtained approximately 100 s after addition of DFOB. The double headed arrows indicate the magnitude of the decrease in Fe-SRFA at equimolar DFOB additions. The red diamonds correspond to the addition of 15 nM DFOB in Fig 10 shown for comparison. 74*

***Figure 15**. Effect of divalent cations on the kinetics of iron ligand exchange: time course for the first 4 h (to highlight the lack of fast initial signal drop) of the concentration of Fe-SRFA complexes after addition of 30 nM DFOB to 1 mg SRFA L-1 saturated at 90% in UV seawater and in 0.72 M NaCl. Insert plot: the complete experiment. 76*

***Figure 16**. Time course of the concentration of Fe-SRHA complexes when SRHA at a concentration of 1 mg L-1 dissolved in UV-digested seawater and saturated to 90% of its iron binding capacity is spiked with different concentrations of DFOB. The solid red line marks the BC_{SRHA}. The dashed red line marks the initial concentration of Fe-SRHA complexes (except for the addition of 10 nM DFOB, see text for details). The lines are the result of fitting the concentration kinetics to the reaction model shown in Section 5.2 4.10..... 78*

***Figure 17.** (A) Time course of the normalized concentration of Fe-SRFA and Fe-SRHA complexes in UV-digested seawater in response to the addition of 1.3 mM EDTA. The initial concentrations were 2 mg SRFA L-1 and 1 mg SRHA L-1, respectively (equivalent to iron BC of 29 nM and 32.6 nM Fe, respectively). (B) Same experiment with the addition of 15 and 30 nM PPIX; it was checked that at the end of the experiment the pH drop was less than 0.1 pH units. All solutions were spiked with iron in order to almost saturate (90%) their binding sites. The red arrows indicate the first concentration obtained approximately 100 s after the addition of the competing ligand. 80*

Figure 18.. *Kinetic section of the characteristic second-order kinetics plot for all ligand exchange reactions departing from Fe-SRFA complexes shown in Fig.1 3 (0.7 M NaCl). 82*

Figure 19*. A and B: A is the experimental results of the addition of 30 nM DFOB to 1 mg SRFA* L^{-1} *and B is the characteristic plot of second-order kinetics. The lines are non- linear fittings of Eq. 1 (black) and Eq. 1 modified to include two types of binding sites (red). C and D: the same for the addition of 120 nM DFOB to 1 mg SRHA* L^{-1}*. A: the kinetic rate constants obtained according to a heterogeneous mechanism were* k_2*=1.58±0.25 and* k_{-2}*=0.574±0.019 x10*^{4} $M^{-1}s^{-1}$ *for the forward and backward ligand exchange of Fe-SRFA*$_1$ *complexes and* k_1*=4.28±0.36 and* k_2*=59.4±5.8 x10*^{4} $M^{-1}s^{-1}$ *for Fe-SRFA*$_2$ *complexes. B: for the same model,* k_3*=0.161±0.003 and k4=0.278±0.007 x10*^{4} $M^{-1}s^{-1}$ *for the forward and backward ligand exchange of Fe-SRHA*$_1$ *complexes and* k_1*=1.88±0.09 and k2=21.2±1.1 x10*^{4} $M^{-1}s^{-1}$ *for Fe-SRHA*$_2$ *complexes..... 83*

Figure 20.. *Kinetic section of the characteristic second-order kinetics plot for all ligand exchange reactions of Fe-SRFA complexes shown in Fig. 10. The lines are linear regressions of the data collected after the initial 20 minutes. They are shown to illustrate the deviations of the initial data from linearity. 84*

Figure 21. *Kinetic section of the characteristic second-order kinetics plot for all ligand exchange reactions departing from Fe-SRHA complexes shown in Fig. 5. The steady-state period at the end has been removed..... 84*

Figure 22*. Time course of Fe-SRFA complex formation when 2 mg SRFA L-1 are added to two aliquots of UV seawater previously spiked with 16 nM of PP IX and DFOB, respectively. The maximum value on the Y-axis is equal to the total concentration of iron in the cell (17.9 nM). .. 87*

Figure 23*. Characteristic plot of second-order kinetics for all data shown in Figs. 12 and 16. Lines are the result of modelling the kinetic data according to the associative irreversible mechanism with two types of SRHS binding sites shown in Eqs. 8 and 9. ..... 90*

Figure 24*. CSV signal obtained in seawater after the addition of 2 mg* L^{-1} *SRFA and 1 mg L1 SRHA, different concentrations of DFOB and Fe in excess of the combined ligand concentrations, allowing equilibration overnight before analysis..... 92*

Figure 25*. Time course of the CSV signal obtained in seawater after the addition of 2 mg* L^{-1} *SRFA, different concentrations of DFOB and Fe in excess of the combined ligand concentrations. After sequential addition of all reagents with 15 minutes equilibration between them, the concentration of Fe-SRFA complexes was monitored..... 105*

Lista de Tabelas

Tabela 1 *Parâmetros voltamétricos para análise de DFe, HS e especiação orgânica do ferro. Baseada em Laglera et al (2013).* *25*

Table 2. *DFe (nM), ligand (nM), log K'Fe'L, HS (µg SRFA L^{-1}) and Fe-HS (nM) a determined from the SBB samples. LS means lost sample. LT means the linearity of the titration that prevent the calculation of log K'Fe'L. <LOD means values less than limit of detection* *50*

Table 3. *Binding capacities of different batches of IHSS fulvic acid and humic reference materials determined after titration with iron as described in Laglera et al. [2009]. Uncertainty as the standard deviation of two determinations, three in the case of SRFA 1R101F* *69*

Table 4. *Kinetic rate constants obtained from fitting the data shown in Figs. 1 and 4 according to the reaction mechanism described by Eqs. 8 and 9. Irreversibility in the time scale of the study was achieved by setting k3 and k6 to a value of 1.5 10-6 s-1. *Value 3 orders of magnitude lower than the other two k4, **value had to be fixed to achieve convergence.* *89*

Lista de Acrônimos e Abreviações

A

AF – Ácidos húmicos

AH-Ácidos fúvicos

B

Bc – capacidade de complexação

BC$_{HS}$– capacidade de complexação das substâncias húmicas

C

CLE-AdCSV – Voltmetria de redissolução catódica aliada à técnica de competição de ligantes (competing ligand Exchange-absortive cathodic stripping voltammetry)

CSV-*Cathodic stripping voltammetry*

CTD – Sistema Condutividade-Temperatura-Profundidade (*Conductivity-Temperature-Depth*)

D

DFe – ferro dissolvido, no inglês dissolved iron

DFO- deferroxiamina

DOM - dissolved organic matter

DHN-2,3-Dihidroxinaftaleno, ligante artificial

E

EDTA–ácido etilenodiamino tetra-acético

F

Fe – ferro

Fe' – ferro inorgânico

Fe-DFOB- ferro complexado por sideróforos

Fe-HS– ferro complexado com substâncias húmicas

H

HNLC – zona de alta concentração de nutriente e baixa de clorofila, no inglês *high nutriente low chlorofill*

HS- substâncias húmicas

K

K'$_{FeL'}$ – constante de estabilidade

$K'_{Fe'HS}$- constantes de estabilidade de Fe inorganico complexado com HS

L

L$_T$ – ligantes totais ou capacidade de complexação

Lad – ligantes adicionados

Lad' – ligantes adicionados não complexados

P

PPIX – protoporfirina IX

POPSO - piperazina-1,4-bis 2-hidroxipropanossulfônico di-hidratado, solução tampão

PPW- Plata Plume water

S

SRFA – *Suwannee River fulvic acid*

SRHA- *Suwannee River humic acid*

SACW – South Atlantic Central Wate

T

TPD - *Transpolar drift*

TW- *Tropical Water*

U

UV dig. Sw – *ultraviolet digested seawater*

Resumo

Ferro (Fe) é um oligonutriente e, devido à sua baixa solubilidade, este elemento é encontrado nos oceanos em pequenas concentrações (0,1 – 1 nanomolar). Atualmente, reconhece-se que 99 % do ferro dissolvido no ambiente marinho ocorre na forma complexada com substâncias orgânicas, denominadas ligantes, dentre as quais encontram-se as substâncias húmicas (SH). Essas substâncias estão relacionadas a aportes continentais e, consequentemente, a presença destes ligantes tende a ser elevada em zonas costeiras. Somente recentemente, foi proposto um novo método que tornou possível analisar o ferro efetivamente complexado com substâncias húmicas, o Fe-HS, e, assim, verificar a predominância de HS sobre os demais ligantes. Diferente de outras regiões oceânicas, a costa brasileira apresenta alta concentração de ferro e, possivelmente, de ligantes. Para comprovar a presença de ligantes e quantificar o que poderia ser o ligante mais importante, este trabalho tem como duas hipóteses que as substâncias húmicas, devido à forte influência das descargas fluviais, são o principal agente complexante na Região de Santa Marta e sendo um ligante heterogêneo esse ligante pode competir com os demais ligantes. Para testar essa hipótese, esse trabalho foi dividido em duas etapas: análise de amostras costeiras e testes de competição entre ligantes já conhecidos (sideróforos, protoporfirina, Etilenodiaminotetracético). Os resultados do primeiro capítulo, embora mostrem uma forte relação entre a produção primária e a manutenção do ferro na quebra do talude, não apresentam as substâncias húmicas como principal ligante. Entretanto, resultados obtidos somente em uma zona de ressurgência não podem ser representativos das demais localidades. O segundo capítulo permite observar as interações entre os ligantes já estudados e as substâncias húmicas, esse capítulo tem um enfoque direto em como os ligantes devem se comportar quando águas costeiras encontram águas oceânicas. Os resultados obtidos nesse trabalho mostraram o quão negligenciadas as substâncias húmicas vêm sendo ao longo dos anos, uma vez que sua heterogeneidade proporciona diversas vias de complexação com o ferro. Ambos os artigos mostraram a importância das substâncias húmicas em meio aquoso, demonstrando que embora HS não seja o principal complexo do ferro, ele é de suma importância em estudos costeiros e oceânicos e ele pode ser sim um grande sequestrador de ferro competindo com os demais ligantes.

Abstract

Iron (Fe) is a micronutrient, and due to its low solubility, this element is found in the oceans in small concentrations (0.1 - 1 nanomolar). Currently, it is recognized that 99% of the dissolved iron in the marine environment occurs in complexed form with organic substances known as ligands, among which humic substances (HS) are found. These substances are related to continental inputs, and consequently, the presence of these ligands tends to be high in coastal areas. Only recently, a new method has been proposed that made it possible to effectively analyze iron complexed with humic substances, Fe-HS, and thus, assess the predominance of HS over other ligands. Unlike other oceanic regions, the Brazilian coast has a high concentration of iron and possibly ligands. To confirm the presence of ligands and quantify what could be the most important ligand, this study has two hypotheses: those humic substances, due to the strong influence of river discharges, are the primary complexing agent in the Santa Marta region, and that being a heterogeneous ligand, it can compete with other ligands. To test this hypothesis, this work was divided into two stages: analysis of coastal samples and competition tests between known ligands (siderophores, protoporphyrin, ethylenediaminetetraacetic acid). The results of the first chapter, although showing a strong relationship between primary production and the maintenance of iron in the slope break, do not indicate humic substances as the primary ligand. However, results obtained in only one upwelling zone may not be representative of other locations. The second chapter allows us to observe the interactions between the already studied ligands and humic substances, focusing on how ligands behave when coastal waters meet oceanic waters. The results obtained in this study show how neglected humic substances have been over the years, as their heterogeneity provides various pathways for iron complexation. Both articles highlight the importance of humic substances in aqueous environments, demonstrating that although HS is not the primary iron complex, it is of paramount importance in coastal and oceanic studies and can indeed be a major iron sequestrant competing with other ligands.

Capítulo I: Introdução

Ferro (Fe) é um oligonutriente encontrado em baixas concentrações nos oceanos (0,1-1 nanomolar) devido a sua baixa solubilidade [Liu & Millero, 2002a]. Aproximadamente em 1/3 dos oceanos este elemento é considerado limitante para a produção primária, já que nessas regiões existem altas concentrações de nutrientes (fosfato, nitrato e amônio) e concentrações de Fe são inferiores a necessidade biológica. Tais localidades são denominadas *high nutrient low chlorofill* (HNLC), sendo considerados verdadeiros desertos biológicos [Martin et al., 1990]. Esse elemento é de suma importância para estudos oceanográficos, já que em experimentos de fertilização em zonas de HNLC, onde foram introduzidas altas concentrações de ferro (Fe(II)), demonstraram relação entre a presença desse elemento, assimilação, incremento de fitoplâncton e consumo de dióxido de carbono atmosférico [Martin et al., 1994; Laglera et al., 2017].

Devido a esta relação de aumento de fitoplâncton e diminuição de CO_2 atmosférico, muitos pesquisadores têm buscado compreender a biogeoquímica do Fe em águas

oceânicas. Parte desta compreensão está no entendimento da forma química que o Fe se apresenta no ambiente marinho. Atualmente, é conhecido que aproximadamente 99 % do ferro dissolvido (DFe), fração inferior a 0,2 μm, na coluna d'água está complexado com substâncias orgânicas, denominados ligantes [van den Berg, 1995; Rue & Bruland, 1995] e que esta condição é o principal fator regulador do Fe nos oceanos, quanto à reatividade e biodisponibilidade[Hassler et al., 2011].

A complexação do DFe com ligantes aumenta a solubilidade de 10^{-11} M para 10^{-9} M, retardando a hidrólise e a precipitação [Liu & Millero, 2002a] e, consequentemente, proporciona um aumento no tempo de sua retenção em águas superficiais [Tagliabue et al., 2009]. Neste contexto, os ligantes possuem um papel crucial para o entendimento desta importante fração de DFe, fração esta que efetivamente é assimilada.

Buscando identificar os processos que regulam a complexação do Fe é necessário considerar quais são os fatores chave para descobrir os ligantes, assim como a qual grupo de carbono orgânico dissolvido ele compõe. Dessa maneira, estudos relacionados a complexação orgânica de Fe em água do mar normalmente são obtidos usando um método indireto, denominado voltametria adsortiva de redissolução catótica aliada à técnica de competição de ligante, em inglês *Competing Ligand Exchange - Absorptive Cathodic Stripping Voltammetry* (CLE-AdCSV). Entretanto, os resultados desses estudos somente permitem determinar a concentração de ligantes totais na amostra, também denominada capacidade de complexação (L_T), e suas constantes de estabilidade (K'_{FeL}), [Pižeta et al., 2015] que somente definem a "força" que determinado complexo pode ter e quantoo Fe poderia se manter na água, não permitindo inferir a qual específico candidato a ligante pertencem àquela determinada água.

Os ligantes estão associados a mecanismos de prevenção de estresse férrico, tais como, por exemplo, a produção de algumas exsudações [Norman et al., 2015], onde algas podem produzir substâncias orgânicas ricas em lipídios na manutenção de Fe em sua forma solúvel na superfície. Apesar do forte interesse em conhecer as fontes e o comportamento desses ligantes, sua caracterização ainda permanece desconhecida em sua totalidade [Breitbarth et al., 2010]. Atualmente é conhecido que existe uma grande variedade de ligantes, denominada por alguns autores como "sopa de ligantes"[Tagliabue et al., 2017], com diferentes afinidades com o Fe, interações químicas, alguns suscetíveis à fotodegradação ou mesmo maior biodisponibilidade [Gledhill, & Buck, 2012]. Dentre os

candidatos encontram-se os sideróforos [Mawji et al., 2008], grupo heme [Gledhill, 2007], polissacáridos [Hassler et al., 2011] e as substâncias húmicas (SH) [Laglera & van den Berg, 2009].

Alguns candidatos a ligantes de Fe já foram quantificados quanto a sua concentração total presente na água do mar, como o caso dos sideróforos e grupo heme, onde foi empregada a cromatografia líquida para sua quantificação[Hogle et al., 2014; Bundy et al., 2018], assim como substâncias húmicas e polissacáridos por voltametria [Hassler et al., 2011; Laglera et al., 2007]. Embora seja comum classificar os sideróforos como substâncias que representam as classes de ligantes mais fortes e com maior distribuição ao longo dos oceanos [Vraspir & Butler, 2009], uma vez que são produzidos por microorganismos que necessitam ferro, atualmente medidas diretas de capacidade de complexação somente detectaram 10 % desse *pool* como sendo Fe-sideróforo complexo [Kustka et al., 2015; Bundy et al., 2018]. Tornando os demais 90 % dos ligantes totais quantificados ainda não em relação a predominância quando complexado com DFe em determinadas regiões.

Dentre esses candidatos que podem complexar Fe estão as SH. Tais substâncias são uma complexa e heterogênea mistura de materiais polidispersos formados por reações bioquímicas e químicas durante a decomposição e transformação de restos de plantas e microbianos. Embora sua origem seja principalmente terrestre, HS são um componente importante do *pool* de matéria orgânica natural na água do mar, podendo ter como origem a degradação fitoplactônica. Do ponto de vista analítico, HS são definidos como a fração retida em uma coluna hidrofóbica e eluida por uma solução alcalina (Sociedade Internacional de Substâncias Húmicas), além de apresentarem muitos grupos fenólicos e carboxílicos aromáticos, ambos fortes grupos de ligação [Buffle & Cominoli, 1981]. Essas substâncias podem ser divididas em ácidos fúlvicos (AF) e ácidos húmicos (AH), dependendo de sua solubilidade em água em pH 1, ambos são os componentes principais de carbono dissolvido em água doce (valores de 15 a 100 %) [Whitby & van den Berg, 2015].

Estas substâncias em estuário tendem a co-precipitar com o aumento de salinidade, assim como o ferro dissolvido (DFe), que pode precipitar até 99 % de sua concentração total e, portanto, em princípio pensava-se que devido a tais processos de remoção em estuários, a concentração de ferro complexado com húmicos poderia ser irrelevante quando aportada na região costeira. Todavia, ficou comprovado exatamente o contrário. Devido

a sua alta concentração nos oceanos na ordem de 100 µg de HS L^{-1} [Obernosterer & Herndl, 2000], foi possível comprovar que essas substâncias são importante candidatas na complexação de ferro em água do mar, demonstrando que embora grande parte da sua remoção ocorra em regiões costeiras, ainda assim o HS desempenha um papel considerável na manutenção do DFe [Laglera & van den Berg, 2009].

Existem inúmeras formas de determinar os HS totais em águas naturais, tais como a quimiluminescência, espectroscopia, voltametria e fluorescência e, dentre estes métodos, o mais empregado é o método clássico que faz uso da eletroquímica para determinar a concentração de HS totais em amostras [Laglera et al., 2007; Sukekava, 2018]. Este método já foi usado em distintos estuários e regiões oceânicas [Sukekava et al., 2023; Su et al., 2018; Bundy et al., 2015; Laglera et al., 2019] , por ser um método barato e sensível. Recentemente, este método foi modificado tornando possível pela primeira vez determinar ferro efetivamente complexado com substâncias húmicas (Fe-HS) [Sukekava et al., 2018]. De maneira que finalmente seria possível determinar ligantes totais, usando o método indireto de CLE-AdCSV e qualificar o percentual de Fe complexado com húmicos, definindo se essas substâncias poderiam ser majoritárias na complexação de ferro.

O método para determinação de Fe-HS já foi aplicado em águas com alta concentração de matéria orgânica devido à influência de rios e derretimento de gelo no Oceano Ártico. Este estudo evidenciou que mais de 70 % do ferro dessa região estava complexado por substâncias húmicas [Laglera et al., 2019], reafirmando a hipótese de que essas substâncias seriam importantes no transporte e manutenção do ferro. O Oceano Ártico apresenta forte influência de descarga fluvial e alta concentração de matéria orgânica dissolvida [Dittmar, 2004], denominada *Transpolar Drift e,* portanto, forte influência continental em sua biogeoquímica, assim como para a plataforma continental sul brasileira [Möller et al., 2008].

Embora esse método seja eficiente e sensível, este foi aplicado pela primeira vez no Atlantico Sul por Longhini et al. [2021] com o intuito de verificar a presença de HS na manutenção de um desastre ambiental. Da mesma forma que existem poucos trabalhos relacionados ao Oceano Atlântico Sul, tanto na região costeira quanto *offshore*. Recentemente, Gerringa et al. [2015] determinou ferro complexado no Atlântico Sul. As concentrações encontradas atingiram elevados valores de ferro dissolvido e ligantes

próximos às influências de rios, como o Rio Amazonas e Rio de La Plata (faixa de 2 nM). Outro trabalho realizado na região costeira do sul do Brasil demonstrou concentrações de até 3 nM/dia de ferro na plataforma continental do Rio Grande do Sul [Windom et al., 2006]. Esse trabalho, entretanto, não indicou o quanto de ferro dissolvido encontra-se biodisponível.

Os recentes trabalhos mostraram que ainda existe um desconhecimento sobre a biogeoquímica do ferro no Atlântico Sul, principalmente ao que se diz a respeito de especiação orgânica e, principalmente, substâncias húmicas. Pensando nisso, essa tese foi dividida em dois artigos científicos que buscavam compreender a dominância e importância de substâncias húmicas como ligantes, mostrando como esse ligante age, afetando assim a complexação do ferro e modificando a especiação desse elemento e, dessa maneira permitindo a maior resiliência do ferro na coluna d´água e a sua manutenção.

Na primeira parte dessa tese, é buscado uma melhor distribuição de HS durante um processo de ressurgência na região de Santa Marta Grande, avaliando a concentração de ferro, e através da análise da especiação orgânica e determinação de ferro complexado por substâncias húmicas uma compreensão de como esse elemento está na coluna d'água em relação a sua disponibilidade. Assim, com esses resultados foi possível observar de forma mais abrangente a manutenção deste elemento nessa região costeira. Já na segunda parte dessa tese foi possível conhecer um pouco do comportamento de HS frente aos demais ligantes estudados (sideróforos, protoporfirina e EDTA), descobrindo através de testes cinéticos como esse elemento se comportaria quando passasse de água costeiras, ricas em HS, para águas oceânicas, de baixa concentração dessas substâncias. Esses testes demonstraram que em inúmeros trabalhos os valores de HS podem estar subjugados devido ao pequeno relato de sua presença no meio oceânicos. Assim, com os resultados obtidos em ambos os trabalhos foi possível compreender melhor a disponibilidade de HS, seu comportamento e responder a seguinte questão: substâncias húmicas seriam o principal agente complexante do ferro?

.

Capítulo II Hipótese

- Substâncias húmicas são os ligantes responsáveis pela manutenção do ferro dissolvido na região costeira do Rio Grande do Sul e um importante complexante de ferro.
- Substâncias húmicas são compostos heterogêneos e possuem alta capacidade de complexação podendo competir com os demais candidatos a ligantes

Capítulo III Objetivos

3. 1 Objetivo geral

- Avaliar a especiação orgânica, porcentagem de (complexos de ferro e substâncias húmicas) Fe-HS e concentração de ferro dissolvido total presente nas amostras da Costa Sul do Brasil e estudar como se comporta esses complexos frente a outros ligantes.
-

3.2 Objetivos específicos

- Descrever o processo comportamental das substâncias húmicas frente aos demais ligantes, sendo eles sideróforos, protoporfirina e ácido etilenodiamino tetra-acético (EDTA).
- Avaliar a distribuição da concentração de ferro complexado com substâncias húmicas (Fe-HS) ao longo do perfil amostral.
- Determinar as diferenças espaciais ao longo da plataforma continental e talude como: fontes de ligantes, redução na formação de complexos e distribuição de ferro complexado.

Cápitulo IV-Material e Métodos

4.1 Reagentes

Todo o material que foi limpo e o preparo das soluções foi utilizado água ultrapura Milli-Q (Millipore®, Reino Unido). Para o preparo dos padrões de ferro (III) foi utilizado água ultrapura acidificada (pH ~1,8) de uma solução padrão de Fe, espectrometria de absorção atômica de 1 ppm (BDH, Reino Unido). O ligante de ferro DHN (2,3-dihidronaftaleno) (Fluka) foi preparado também em água ultrapura acidificada (pH ~1,8) a uma concentração de 10 mM. A solução tampão/catalisador usada tanto na determinação de ferro dissovido (DFe), como substâncias húmicas (SH) foi preparada de uma mistura contendo 0,1 M de POPSO (piperazina-1,4-bis(2-hidroxipropanossulfônico) di-hidratado da Sigma Aldrich) e 0,4 M de bromato de potássio (Sigma Aldrich). O pH dessa mistura foi ajustado para 8,2 usando amônia (Ultratrace Fluka) para DFe e pH 8,35 para HS. Para o preparo de tampão que foi usado na especiação orgânica do ferro, somente 0,1 M de POPSO, sem que fosse adicionado bromato de potássio. Isso ocorre porque o método usa o oxigênio como agente catalizador. Todos esses reagentes foram limpos

usando MnO_2. Esse composto age como um agente limpador complexando os demais metais, considerados impurezas nos reagentes. Para que haja uma completa descontaminação do reagente foi esperado cerca de 16 horas aproximadamente, assim todos os metais que poderiam interferir seriam precipitados junto ao MnO_2, após esse período de espera foi possível fazer uma filtração (nitrato de celulose 0,2 μm, Whatman) retirando os elementos indesejados. Recomenda-se a filtração sem uso de bomba a vácuo para que não haja rompimento das moléculas filtradas. Uma solução de NaCl (ultratraço, Fluka) foi preparada a uma concentração de 0,72 M para reproduzir a força iônica da água do mar oceânica. Essa solução não foi limpa para análise, entretanto sua concentração de ferro foi descontada dos experimentos. Isso, porque o objetivo das análises foi verificar complexos de ferro formados por substâncias húmicas, quando saturado com Fe, se esse elemento não fosse descontado da concentração final, a solução teria excesso de ferro influenciando no estudo da cinética.

O ácido fúlvico (SRFA, 1S101F) e o ácido húmico (SRHA, 1S101H) do Rio Suwannee foram adquiridos da Sociedade Internacional de Substâncias Húmicas (IHSS) e utilizados como SH. Soluções estoque de 0,2 g L^{-1} foram preparadas em água Milli-Q e armazenadas em baixas temperaturas até o uso. Ultrassom ou tratamentos combinados de alcalinização/neutralização não alteraram a capacidade de ligação do ferro do HS-modelo. O sideróforo desferrioxamina B (DFOB, (N'-[5-(Acetil-hidroxi-amino)pentil]-N-[5-[3-(5-aminopentil-hidroxi-carbamoil)propanoilamino]pentil]-N-hidroxi-butano diamida)) foi adquirida como sal mesilato (Sigma Aldrich) e dissolvida em água ultrapura. Uma solução estoque aquosa de DFOB foi diluída para uma concentração de 5 μM e mantida na geladeira entre os usos. O protoporfirina IX (PP-IX, (3,7,12,17-tetrametil-8,13-divinil-2,18-porfinadi-propiônico) foi escolhido como ligante típico de lise celular. Devido à sua baixa solubilidade em água e sua tendência à dimerização e polimerização em função do pH [Scolaro et al., 2002], soluções aquosas de PP-IX requerem um planejamento específico uma vez que pequenas adições de PPIX podem mudar a sensibilidade do método, alterando o pH do tampão/catalisador usado.

Soluções estoque foram preparadas dissolvendo alguns miligramas em 1 M de uma solução de EDTA (ácido etilenodiaminotetracético, Merck) e, a solução de 0,1 M foi preparada em água ultrapura. O pH da solução foi elevado para 8,2 com amônia grau ultra-traço.

A água do mar livre de ligantes utilizada no segundo artigo foi proveniente de uma mistura de amostras filtradas (0,2 μm) restantes da campanha Polarstern ANT-XXV/3 realizada nas águas do Oceano Antártico [Laglera et al., 2017]. A mistura de água do mar foi homogeneizada em um frasco de polietileno de baixa densidade (LDPE) (Nalgene) limpo e digerida por UV antes do uso para remover qualquer matéria orgânica interferente.

Soluções reagentes e misturas de água do mar foram preparadas em recipientes de LDPE, que foram previamente limpos sequencialmente com detergente (BIO-SEL), HCl 10 % e HCl 1 M, com enxágues de água ultrapura entre eles e antes do uso.

4.2 Equipamentos

Para as análises usadas no primeiro artigo, tais como de ferro dissolvido e sua especiação orgânica, assim como a determinação de substância húmicas e a sua complexação com o ferro, as análises usadas para os testes de cinética de competição entre os ligantes e HS, foram usados CSV (*cathodic stripping voltammetry*) monitorado por três eletrodos em uma célula voltamétrica, sendo eles: um eletrodo de trabalho *mercury drop working electrode* (HMDE) , um eletrodo auxiliar de carbono vítreo e um eletrodo de referência, com uma junção *doble* Ag/AgCl.

Embora fosse usado um sistema parecido para as análises do primeiro artigo e segundo artigo, para os testes feitos no Laboratório de Hidroquímica usou-se um potenciostato modelo PST101 Autolab e do segundo artigo todos os testes foram feitos no Laboratório Fi-*Trace* usando o potenciostato μAutolab III, ambos controlados pelo sofware NOVA 2.1.5 conectados por um stand VA663 (todos Metrohm AG).

Devido ao longo tempo de análise das cinéticas o programa NOVA foi programado para reproduzir os dados com frequências de 15 minutos cada leitura.

Para a produção de uma água de baixo complexante de ferro e a determinação de ferro dissolvido, as amostras de água do mar foram digeridas por sistemas UV de Digestão

ambos *homemade* em que foram formados por uma lâmpada de mercúrio de 150W (2 horas) e 60W (4 horas), para o segundo e primeiro artigo, respectivamente.

4.3 Parâmetros eletroquímicos

Como o comportamento voltamétrico dos complexos Fe-HS e Fe-DHN no HMDE é similar, ambos os métodos compartilham os mesmos parâmetros eletroquímicos descritos em publicações anteriores (Laglera et al., 2007; Laglera et al., 2013), como indicados na Tabela 1.

Tabela 1 Parâmetros voltamétricos para análise de DFe, HS e especiação orgânica do ferro. Baseada em Laglera et al (2013).

Parâmetros voltamétricos	
Modo	DC
Purga	300 segundos
Potencial de deposição	-0.1V
Tempo de deposição	90 segundos
Tempo equilíbrio	7 s
Step	-5mV
Velocidade de Scan	50 mV/s
Potencial inicial e final	-0.1 a -1.15V

4.5 Determinações de ferro dissolvido total

Para a determinação de ferro, primeiramente todas as amostras (subamostras para os testes de cinética: UVseawater e NaCl e amostras do coletadas em Santa Marta) passaram por uma digestão com luz ultravioleta. Em seguida, foram determinadas por AdCSV após

acidificação durante a noite a pH 2,0 e neutralização com amônia na presença de 1,2 diidroxinaftaleno (DHN) e bromato [Laglera et al., 2013]. A contaminação de ferro nas soluções de bromato/POPSO e DHN foi medida repetindo a análise de água ultrapura adicionada de 30 µM de DHN, 20 mM de KBrO3 e 5 mM de POPSO (solução combinada) antes e depois de triplicar a concentração de DHN ou KBrO3 e POPSO e subsequente calibração interna com ferro.

4.6 Determinação de especiação orgânica do ferro

Amostras de água do mar (120 mL) foram misturadas em uma garrafa de Teflon, após um pré-condicionamento (Figura 1A), com DHN em uma concentração de 1 µM e um tampão de POPSO em uma concentração de 5 mM, respectivamente (Figura 1B). Cada amostra foi dividida em 12 alíquotas de 10 mL, e o Fe foi adicionado em concentrações variando de 0 a 20 nM (Figura 1C). O método CLE-CSV com DHN foi originalmente descrito por van den Berg [2006], mas foram feitas modificações para evitar subestimar a contribuição de HS para as concentrações de ligantes [Laglera et al., 2011], já que a presença de HS e Fe-DHN podem se sobrepor durante análise, e excluir a purga durante a medição [Caprara et al., 2015].

Todas as alíquotas foram deixadas em equilíbrio durante a noite em temperatura ambiente. No dia seguinte, a concentração do complexo Fe-DHN foi determinada usando análise de AdCSV (Figura 1C). Os parâmetros voltamétricos utilizados foram os mesmos descritos Tabela 1.

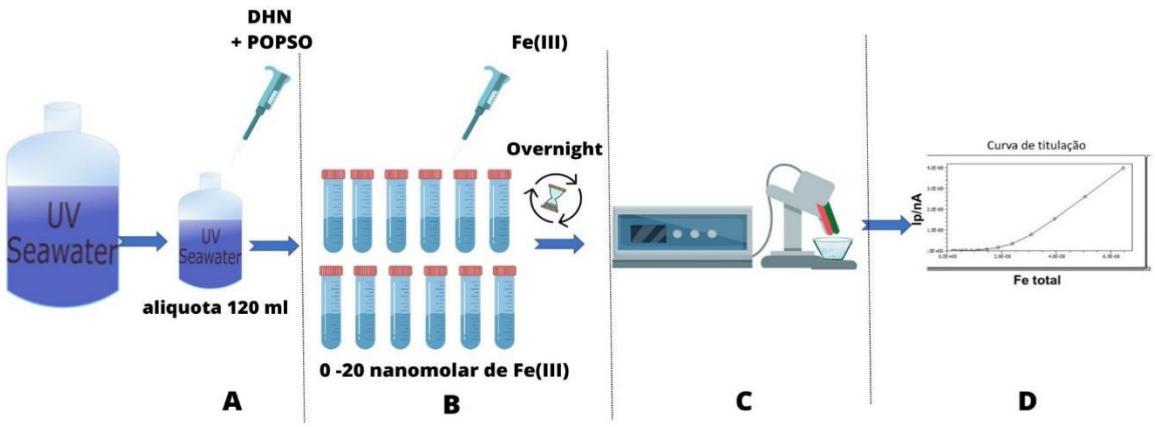

Figura 1. Etapas de para análise de especiação orgânica de ferro. A) separação de 120 ml de amostra e adição do tampão e ligante artificial. B) Separação da amostra em 12 alíquotas e adição de ferro dissolvido, seguida de uma espera *overnight* de equilíbrio. C) Análise de AdCSV D) Tratamento da curva de titulação.

As concentrações de ligantes e as constantes de estabilidade condicional de seus complexos com o ferro (K'Fe'L) foram determinadas ajustando os dados de titulação CLE-AdCSV em um modelo linear Rûzic/van den Berg, conforme descrito em Pižeta et al. [2015]; Ružić [1982] evan Den Berg [1982]. As concentrações de ligantes são relatadas em nM, e os valores de $K'_{Fe'L}$ são relatados em escala logarítmica, em relação à concentração de ferro inorgânico (Fe') como log $K'_{Fe'L}$ (Figura 1D).

4.7 Determinação de substâncias húmicas

Para determinação de substâncias húmicas foi usado o método descrito em Sukekava [2018] em que consiste nas seguintes etapas:

1. Adição de 10 mL de amostra e adição de 500 µL da mistura Bromato/POPSO na célula voltamétrica, duas vezes com 5 minutos de condicionamento em cada uma delas. Amostras com picos muito pequenos devem ser adicionados até 3 vezes a quantidade de bromato/POPSO, a fim de aumentar o efeito catalizador (Figura 2A).
2. Adição novamente da mesma solução, fazendo ao todo 5 a 10 leituras de maneira que haja alturas de pico semelhante entre elas. A média dos resultados obtidos nessas leituras serão equivalente p_0 (Figura 2B).
3. A amostra deve, então, ser saturada com ferro dissolvido. As adições de ferro serão entre 20 -60 nM. Durante, aproximadamente, 1 hora a altura do pico deve diminuir até um valor constante, quando for alcançado a estabilidade do sinal a média entre as 5 leituras finais (ip_{final}) serão usadas para o cálculo de porcentagem de HS que pode ser complexado com ferro ($\frac{ip_0}{ip_{final}} x100$). (Figura 2C)

4. Por fim, a determinação de HS total será feita com adições da solução padrão de $SRFA_{saturado\ com\ ferro.}$ (Figura 2D)

Para a determinação da capacidade de complexação que os HS naturais da amostra possuem usa-se a concentração total de HS da amostra dividido pelo valor obtido de capacidade de complexação da solução padrão ($L_{HS} = [HS]/BC_{SRFA}$) . E para a determinação do ferro efetivamente complexado por HS (Fe-HS), os valores obtidos para L_{HS} multiplicado pelos valores obtidos da porcentagem de Fe capaz de saturar HS. ($[Fe - HS] = L_{HS}\ x\ \%Fe\ saturado\ por\ HS$.

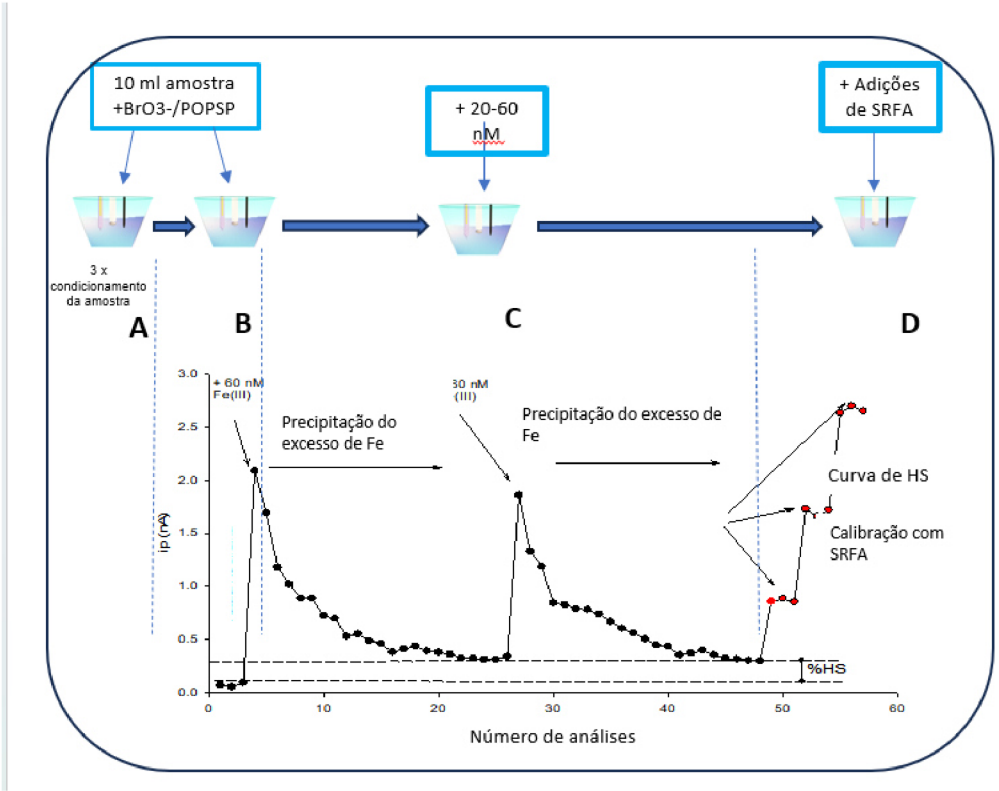

Figura 2. Esquema do método determinação de HS e como ficariam os resultados de uma amostra ambiental. A) Período de condicionamento da amostra. B) Primeiras medidas com tamanho de pico constante (ip0). (C) Duas adições de ferro de 60 nM para saturar SH, resultado final indica $ip_{final.}$ (D) Adições de SRFA para determinação de HS

4.8 Capacidades de complexação de substâncias húmicas

Para a determinação dos ligantes complexados com substâncias húmicas é necessário saber a capacidade de complexação da solução padrão de HS, para isso é necessário a determinação da capacidade de ligação do ferro em soluções de padrão de ácido fulvicos e ácidos húmicos (SRFA e SRHA) (BC_{SRFA} e BC_{SRFA}). Esse processo foi realizado de acordo com um procedimento estabelecido por Laglera & van den Berg [2009]. Resumidamente, soluções de SRFA ou SRHA a 1 mg L^{-1} foram tituladas em uma matriz livre de ligantes (água ultrapura, NaCl 0,72 M ou água do mar exposta ao UV) com adições sucessivas de alguns nanomols L^{-1} de ferro. O pico de Fe-HS aumenta linearmente em função da concentração do ferro adicionado até que os grupos de ligação de HS se tornem saturados. Além dessa etapa, os picos de CSV ficam abaixo da tendência linear e diminuem com o tempo devido à lenta precipitação de ferro que estava em excesso. A concentração de ferro correspondente à interseção das duas seções relacionadas foi usada para determinar o BCSRHS de ferro (Figura 3).

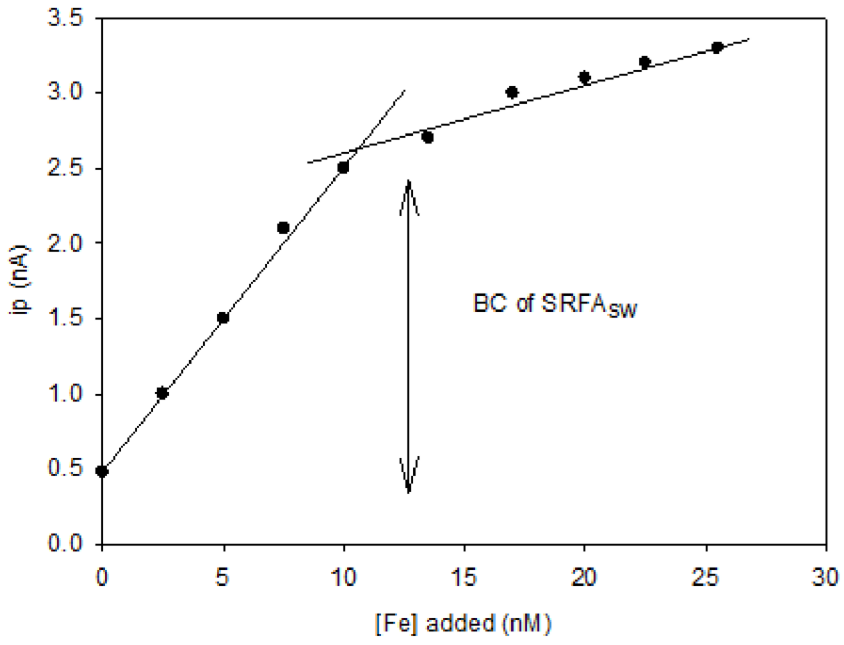

Figura 3. Gráfico de capacidade de complexação da solução padrão de SRF. Corrente (ip em nano amperes) por adições de Fe em nanomolar.

4.9. Reversibilidade: separação do ferro ligado a FOB e PPIX por HS

Nesse teste foi estudado se e quando houve troca de ligantes, ou seja, a troca de ligantes dos complexos Fe-FOB ou Fe-PPIX em solução após a subsequente adição de HS. Foram utilizados apenas SRFA porque SRHA, possivelmente já estava saturado com ferro em suas ligações mais fortes. Em casos anteriores em que foi usado diferentes resinas para remover a contaminação de ferro de SRHS foi introduzido contaminação orgânica que interferiu na nossa linha de base analítica. Para esse teste foi feito dois experimentos separados, adicionamos água do mar UV com 1 mL da solução de POPSO/bromato e 16 nM de DFOB ou PPIX e ferro em uma concentração suficiente para atingir uma concentração celular de 16 nM de ferro, considerada o BC_{SRFA} dos testes anteriores. Anteriormente, foi preenchida a célula com a mesma solução duas vezes para condicionar as paredes da célula. Para análise, após 5 minutos de condicionamento e várias varreduras de CSV para garantir a ausência de complexos de ferro interferentes eletrolábeis, foram adicionados à solução 2 mg SRFA L^{-1} para uma capacidade de ligação de 29,0 nM Fe e monitoramos a formação de complexos Fe-SRFA eletroativos por várias horas. Ao final da coleta de dados, o Fe-SRFA foi calibrado com três (DFOB) e quatro (PPIX) adições internas de 2 nM de ferro para determinar a sensibilidade.

4.10. Estudos da formação de adutos de HS e DFOB

Foram projetados dois tipos de experimentos para estudar se HS e DFO interagem, formando adutos HS-DFO e/ou HS-Fe-FO. Apesar das limitações de métodos não espectroscópicos, os métodos eletroquímicos permitem concentrações experimentais próximas das condições naturais. Em ambos os experimentos, as concentrações de ferro adicionadas foram bem superiores às capacidades de ligação combinadas de FO e HS, evitando qualquer troca de ligantes de ferro. Desvios do sinal esperado de Fe-HS saturado poderiam ser causados por uma diminuição na concentração de ligante lábil devido às

interações orgânico-orgânicas. Detalhes sobre a interpretação dos resultados são discutidos abaixo.

Primeiro, várias alíquotas de 20 mL de água do mar digerida por UV foram colocadas na célula voltamétrica com 1 mL da solução de bromato/POPSO. Para a primeira alíquota, foram adicionados 2 mg de SRFA L^{-1} (para uma capacidade de ligação de 29,0 nM Fe) e 300 nM de ferro, e foi permitido um período de equilíbrio de 15 minutos para garantir a saturação completa dos grupos de ligação de ferro do SRFA. Em seguida, adicionou-se 5 nM de DFOB, e o desvio do sinal de Fe-SRFA foi monitorado por muitas horas, ou até o equilíbrio, para verificar se o DFOB cancelava uma fração da complexação de Fe-SRFA estabelecida nessas condições experimentais. O experimento foi repetido com concentrações de DFOB na faixa de 5 a 100 nM. Na ausência de interações orgânico-orgânicas e artefatos do método, o sinal de Fe-SRFA deve permanecer constante em todos os experimentos.

Em segundo lugar, foram preparados dois conjuntos de frascos de LDPE contendo 10 mL de alíquotas de água do mar irradiada por UV. Em seguida, o SH foi acrescentado em sequência (o primeiro conjunto com 2 mg L^{-1} de SRFA e o segundo conjunto com 1 mg L-1 de SRHA, para capacidades de ligação de 29,0 e 32,1 nM Fe, respectivamente), DFOB (faixa de 0 a 100 para SRFA e 0 a 300 para SRHA, com tempo suficiente para interagir) e, finalmente, 600 nM de ferro para saturar todos os ligantes. A mistura interagiu durante a noite para permitir a precipitação de ferro em excesso, e no dia seguinte todas as alíquotas foram adicionadas com reagente de bromato/POPSO e analisadas por CSV para verificar se as interações sideróforo-HS poderiam ter impedido a formação igual de complexos Fe-HS eletrolábeis.

Capítulo V: Artigos Científicos

Para a obtenção do título de Doutor pelo Programa de Pós-Graduação em Oceanologia é requerido que o discente realize a submissão de pelo menos um (dois) artigo(s) científico(s) como primeiro autor em periódico com corpo indexado. Desse modo, os resultados da pesquisa desenvolvida durante o período de doutorado e a discussão dos resultados serão apresentados em forma de artigos neste Capítulo.

O primeiro manuscrito, de autoria de Camila Fiaux Sukekava, Carlos Francisco Ferreira de Andrade, Luis Felipe Hax Niencheski, Marcio Silva de Souza, Luis M. Laglera, é intitulado "**Macronutrients, iron and humic substances summer cycling over the extended continental shelf of the South Brazil Bight**" e publicado no periódico "**Science of Total Environment**".

O segundo manuscrito, de autoria de Camila Sukekava, Javier Downes, Monserrat Filella, Bartolome Vilanova, Luis Miguel Laglera que foi intitulado "**Ligand exchange provides new insight into the role of humic substances in the marine iron cycle**" e foi submetido no periódico "**Geochimica et Cosmochimica Acta**"

5.1 “Macronutrients, iron and humic substances summer cycling over the extended continental shelf of the South Brazil Bight”

Abstract

We surveyed macronutrients and dissolved iron (DFe) concentrations and speciation in a transect over the shelf of the South Brazil Bight (SBB) at Santa Marta Grande Cape (SE Brazil) during a coastal downwelling episode. Driven by dominant NE winds, coastal downwelling is a common feature during the austral summer and force after water convergence, with contribution of internal wave breaking at the shelf edge, upwelling of macronutrients into the nutrient-depleted waters of the southbound Brazil Current at ~100 km from the coastline. As a result, we found a plume of high turbidity that reached the euphotic layer, a deepening of the silicate, nitrate, and phosphate isolines over the shelf and a bulging of the nitrate and phosphate isolines over the shelf edge and the slope. Our first measurements of DFe concentration and speciation in the area revealed that against prior findings in other coastal areas, macronutrients, DFe, and iron ligand cycles were disentangled. Higher DFe concentrations were often found at the surface indicating aerial deposition. Secondary DFe maxima over the sediment-water interface and in the upwelled plume indicated DFe fluxes from the sediment and from resuspended instable colloids. Iron ligand concentrations were higher than DFe concentrations in most stations with a clear land-to-ocean gradient. Subtraction of HS iron ligands revealed that except in upwelled water, the bulk of surface ligands was the result of local biological processes. The analysis of the concentrations of Fe-HS complexes showed that the contribution of HS to DFe was dominant in upwelled waters, significant in waters close to the coast, but nearly negligible in the rest of the studied area. We hypothesize that the injection of iron-humic complexes into the euphotic layer during summer upwelling episodes is the key to understanding the persistent high chlorophyll meanders found over the shelf edge of the SBB coast.

5.1.1 Introduction

The Santa Marta Grande (SMG) Cape is located on the Southeast coast of Brazil, in the southern section of the South Brazil Bight (SBB). The SBB starts in Rio de Janeiro (23ºS) and ends in the Santa Catarina state (28.5ºS). From an economic perspective, the SMG is a relevant fishing area and serves as a fish nursery for many species [Franco et al., 2020]. The SBB shelf is remarkably wide with an average width of approximately 150 km (maximum of 230 km), whose edge is found at 150 to 185 m deep[Martins & Coutinho, 1981]. The bathymetry at the SMG Cape is particularly characterized by a nearly flat shelf (declivity 1:300/600) and a shelf edge line located ~100 km from the coast, which is closer to the coast than in most of the SBB region. The SBB is an example of the poorly studied coastal systems defined by low terrestrial waters inputs and biogeochemical processes ruled by the effect of wind dynamics.

The oceanography of the SMG area presents a stratified water mass structure. Freshwater river discharge has a small contribution concealed to the inner shelf [Campos et al., 1995]. The Brazilian Current (BC), the southbound split of the Atlantic South Equatorial Current after bifurcation off Cape São Roque [Stramma et al., 1990], which is defined by warm and high salinity waters, occupies the outer shelf edge. The BC is a relatively weak South Atlantic western boundary current that flows southwards as a shallow current (confined to the upper 500 m) carrying warm and saline tropical waters. It is composed of two water masses: the shallow Tropical Water (TW) and the deeper South Atlantic Central Water (SACW). TW transports low macronutrient concentrations, opposed to the high macronutrient concentrations found in the SACW [Piola et al., 2000; Braga et al., 2008; Niencheski et al., 2014]. Seasonally changing wind dynamics force strong episodes of Ekman transport, with temporal episodes of combined coastal downwelling/shelf edge upwelling, and substantial changes of the SACW upper limit across the shelf–during summer, the elevation of the SACW upper limit often reaches the euphotic layer. Winter freshwater inputs and summer upwelling pulses bring enough macronutrients to surface waters to increase biological productivity significantly of the otherwise macronutrient-depleted TW [Ciotti et al., 2014; Muelbert et al., 2008]. Biogeochemical studies conducted in the SBB have revealed two major sources of macronutrients over the shelf

and the slope with strong seasonal variations: continental exchanges and some upwelling pulses [Muelbert et al., 2008; Niencheski et al., 2014; Braga et al., 2008; Acha et al., 2004]. Moreover, in restricted areas of strong bathymetry changes as shelf edges, the dissipation of internal waves generated by the effect of tidal currents over the topography may generate turbulence and localized macronutrients upward pulses (upwelling) [Cullen et al., 1983]. This process has been verified in the outer shelf of the SE coast of Brazil with a peak during summers [Lorenzzetti & Dias, 2013].

Despite the oceanographic relevance of the SBB area, prior studies focused only on biological parameters and macronutrients (nitrate, silicate, phosphate) [Niencheski et al., 2014; Braga et al., 2008; Muelbert et al., 2008]. To our knowledge, there are no reports in the area about the concentration and possible upwelling of micronutrients such as the essential element iron.

Iron is usually not limiting in coastal areas, although this has been questioned in the narrow shelf area of the Southern part of the California upwelling region for periods of low riverine inputs [Biller & Bruland, 2014; Bruland et al., 2001; Till et al., 2019]. Iron uptake is key to primary productivity and the composition of the biological community [Geider & La Roche, 1994; Till et al., 2019]. Iron is of relevance to CO_2 exchange between the atmosphere and the ocean in coastal areas [Ito et al., 2016]. In shallow continental shelves, iron resuspension from sediments may be necessary for a substantial drawdown of upwelled nutrients by phytoplankton blooms [Capone & Hutchins, 2013].

The solubility of iron in seawater is extremely low (about 10^{-11} M in organic matter free seawater) due to the thermodynamical stability of the Fe(III) species, where inorganic speciation in seawater is dominated by the $Fe(OH)_3^0$ species [Liu & Millero, 2002b]. Low iron solubility limits its transition from continental waters into the open ocean. However, the presence of organic matter, and more specifically iron ligands, prevents iron precipitation resulting in dissolved iron concentrations on the coast (DFe) in the nanomolar range [Liu & Millero, 2002a]. The concentration of iron ligands and the conditional stability of their organic matter-DFe complex is routinely determined after competing ligand equilibrium and analysis by cathodic stripping voltammetry (CLE-CSV) in a set of sample aliquots titrated with DFe to which is added an artificial ligand for competition that forms an electroactive complex [Gerringa et al., 2014]. Current research has proposed a short list of groups of organic substances as candidates to

constitute the bulk of iron binding ligands in seawater: siderophores and their degradation products [Bundy et al., 2018; Boiteau et al., 2016; Mawji et al., 2008], pigments [Gledhill et al., 2013], polysaccharides [Hassler et al., 2011] and humic substances (HS) [Laglera & van den Berg, 2009]. HS are the product of the biological and chemical transformations of terrestrial plant tissues and microbes that constitute a physical and chemical heterogeneous mixture of hydrophobic organics, ubiquitous in natural waters. In coastal waters, terrestrial-derived HS are expected to dominate iron complexation [Laglera & van den Berg, 2009], although there are doubts whether this effect, which is of major importance at high latitudes, is extended to lower latitudes [Krachler & Krachler, 2021].

Here, we present measurements of macronutrients and the micronutrient iron, including its organic speciation and the contribution of HS to DFe concentrations in a coast to ocean transect off the SMG cape. We sampled the water column over the whole shelf and the initial section of the slope during a coastal downwelling. Our aim was to determine the effect of such episodes in the distributions of macronutrients, DFe and HS. This study is the first to report iron concentrations and speciation on the SBB coast where the spatial distribution of nutrients and primary productivity are strongly controlled by intense wind variations.

5.1.2. Material and Methods

5.1.2.1 Sampling

Water column samples were collected on board the RV Atlântico Sul in a transect perpendicular to the Southeast coast of Brazil at the Santa Marta Grande Cape (28.5 ºS) in January 2015 (summer) (Fig. 4A). During the campaign, 22 samples were collected at six stations in one transect from the coast to the point of the slope where the sea bottom depth was 1500 m. Bottle closure depths were selected based on the vertical distribution of temperature and salinity to represent all the water masses present at the station. The deepest sample at each station was collected with the help of a pinger (SeaBird SBE19plus) at 5 m over the seafloor at stations 1 to 3 located over the shelf and at 10 m over the seafloor at stations 4 to 6 located over the shelf edge and the slope.

Macronutrients and iron samples were collected using 12-liter Teflon-coated Go-Flo bottles suspended on a Kevlar line. The hydrographic data (CTD and dissolved oxygen) were collected using the SeaBird SBE9plus and SeaBird SBE19plus probes.

All samples for macronutrient analyses were filtered through 0.45 µm filters (cellulose acetate, Millipore®) immediately once onboard, with the help of a vacuum pump. Filtered samples destined to nitrate, phosphate, and silicate analyses were stored in polyethylene bottles, with chemicals added for analyte stabilization when needed, and then frozen pending later analysis. The analytical methodology is described in [Strickland & Parsons, 1972]. A failure of the fluorescent probe after sampling the first two stations impeded the collection of fluorescence profiles thereafter. Instead, we used chlorophyll satellite images as a proxy for the distribution of primary producers at the surface. Chlorophyll concentrations were estimated using satellite images (https://www.star.nesdis.noaa.gov/socd/mecb/color/index.php).

Samples for DFe, organic iron speciation and humic substances analysis were immediately filtered by 0.2 µm cellulose nitrate membrane filters, Millipore® once onboard, stored in 250 ml low density polyethylene bottles and samples for analysis of DFe acidified to pH 2. Filters and bottles were treated before use according to standard GEOTRACES protocols [Cutter et al., 2017] Speciation and HS samples were immediately frozen, and all analyses were carried out at the laboratories of the Federal University of Rio Grande.

5.1.2.2 Reagents

Water used for solution preparation and for rinsing containers was ultrapure (Milli-Q, Millipore®). A combined solution of Piperazine-*N,N′*-bis(2-hydroxypropanesulfonic acid (POPSO, Sigma-Aldrich) and potassium bromate (Sigma-Aldrich) was prepared by using aqueous ammonia (Merck, Suprapur 40 %) at concentrations of 0.1 M and 0.4 M, respectively. The concentration of ammonia in this solution was such to set the pH at 8.2 if used for the determination of dissolved iron [Laglera et al., 2013] or 8.35, for the analysis of the concentration of HS and humic iron [Sukekava et al., 2018]. A volume of

500 µL of this buffer/bromate solution was added to 10 mL of each sample. Trace element contamination in the buffer/bromate solution was removed by adding 100 µM suspended particulate MnO_2 which was removed after overnight equilibration (twice) by gravity filtration (0.2µm acetate cellulose, Millipore®) [Gallera et al., 2007, 2013]. For speciation studies, a buffer solution of POPSO (0.1 M) was prepared and cleaned of contamination with colloidal MnO_2 as described above. Procedural blanks were lower than 0.3 nM Fe per 500 µL addition of the combined bromate/POPSO solution and below the limit of detection for the POPSO and DHN solutions. A stock solution of 5 µM iron (III) was prepared from an atomic absorption spectrometry standard solution (1 ppm, BDH) with two dilution steps in acidified (HCl) ultrapure water (pH=2.0). The 2,3-dihydroxynaphthalene (DHN, Merck) solution was prepared in pH 2 ultrapure water at a concentration of 10 mM. The Suwannee River fulvic acid (SRFA) standard (1S101F, International Humic Substances Society, IHSS) was prepared in Milli-Q water, at a concentration of 0.2 g L^{-1}. Before use, an aliquot of the SRFA standard solution was carefully saturated with the required concentration of iron to equal the binding capacity of the HS in ultrapure water [Sukekava et al., 2018] which was determined as described in [Laglera et al., 2007].

5.1.2.3 Equipment

The voltammetric system consisted of an Autolab PS101T potentiostat (Ecochemie, Netherlands), connected to a voltammetric stand (Metrohm model 663VA) containing a hanging mercury drop electrode (HMDE), a glassy carbon rod counter electrode and a double junction, Ag/AgCl, reference electrode with a salt bridge filled with 3M KCl. The instrument was controlled by NOVA 2.15 software (Metrohm). Samples (10 mL) were placed in a quartz voltammetric cell and stirred by a rotating PTFE rod.

5.1.2.4 Dissolved iron

DFe concentrations were determined after acidification (10 µL of 37% HCl ultrapure) following a well-established CSV method in the presence of 30 µM DHN [Laglera et al., 2013] but adding a UV digestion step. Acidified samples were transferred to 30 mL quartz tubes and irradiated for 3h using a home-built system including a 60 W high-pressure mercury vapor lamp. Before CSV analysis, the pH of samples was neutralized with ammonium (Merck, Suprapur 40%) and the sensitivity was determined in every sample through internal additions of DFe. The accuracy of the analytical results was verified through replicate analyses certified seawater NASS-5 (National Research Council of Canada, NRC). We determined a concentration of 3.68±0.14 nM, (n= 6), which was in excellent agreement with the certified value of 3.71±0.63 nM. The detection limit (3σ of blank) was 0.024 nM.

5.1.1.5 Iron ligand concentrations and the stability constant of their complexes

Seawater samples (120 mL) were mixed in a Teflon bottle with DHN at a concentration of 1 µM and POPSO buffer at a concentration of 5 mM, respectively. Every sample was split into 12 aliquots of 10 mL to which iron was spiked in the range of 0 to 20 nM. The CLE-CSV method with DHN was described initially by [van den Berg, 2006], but was modified by removing the addition of bromate from the original method to avoid any underestimation of the contribution of HS to ligand concentrations [Laglera et al., 2011] and excluding the purge during the measurement [Caprara et al., 2015]. All aliquots were equilibrated overnight at room temperature. The next day, each aliquot was spiked with 500 µL of the POPSO solution in order of increasing iron concentration and the concentration of the Fe-DHN complex determined by CSV analysis. The voltammetric parameters were as follows: a deposition potential of 0 V, adsorption time of 90 s, -5 mV of potential step with step intervals of 0.1 seconds and a potential scan using sample DC from -0.1 to −1.1 V.

Ligand concentrations and the conditional stability constants of their complexes with iron ($K'_{Fe'L}$) were obtained by fitting the CLE-CSV titration data into a linear Rûzic/van den Berg model, as described in [Ružić, 1982; Pižeta et al., 2015; van Den Berg, 1982].

Ligand concentrations are reported in nM and $K'_{Fe'L}$ values, reported in a logarithmic scale, and referred to the concentration of inorganic iron (Fe') as log $K'_{Fe'L}$.

5.1.1.6. Determination of humic substances and Fe-HS complexes

Samples were thawed and analyzed for HS concentrations and Fe-HS concentrations following established CSV procedures [Sukekava et al., 2018; Laglera et al., 2007]. Briefly, the voltammetric method consisted in the deposition of Fe-HS complexes onto the HMDE at -0.1 V for 90 seconds before switching the potential to -1 V using DC sample at 50 mV s^{-1}, to force the reduction of adsorbed Fe(III)-HS complexes. The analysis included 3 steps: (1) measurement of HS concentrations in the samples, (2) saturation of the natural HS with added iron (20-60 nM depending on the magnitude of the initial signal), while monitoring the precipitation of excess dissolved iron until completion (marked by the stability of the Fe-HS CSV signal) and (3) determination of total HS using standard additions of a SRFA iron-saturated solution.

5.1.3 Results and discussion

5.1.3.1 Hydrography

Our area of study consists of a 100-km wide continental shelf and the adjacent slope influenced by many hydrographic features with strong seasonality [Campos et al., 2013; Piola et al., 2005]. In general, high salinity and warm waters of the BC tend to separate from the coastal waters as the shelf widens. Samples were collected in a transect designed to cut perpendicularly the BC in its transit across the SMG Cape (Fig. 4). During fall and winter, SW winds are prevalent, and Plata Plume waters (PPW), characterized by low surface temperature (<18-20ºC) and salinity (<33.5), occupy the vicinity of the coast [Möller et al., 2008]. However, during spring and summer, when NE winds are predominant, the PPW is retracted southwards and Itajaí River waters of low salinity and

high temperature are found close to the coast [Campos et al., 2013]. At the first few kilometers from the coast (Stations 1 and 2) we found high temperature (>23ºC) and low salinity (<34.5) waters (Fig. 4), confirming the contribution of the Itajaí River to coastal waters [Campos et al., 2013].

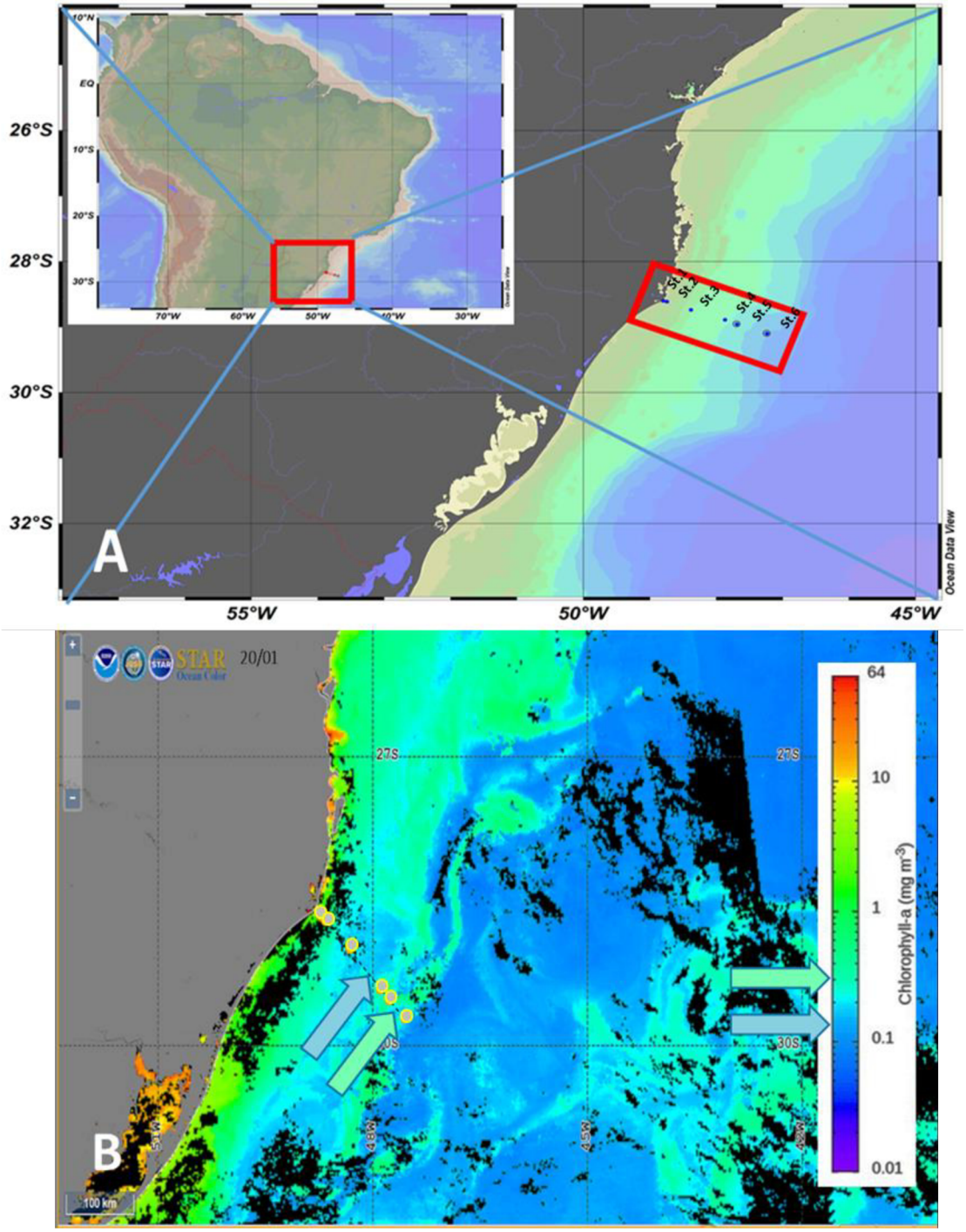

Figure 4. (A) Map of the Southeast coast of Brazil showing the location of the transect sampled in this study, and name of each station. (B) Surface chlorophyll map of the studied area showing the sampled transect. The arrows point to two important features of the Brazilian Current, the intermediate area of lower biomass, and to the outer string of high biomass.

Other distinctive local feature during the summer would be common wind-field variations that change the distribution of water masses alternating upwelling and downwelling pulses across the shelf depending on whether NE or SE winds prevail [Campos et al., 2000, 2013]. The depth of the 18.5 ºC isotherm and the 35.3 PSU isohaline (upper boundary of the SACW) have been usually accepted as indicators of whether waters over the shelf are dominated by downwelling or upwelling periods at any given time during the summer [Ciotti et al., 2014; Campos et al., 2013]. Since both isolines barely penetrated shelf waters (Fig. 4), the overall situation indicated downwelling in the first 70 km from the coastline. This was in line with the prevalent NE winds registered in the area during the 4 days prior to the sampling (Fig. 5). Coastal water downwelling forces by water convergence an upwelling of deep waters from the outer shelf (~100-120 km from the coast) to replace surface water close to the coast [Campos et al., 2000; Brandini et al., 2014]. During our study, temperature and salinity isolines featured a domed shape at 100 km from the coastline, confirming water upwelling over the shelf edge (Fig. 6A and 6B). During strong episodes of upwelling, macronutrient rich SACW waters can be injected into the euphotic layer [Brandini et al., 2014].

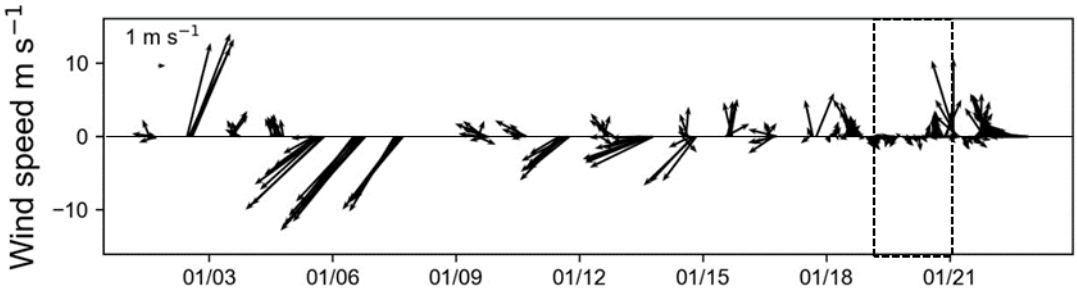

Figure 5. Wind speed and direction measured 15 days before sampling, 3 days during the cruise (in rectangle). Positive values indicate S/SW winds.

5.1.3.2 Other ancillary parameters

Oxygen concentrations showed a patchy pattern along the transect, albeit oxygen saturation showed a more coherent distribution. Local biogeochemical processes appeared to generate two major oxygen undersaturation sites: one near the coast in low salinity waters and another around the shelf edge region (Fig. 6C). Coastal oxygen undersaturation sites might result from the combination of intense respiration activity of grazers and large phytoplankton biomass [Ito et al., 2016].

The turbidity was high and nearly constant along the shelf and therefore across the salinity gradient that separated coastal freshwater inputs and TW (Fig. 6D). This lack of relationship with the salinity suggests a local resuspension of particles from the shelf sediments. At the shelf edge region, an area where water convergence and turbulence caused by the dissipation of internal waves combine to generate upwelling, there is a remarkable surge of turbidity (Fig. 6D). Our data indicate that the referred upwelling at the shelf edge was strong enough to bring along low oxygen interstitial waters with a high content in particles. For later comparison with chemical species measured in filtered samples, it is important to remark that turbidity is measured in unfiltered water and that light is not scattered below a particle size threshold.

Satellite pictures (Fig. 4B) show two maxima of chlorophyll-*a* concentrations along the transect which were related to the general distribution of biomass in the SBB region during our sampling. One along the first 20 km from the coastline (>2 $mg.m^{-3}$) and a secondary with moderate concentrations around the shelf edge (~ 0.35 $mg.m^{-3}$). Intermediate concentrations were below 0.14 mg m^{-3} (Fig. 4B). Over the studied area, this secondary maximum is generalized and appears in the satellite images as a high biomass meander separated from high biomass coastal waters by an area of low biomass area (Fig. 4B).

For the area that is very close to Santa Catarina State, concurrent relationships between the same oceanographic features described here and the spatial distribution of phytoplankton biomass were found. This coincidence suggests that the combination of shelf downwelling / slope upwelling and its repercussion in the formation of a secondary chlorophyll maximum at ~100 km from the coastline may be a generalized scenario in the region during the summer [Brandini et al., 2014].

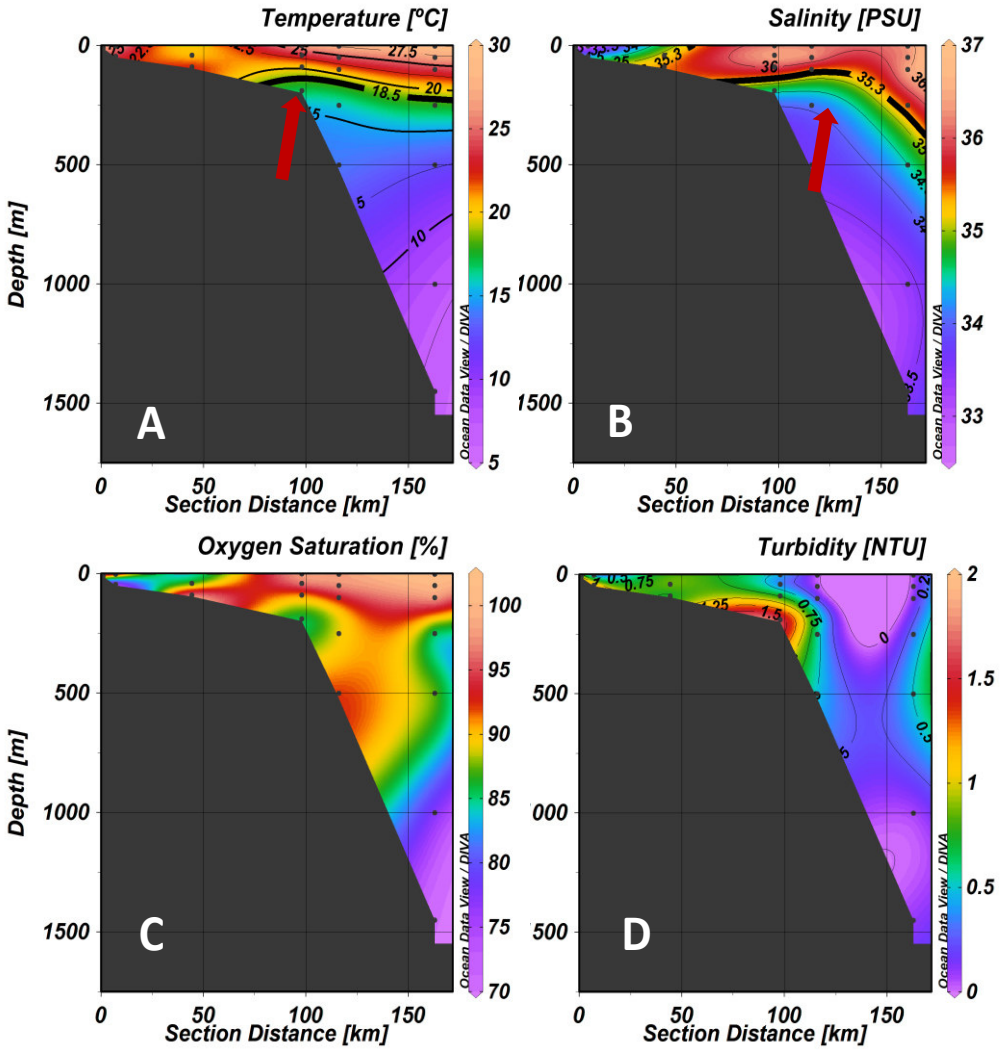

Figure 6. Spatial distribution of temperature (ºC) (A), salinity (PSU) (B), oxygen saturation (%) (C), and turbidity (NTU) (D) in the transect off the Santa Marta Grande cape. The arrows remark the dome shape of the 18.5 ºC isotherm and the 35.3 ºC isohel, upper limit of the South Atlantic Central Water (SACW), indicative of upwelling in the transition from shelf to slope.

5.1.3.3 Macronutrients

The BC is depleted in macronutrients although local coastal processes, such as the aforementioned freshwater discharge by rivers and wind-driven upwelling episodes, play a modulating role [Braga et al., 2008; Ciotti et al., 1995]. Surface silicate concentrations were in the range of 2-18 µM (Fig. 8C). Previous studies have reported silicate concentration of 1–12 µM within SACW [Piola et al., 2000].

The three macronutrients correlated highly over the entire data set with Pearson correlations for nitrate vs phosphate and nitrate vs silicate of 0.804 ($p<0.001$) and 0.710 ($p<0.001$), respectively. This high correlation indicates that macronutrient concentrations were probably the result of the same processes. The isolines of the three macronutrients sink and move away from the sea surface over the shelf whereas they showed a domed pattern over the shelf edge and beyond suggestive of upward transport. (Fig. 8). This scenario was in accordance with the referred coastal downwelling process leaving behind exhausted nutrient levels at the surface coupled to an upwelling of nutrient-rich upwelled waters near the shelf edge. Although it is difficult to estimate the exact contribution of this nitrate (and phosphate) input into the euphotic layer, it is safe to hypothesize that upwelling pulses contribute to form the high chlorophyll meander located at about 100 km from the coastline. Seawater N:P ratios were below the Redfield ratio of 16 in all but 3 samples. Fig. 7 shows that in the coastal downwelling area nitrogen was limiting but over the shelf edge, N:P ratios well over Redfield requirements formed a well-defined plume coincident with the turbidity maximum indicating nitrogen enrichment with respect to phosphate.

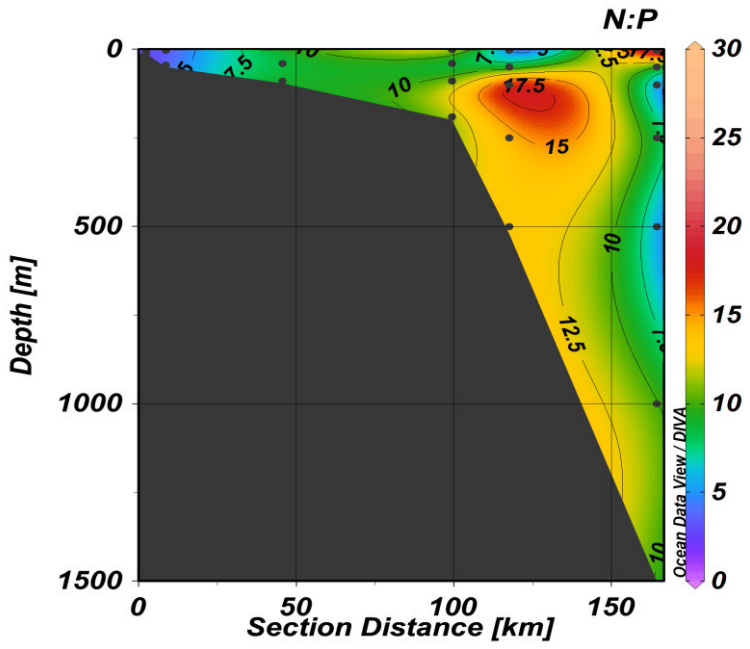

Figure 7. Distribution of nitrogen and phosphorus ratio (N:P) in the transect off the Santa Marta Grande cape.

Silicate concentrations were minimum at the surface coincident with the chlorophyll maximum indicating that its surface distribution is modulated by primary productivity

drawdown (Fig. 4B and 8C). There was no apparent upwelling of silicates at the shelf edge region (Fig. 8C). Since particles and other nutrients were substantially upwelled, we can suggest that sediments at that region were silica depleted.

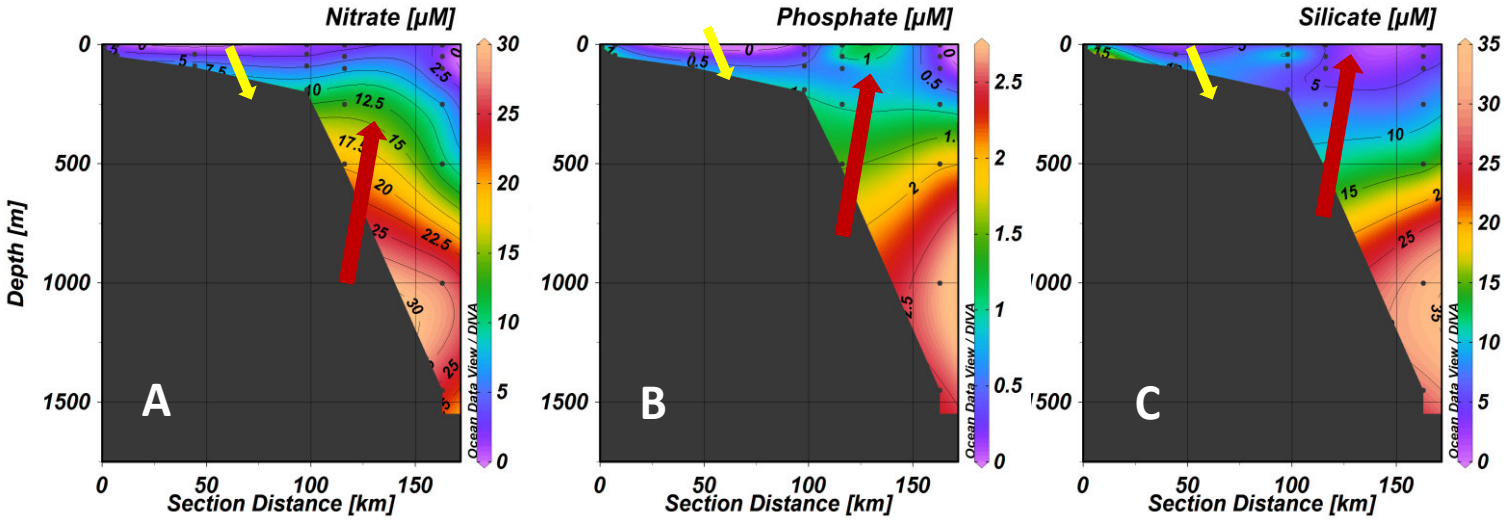

Figure 8. Spatial distribution of nitrate (µM) (A), phosphate (µM), (B) and silicate (µM) (C) in the transect off Santa Marta Grande cape. Yellow arrows indicate location of the downwelling and red arrow's location of upwelling.

5.1.3.4 Dissolved iron

In the studied area, DFe concentrations (all > 0.9 nM) were one order of magnitude higher than what is considered limiting, so its role in controlling primary productivity was possibly not relevant (Fig. 9A). Fe:NO_3^- ratios in the upper 200 m over the area of study were in the range 0.17 to 4.2 nmol:µmol^{-1} and corroborated that nitrate was the limitant nutrient. These ratios are at least one order of magnitude higher than the ratios of 0.03 nmol:µmol^{-1} that mark the transition from nitrate to iron limitation in the California upwelling region [Biller & Bruland, 2014].

DFe concentrations also responded to the overall circulation pattern proposed and its isolines sank over the shelf and rose over the shelf edge in concomitance with nitrate, oxygen saturation, and turbidity data. However, over the slope, the trend was the opposite with higher DFe concentrations at the surface. Lower DFe concentrations at stations 1 and 2 with respect to station 3 can only be explained by a combination of low discharge

of freshwater to the inner shelf area combined with enhanced, non-terrestrial iron inputs to the upper ocean in the outer shelf region. Aerial deposition, a common feature in the area, seems the most likely source of surface DFe for the first 60 km from the coast [Bif & Yunes, 2016]. High DFe concentrations over the shelf edge and the slope sediments, point to an apparent resuspension of iron. On one hand, this is a regular situation in systems characterized by low oxygen saturation that favors the reduction of Fe(III) species into the highly soluble Fe(II) species. The reoxidation of Fe(II) back to Fe(III) as the oxygen saturation increases usually restricts this effect to the few first meters over the sediment. On the other hand, the DFe surge over the shelf edge is coupled with an increase of the turbidity, suggesting that colloidal and particulate iron is resuspended, with the consequent release of DFe by particulate/solution fluxes. It is difficult to measure the contribution of the two processes to the DFe plume located at the shelf edge. Since at stations 4 to 6 we found high DFe concentrations in all samples collected close to the bottom, the release of DFe (as Fe(II)) from the sediment seems to be a generalized feature. However, only the DFe plume associated to the maximum in turbidity is not confined to the vicinity of the sea floor and seems to make an impact in the euphotic layer. This indicates that particulate iron resuspension, possibly in the form of heterogeneous colloids, was an important feature at the sampling time. Turbidity decreased quickly from station 4 to 5 whereas the rest of chemical parameters affected by the upwelling advanced to station 5. We hypothesize that this decoupling of the distribution of turbidity and chemical species that seem related is caused by the progressive disaggregation of the resuspended particles. Particles, possibly a fraction of which were colloids formed by the interaction in pore waters of polynuclear iron nano-oxides with heterogeneous organic matter, were observed by turbidity but their content only partially analyzed because a significant fraction were too big to pass through our 0.2 μm filters. This mixed material has been observed in coastal plumes of peat-draining rivers [Muller & Cuscov, 2017]. As these colloids penetrated more oxygenated and sunlit waters, they started to disaggregate and cancelled their contribution to the turbidity since became too small to scatter the light of the detector. However, downsizing promoted their incorporation to the filtrate, and increased their contribution to DFe concentrations. Surface DFe concentrations over 4 nM at Stations 5 and 6 (Fig. 9A) could be also explained by the aerial deposition referred above [Bif & Yunes, 2016]. Finally, surface trophic biological processes may play a role in remineralizing part of the particulate iron [Laglera et al., 2017], since blooming surface

waters influenced by upwelling of SACW waters, are characterized by high zooplankton biomass [Resgalla et al., 2001].

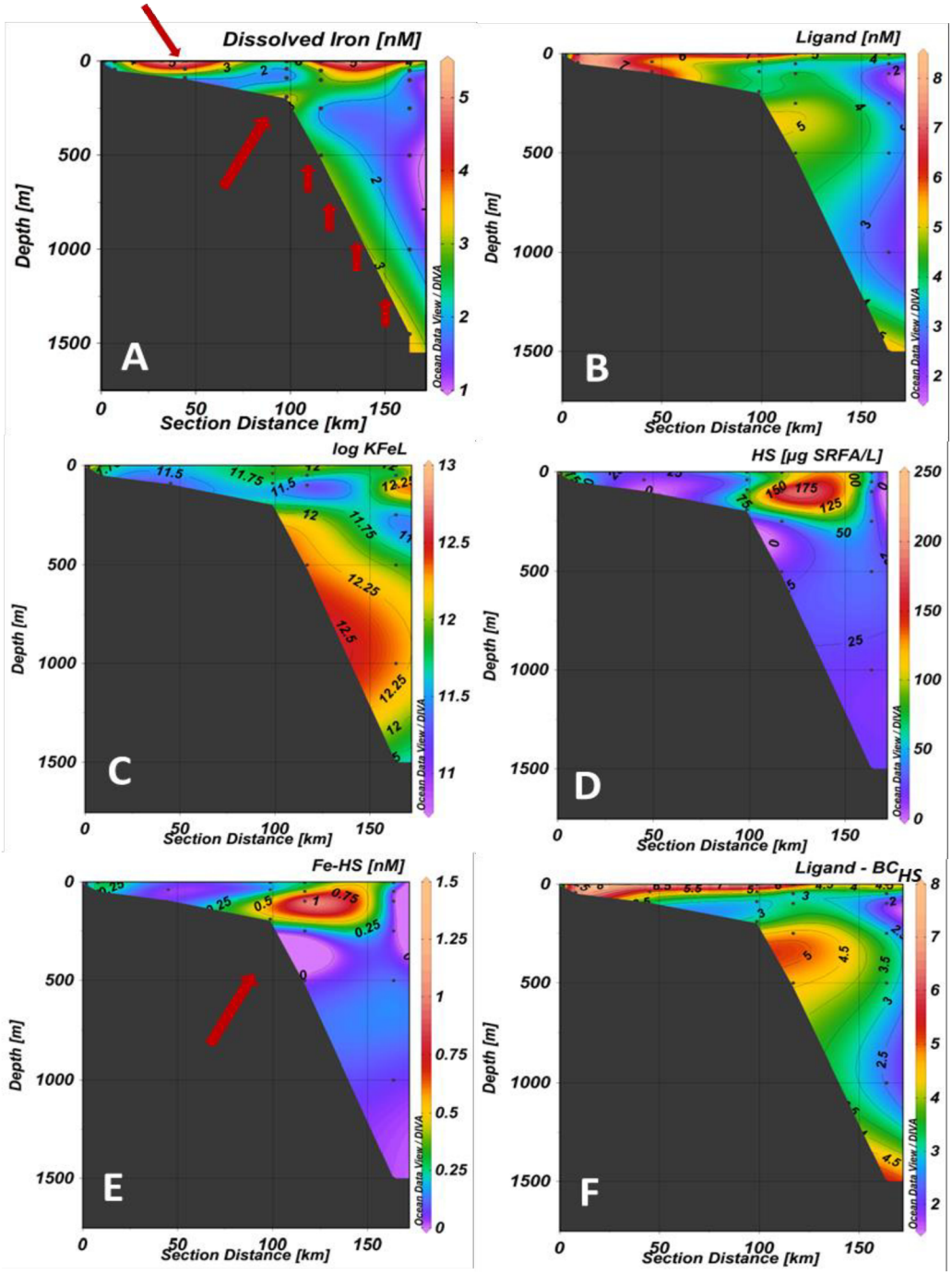

Figure 9. Spatial Distribution of DFe (nM) (A), ligand (nM) (B), constant of stability (C), HS (µg SRFA L^{-1}) (D), Fe-HS (nM) (E) and overall ligands without the contribution of humic (F) in the transect off Santa Marta Grande cape. Yellow arrows indicate downwelling and red in the slope upwelling. The DFe plot had red arrow that show aerial deposition in surface and sediment resuspension.

5.1.3.5 Iron speciation and the role of humic substances as iron ligands

To be able to extract the concentration of ligands and their $K'_{Fe'L}$, plotting of the fraction exchanged with an added ligand that forms an electroactive complex as a function of the iron added to the aliquot must show a characteristic curved shape. However, this is sometimes not the case in coastal waters [Su et al., 2016; Sato et al., 2022]. This is often due to small ligand concentrations (equal or barely below DFe concentrations) of extremely high affinity and already saturated with iron, that interchange iron with the artificial ligand below the limit of detection. In two cases, the 40 m deep sample at station 3 and the bottom sample (190 m deep) at station 5, the linearity of the titration prevented the calculation of the ligand concentration and $K'_{Fe'L}$. In these two cases, and exclusively for studying DFe speciation, we decided to consider a ligand concentration equal to the DFe concentration. This is based on the certainty that ligands were not absent in the sample. The extremely low solubility of inorganic iron requires complexation to maintain concentrations in solution in the nanomolar range. Ligand concentrations close to DFe concentrations were a common feature with ligand to DFe ratios lower than 2 in more than half the samples.

Along the shelf, ligand concentrations were high (2 to 8 nM) with a clear land to ocean gradient, with the highest values (~8 nM) found at the bottom of station 3 (Fig. 8B). This trend does not concur with the well-defined downwelling pattern shown by other variables. In contrast to DFe, ligands did not show high surface concentrations and did not seem to be upwelled at the shelf edge. To the best of our knowledge, the decoupling of DFe and iron ligand concentrations in coastal waters has not been found before [Mellett et al., 2018; Su et al., 2015]. Land to ocean ligand gradients usually indicate that terrigenous ligands, mainly composed of HS, could be the main source of ligands. However, HS were only high at stations 1 and 2 (60 to 110 µg SRFA L^{-1}) and did not follow the horizontal gradient shown by overall ligands with some of the lowest HS concentrations found at station 3 (Fig. 9D). If we take the iron binding capacity of our SRFA standard, 14.6 ± 0.7 nmol Fe mg $SRFA^{-1}$, we can determine that the contribution of HS to ligand concentrations over the shelf was of 0.5 to 1.8 nM, which is only 10 to 20% of the ligand concentrations (Table 2). The exception was station 1 and 2 where ligand concentrations were comprised of HS by 30 to 70%. Our analytical scheme also included the determination of the contribution of Fe-HS complexes to the concentration of DFe. In waters over the shelf, HS binding sites with affinity for iron were found to be

mostly iron-free with saturation indexes from 0 to 25%, and Fe-HS concentrations were in the range below the limit of the detection (LOD, <0.03nM) to 0.43 nM (Fig. 9E, Table 2). Therefore, the contribution of Fe-HS complexes to DFe over the shelf was in the range of ~0 to 25%. This implies that despite the strong horizontal gradient of ligands and the vicinity to the coast, the contribution of HS to iron solubility over the shelf was low.

Table 2. DFe (nM), ligand (nM), log K'Fe'L, HS (µg SRFA L^{-1}) and Fe-HS (nM) a determined from the SBB samples. LS means lost sample. LT means the linearity of the titration that prevent the calculation of log K'Fe'L. <LOD means values less than limit of detection.

Station	Depth [m]	DFe [nM]	Ligand [nM]	log K'Fe'L	HS [µg SRFA L^{-1}]	Fe-HS [nM]
St. 1	2.9	1.68±0.24	3±0.2	12.31±0.88	111.4±12.01	0.081
	11.5	1.59±0.36	3.6±0.20	11.69±0.11	79.5±4.65	0.128
St.2	2.5	2.16±0.33	8.10±0.20	11.83±0.08	59.4±10.71	0.359
	45	1.83±0.42	7.5±0.30	11.87±0.17	88.3±25.07	0.291
St. 3	40	4.49±0.22	4.49[a]	LT	12. 4±1.71	0.007
	90	1.24±0.10	7.5±0.30	11.23±0.11	LS	LS
St. 4	1	1.75±0.14	8.30±0.30	11.75±0.09	82.2±24.71	0.308
	40	1.74±0.33	4.30±0.30	11.94±0.93	32.2±1.38	0.073
	90	0.99±0.01	3.10±0.20	11.94±0.18	27.9±4.11	0.317
	190	3.53±0.38	3.53[a]	LT	57±10.44	0.432
St. 5	2.5	4.93±0.81	5.80±0.20	12.08±0.11	92.7±15.34	0.233
	50	2.32±0.33	2.70±0.60	11.87±0.56	81.2±11.50	0.321
	100	2.95±0.58	5.20±0.80	10.91±0.14	240.5±34.93	1.358
	250	1.27±0.10	5±0.20	12.08±0.11	26.4±2.74	<LOD

	500	2.55±0.41	4.60±0.10	12.33±0.06	19.5±9.85	<LOD
St. 6	2.5	4.33±0.15	5±0.50	12.15±0.21	47.1±3.50	0.275
	50	0.99±0.15	3.30±0.30	11.49±0.24	55±0.68	<LOD
	100	1.55±0.30	1.70±0.04	12.57±0.11	22.8±3.80	<LOD
	250	1.69±0.48	3.10±0.20	11.41±0.12	36.3±4.35	<LOD
	500	0.88±0.06	3.40±0.10	11.95±0.25	34.3±5.03	0.127
	1000	1.67±0.24	2.50±0.10	12.32±0.11	18.2±7.34	0.064
	1500	3.02±0.49	5.50±0.40	11.71±0.34	20.7±6.08	<LOD

With respect to the other major area of interest, the shelf edge and the slope, ligand concentrations were also high except for station 6, which was less affected by water upwelling. At stations 4 and 5, ligand concentrations were in the range of 3 to 8 nM, while at station 6, ligand concentrations were in the range 2 to 5 (Fig. 9B). Since sediments accumulate a high concentration of decaying organic matter, and a part of it is expected to show affinity for iron, upwelling of interstitial waters must pump iron ligands into the water column. Ligand concentrations at the bottom of stations 5 and 6 were higher concurring with the DFe release from sediments shown above. However, this was not the case at station 4. In contrast, in the area affected by upwelled water at stations 4 and 5, HS concentrations were more than double than in surrounding waters (ranges of 30 to 240 and 20 to 40 µg SRFA L-1, respectively) (Fig. 9D). This is the equivalent to ligand concentrations in the range 0.41±0.04 to 3.5±0.17 nM, which is equivalent to a contribution of HS to ligand concentrations ranging from 11 % to 68% at the maximum HS concentration of 240 µg SRFA L-1 at 100 m deep at station 5 (Table 2). The origin of this HS input is clearly related to the upwelling of high-turbidity and nutrient-rich waters at the shelf edge, despite being the maximum HS concentration not found close to the bottom at station 4 (Fig. 9D). We hypothesize that the same disaggregation process mentioned in Section 3.4 was responsible of HS upwelling and explains the lack of correlation of turbidity with HS concentrations despite having a common origin. Another possible source of HS to the water column is the local degradation of the organic matter flux from the euphotic layer, in this case from the high chlorophyll meander. In the upwelled waters, concentrations of Fe-HS complexes up to 1.4 nM were substantial constituting up to 42% of the DFe concentrations (100 m deep station 5) (Fig. 9E).

Samples collected at station 6 and at station 5 below upwelled waters (including samples collected close to the slope bottom) showed a negligible contribution of HS to iron solubility (Fig. 9E).

Another approximation to the nature of the natural ligands can be inferred from the K'Fe'L values. However, there is one strong limitation since $K'_{Fe'L}$ values fall inside a range called "analytical window" determined by the concentration and stability of the complex formed by the added ligand and iron, i.e.: the ability to extract iron from the ligands found in the sample [Gerringa et al., 2014]. In summary, too strong, and too weak ligands are not properly resolved. Weak ligands are fully outcompeted by the added ligand and left out of calculations. Iron complexes with strong ligands do not undergo ligand exchange after the addition of the added ligand, and although contribute to the ligand concentration, strong ligands do not weight in the determination of $K'_{Fe'L}$. Our analytical protocol set the center of our analytical window at a value in the lower end of the analytical windows used with different CLE-CSV methodologies to this date (side reaction coefficient or $\alpha'_{Fe'L}$ = [DHN] x $K'_{Fe'DHN}$ = 22.4) [Gerringa et al., 2021] with the aim to include the contribution of the weakest binding fraction of HS. In the whole area of study, log $K'_{Fe'L}$ values fell into the range of 10.9 to 12.9 (Fig. 9C). Overall, there is a clear depth interval (20 to 200 m) where ligands of lower stability (all < 11.8) are found, mostly over the shelf. Stronger ligands (all >11.8) were found close to the coast, and at stations 4, 5 and 6 above and below the depth range referred to above including all samples collected close to the bottom of the slope (Fig. 9C). The traditional interpretation would point to a possible presence of HS in samples with lower log K'Fe'L based on previous reports that the affinity of HS for iron is about one order of magnitude lower than that of other natural ligands such as siderophores and porphyrins [Laglera & van den Berg, 2009; Witter et al., 2000]. However, this is not the case here because of the lack of relation between the distributions of ligands, HS and log K'Fe'L (Fig 9B and 9D). This same traditional approach shows that due to the high log K'Fe'L values found in surface waters, local biological production of ligands would be more important in the upper 20 m and below 200 m over the studied area. Theoretically, the use of an analytical window centered at a higher α'Fe'L could have removed the contribution of weak ligands, many of HS nature, and become an arguable approach to resolve non humic ligands without our subtraction step. However, shifting of the CLE-CSV analytical window for iron speciation has been barely tested because the flexibility of many CLE-CSV methods to reduce or increase the concentration of the artificial ligand is very limited or require huge

side corrections due to the presence of non-electroactive Fe-artificial ligand species [Mahmood et al., 2015] and the combined use of different artificial ligands has recently shown drawbacks [Gerringa et al., 2021]. Moreover, the use of a higher analytical window could reduce the number of reliable results since out competition of weak ligands increases the possibility to obtain straight titrations like the two cases reported above.

Here we present for the first time a way to clarify the origin of ligands via the subtraction of the contribution of HS to iron speciation. Fig 9F shows that once the contribution of HS to ligand concentrations is removed, the color plot of ligand distribution becomes more coherent. In the upper 200 m over the whole transect, non-humic ligands show a clear gradient from coast to open waters and from surface to bottom. Since high surface ligand concentrations extended well beyond the area of coastal influence, biological production (exudation or cellular lysis) must be the main source of non-humic ligands in the upper 200 m. Bottom samples at stations 5 and 6 also showed higher non-humic ligand concentrations, probably indicative of sediment release or bacterial remineralization [Burdige et al., 2004]

Fig. 9E shows that there are two areas of significant contribution of Fe-HS complexes to DFe concentrations: close to the coast and in upwelled waters. Apart from their iron binding ability, HS are characterized by their photolability and promote Fe reduction which increases substantially in the bioavailability of iron [Chen & Wang, 2008; Lis et al., 2015]. The upwelling of DFe into the euphotic layer in the form of Fe-HS complexes probably increases its bioavailability with respect to other areas where other iron species are predominant [Muller, 2018]. At the sediment-water interface of these two areas, DFe and ligand concentrations were high, and HS were absent, indicating that in sediments not affected by the upwelling, HS were either not present or, due to their size and/or chemical properties, remained in the interstitial waters. Only when the physical force at the water-sediment interface is strong enough to resuspend particles, are Fe-HS complexes a substantial contributor to upwelled DFe concentrations.

5.1.4 Conclusions

We observed upwelling of macronutrients and DFe over the shelf edge at 100 km from the coast as a response to NE summer wind regimes and turbulence generated by the dissipation of internal waves on the shelf edge. Our data do not allow us to estimate which one of the two processes-controlled upwelling. Macronutrient injection reaching the euphotic layer helps to explain the discontinuity in coastal chlorophyll concentration and the formation of high biomass meanders parallel to the coast.

Surprisingly, DFe and iron ligands distributions were uncoupled with strong vertical gradients of DFe, suggesting aerial deposition, and a strong horizontal gradient of ligands. Uncoupling of HS and overall ligands showed that most of surface ligands were of local biological origin although further investigation would be required to study the sources and fate of such ligands. DFe and ligands were also high in nearly all the stations where we collected samples close to the bottom, suggesting sediment to water column fluxes.

We detected an important source of Fe-HS complexes, clearly related to the upwelling of high-turbidity nutrient-rich waters over the shelf edge, that were stable enough to reach the euphotic layer at the shelf edge, and that contributed significantly to iron solubility. We conclude that high dissolved Fe-HS concentrations could be caused by disaggregation and dissolution of resuspended colloidal material of sedimentary origin. Future research to understand micronutrient dynamics should focus on the study of the composition and stability of particles upwelled from the outer section of continental shelves. The use of advanced methods to disentangle the contribution of HS to iron speciation from the rest of the binding components of DOM show that the contribution of HS to iron dynamics in the SMG is concealed to upwelling areas due to the low input of freshwater and the absence of dissolved HS fluxes from sediment to water.

Data availability

Data available on https://doi.org/10.1594/PANGAEA.951154

5.2 Ligand exchange provides new insight into the role of humic substances in the marine iron cycle.

Abstract

Organic complexation of iron plays a crucial role in preventing its precipitation, facilitating its transport, and modulating its reactivity and bioavailability in natural waters. Although humic substances (HS) complexes serve as the primary source of terrestrial iron reaching ocean waters, the transition from Fe-HS species to other forms of organic complexation with ocean autochthonous ligands has not yet been properly described. Taking advantage of the electrolability of Fe-HS complexes, we monitored the ligand exchange of iron-saturated Suwannee River fulvic and humic acids (SRFA and SRHA) after the addition of desferrioxamine B (DFOB) and other ligands for comparison. We observed that Fe-HS concentrations gradually decreased until reaching an apparent steady state, typical of a reversible reaction within 1 to 15 h. The dissociation kinetics and species partitioning of $FeSR_{HS}$ complexes at the equilibrium showed some features contrary to the current paradigm of HS iron complexation. The affinity of SRFA to bind iron is close to that of DFOB and for SRHA is even higher. The heterogeneity of the HS iron binding groups was confirmed, although experiments in NaCl solutions revealed that in seawater it is substantially caused by the interaction of major divalent ions. The different dissociation kinetics of Fe-SRHS complexes obtained with different competing ligands and the absence of Fe-DFOB dissociation in the presence of iron-free SRFA indicate an intimate associative mechanism of ligand exchange, with the presence of a ternary complex (SRHS-Fe-DFOB) that does not form if the departing complex is Fe-DFOB. We hypothesize that at the concentrations of HS and siderophores found in the open ocean, iron ligand exchange is limited, and organic iron speciation will be close to being regulated on a “first come, first served” basis. Experiments conducted under saturation of all iron complexes support the formation of a permanent concentration of a ternary complex. Our findings show the real complexity of cation-ligand interactions in seawater, with implications for the interpretation of recent chromatographic and electrochemical measurements and for the understanding of iron partitioning in the presence of ubiquitous HS.

5.2.2 . Introduction.

Organic complexation is the key process in regulating iron concentration, transport, reactivity and bioavailability in the ocean [Gledhill, & Buck, 2012]. Due the high biological requirements of marine organisms for iron and the very limited solubility of the element in seawater[Liu & Millero, 2002a], organic complexation and reduction to the more soluble Fe(II) form are paramount to ocean ecology and, subsequently, to carbon cycling. The formation of complexes with a fraction of dissolved organic matter (DOM), hereafter referred to as ligands (L), prevents the formation and aggregation of iron hydroxides and facilitates, via ligand to metal charge transfer reactions, the formation of the more bioavailable Fe(II).

HS are complex organic mixtures resulting from biological and chemical and biochemical transformations of dead plants tissues and microorganisms. HS are a physically and chemically heterogeneous mixture characterized by their hydrophobicity, a wide range of molecular sizes, and, related to the problem targeted here, the presence of a high number of cation-binding moieties [Tipping & Hurley, 1992] of which a fraction are hard bases showing a high affinity for iron [Laglera & van den Berg, 2009]. HS are operationally divided into humic acids (HA) and fulvic acids (FA) depending on whether they are soluble (FA) or not (HA) at pH 1. As a result of their formation in most terrestrial and possibly marine ecosystems and their refractory character, HS are ubiquitous in natural waters, including remote areas such as the deep ocean.

Iron export from estuaries was considered irrelevant for ocean inventories due to estuarine trapping, a process caused by the aggregation and coprecipitation of terrestrial DOM, mostly composed of HS, and iron, mostly colloidal hydroxides, as the increase of the ionic strength overrides DOM repulsion electrostatic forces [Sholkovitz, 1978]. This paradigm has been modified in the last two decades, leading to a common understanding that a fraction of riverine DFe is exported to the ocean as stable, and importantly, rather refractory Fe-HS complexes [Heerah & Reader, 2022; Krachler et al., 2015; Laglera & van den Berg, 2009; Muller, 2018; Oldham et al., 2017]. From an ecological perspective, humic iron exports should be an important source of iron that feeds coastal blooms

[Heerah & Reader, 2022; Krachler et al., 2019; Sukekava et al., 2023]. Iron complexed to HS can be taken up directly by biota, but a significant fraction is expected to be sequestered by autochthonous L formed by biological processes in seawater. Although recent field studies on the interaction of HS and iron in seawater are available [Batchelli et al., 2010; Laglera et al., 2019; Laglera & van den Berg, 2009; Sukekava et al., 2023; Whitby et al., 2020a; Yang et al., 2017], the kinetics of iron ligand exchange from humic iron to other autochthonous biological ligands have not yet been described.

Most of our knowledge about the concentrations of trace element ligands in natural waters, including the calculation of the stability constant of their complexes with trace elements, comes from the use of competing ligand equilibration (CLE) with analysis by adsorptive cathodic stripping voltammetry (AdCSV) [Gerringa et al., 2014; Gledhill & van den Berg, 1995]. The result is presented as a ligand concentration and the conditional stability constant (K′) of the corresponding complex. In some cases, if the affinity of the different iron binding groups present in natural samples is grouped into classes, CLE-AdCSV can provide further insight into the heterogeneity of iron complexation by defining a stronger and a weaker ligand (L1 and L2, K′Fe′L1 >> K′Fe′L2). Remarkably, CLE-AdCSV techniques have failed to describe in detail the natural heterogeneity of HS binding sites [Laglera et al., 2011] . During the CLE step, iron undergoes ligand exchange following competition from the added free Lad (artificial ligand). There is little information on the intimate mechanism of the reaction that regulates the kinetics (i.e, time period) before reaching the equilibrium, a period that has been described for iron in a wide range, from many minutes to nearly three days depending on the combination of natural and Lad used in the experiement [Wu & Luther, 1995; Rue & Bruland, 1995]. A comprehensive summary of published kinetics and the intimate mechanisms of iron ligand exchange and their implications in CLE studies can be found elsewhere [Laglera & Filella, 2015]. CLE-AdCSV studies and current speciation models are based on a number of assumptions such as the dissociative mechanism of complexes dissociation, reversibility, absence of ligand interactions with other organic components of the matrix, etc. [Stockdale et al., 2011; Gerringa et al., 2014; van den Berg, 1995].

Here we present the first CLE-CSV follow-up to equilibrium using HS as an electrolabile ligand against the competing effect of the siderophore desferroxamine B (DFOB) and other ligands commonly used in CLE experiments. This is the same process that terrestrial iron undergoes during estuarine transition. In contrast to all previous experiments,

departing and competing ligands compounds are part of natural DOM. The exchange or iron from HS complexes to biological ligands is the same process that occurs when riverine iron mixes with coastal seawater.

5.2.2. Conceptual framework

In the following, we will present only the basic concepts and equations needed to interpret our results. A short summary of the conceptual framework may be found in the supplementary file. For a complete overview of ligand exchange from a mechanistic point of view, we refer the reader to our previous publication on the intimate mechanism and kinetics of iron ligand exchange in seawater and its application to CLE studies [Laglera & Filella, 2015].

The iron ligand exchange of the departing complexes (Fe-HS here) caused by competition with an added ligand (L_{ad}), a situation similar to the arrival of DOM and Fe rich riverine waters to estuaries, is defined according to Eq. 1:

$$\mathrm{Fe-HS} \quad + \quad \mathrm{L'_{ad}} \quad \overset{kobs}{\longleftrightarrow} \quad \mathrm{HS'} \quad + \quad \mathrm{Fe-L_{ad}} \qquad (1)$$

the prime superscript (HS′ and L′ad) combines all the non-ferric forms and mass balances for both ligands are defined as follows:

$$[\mathrm{HS}]_{\mathrm{TOT}} = [\mathrm{HS'}] + [\mathrm{FeHS}] \qquad [\mathrm{L_{ad}}]_{\mathrm{TOT}} = [\mathrm{L'_{ad}}] + [\mathrm{FeL_{ad}}] \qquad (2)$$

This simplification implies the conditionality to the matrix composition of all stability constants:

$$K'_{Fe'HS} = \frac{[Fe'-HS]}{[Fe'][HS']} \qquad K'_{Fe'L_{ad}} = \frac{[Fe'-L_{ad}]}{[Fe'][L'_{ad}]} \tag{3}$$

where Fe′ is the total concentration of iron inorganic species.

At the equilibrium, we can calculate the ratio between the conditional stability constants of both ligands as [Luther et al., 2021] .

$$\frac{K'_{Fe\prime-L_{ad}}}{K'_{Fe\prime-HS}} = \frac{[Fe\prime-L_{ad}]\cdot[HS']}{[Fe\prime-HS]\cdot[L'_{ad}]} \tag{4}$$

There are two major routes for ligand exchange to happen, depending on whether intermediate chemical species have a lower or higher coordination number.

Dissociative mechanism (D): it is characterized by the complete dissociation of the departing ligand (Fe-HS) before iron establishes any interaction with the incoming ligand. Scientists favour this mechanism because the relationship between the conditional equilibrium constants equal the ratio of association and dissociation kinetic rates:

$$Fe' - HS \rightleftharpoons Fe' + HS' \qquad k_{a,Fe'HS},\ k_{d,Fe'HS} \tag{5}$$

$$Fe' + L'_{ad} \rightleftharpoons Fe' - L_{ad} \qquad k_{a,Fe'L_{ad}},\ k_{d,Fe'L_{ad}} \tag{6}$$

The kinetics of Eq. 5 and 6 are second order kinetics. For the combined reaction, the characteristic 1/[Fe-SRFA] vs. time plot is linear in the kinetic section with a curved transition section before the flat line marking the equilibrium (Fig. 10).

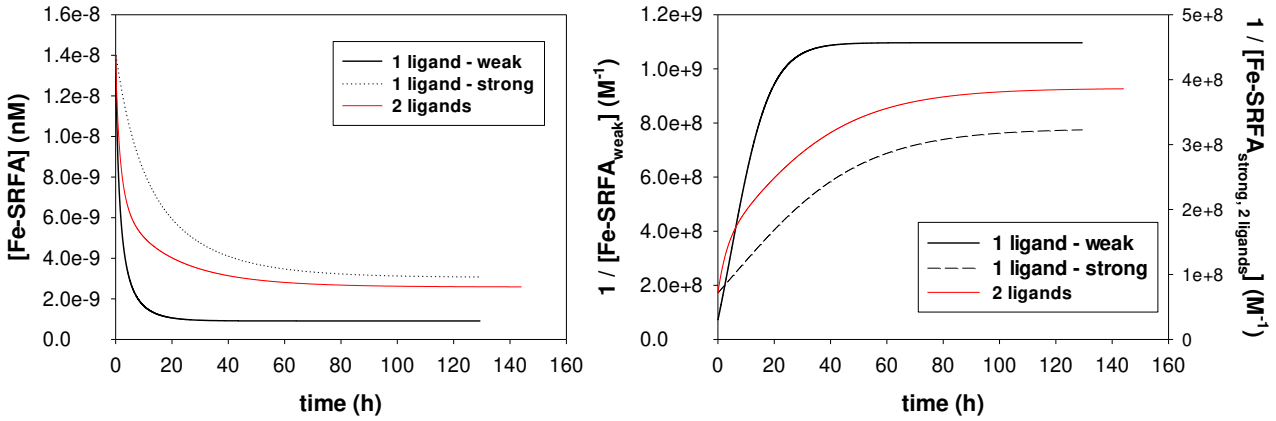

Figure 10. Modelling of the time course of the iron ligand exchange of 14 nM Fe-SRFA complexes after the addition of 15 nM L_{ad} using the following rate constants: $k_{a,FeDFOB}$=2x10^{6} M^{-1}s^{-1}, $kd_{,Fe\text{-}DFOB}$=2x10^{-6} M^{-1}s^{-1}, $k_{a,Fe\text{-}SRFA}$=2x10^{6} M^{-1}s^{-1} and two different $k_{d,Fe\text{-}SRFA}$=1x10^{-5} M^{-1}s^{-1} (strong ligand) and 1x10^{-4} M^{-1}s^{-1} (weak ligand). Red line: same experiment when the SRFA binding groups are divided into 8 nM of the weak ligand and 6 nM of the strong ligand.

Associative mechanism (A): the incoming ligand forms a chemical bound with the departing complex resulting in a ternary complex of higher coordination. The breaking of the initial bond occurs in a secondary reaction.

$$\mathrm{Fe'-HS} \quad + \quad \mathrm{L_{ad}} \quad \overset{A1}{\leftrightarrow} \quad \mathrm{HS-Fe'-L_{ad}} \quad \overset{A2}{\leftrightarrow} \quad \mathrm{Fe'-L_{ad}} \quad + \quad \mathrm{HS'} \qquad (7)$$

Since the D mechanism requires "spontaneous" dissociation of the departing complex and the A mechanisms involves the chemical attachment of the incoming ligand to the initial complex, changes in ligand exchange kinetics with different incoming ligands are indicative of an A mechanism [Helm & Merbach, 2005]. The A mechanism makes the calculations extremely complicated because extra species are added to mass balance equations, the ternary complex has its own stability constant and association and dissociation kinetics. The observation of an A mechanism necessarily accelerates the ligand exchange kinetics with respect to the D case.

Some matrix components known as accelerators, mainly cations or sometimes other organics, present the ability to weaken the bond of the initial iron complex and therefore change the kinetics of Eq. 1.

In the case of HS, due to their binding heterogeneity, each binding group reaches equilibrium after a different period, thus, the 1/[Fe-SRFA] vs. time plot lacks linear sections and it is not valid to study the reaction order or the existence of ternary complexes.

5.2.3. Material and methods

5.2.3.1. Apparatus

The CSV response of Fe-HS complexes was monitored in a three-electrode electrochemical cell consisting of a hanging mercury drop working electrode (HMDE), a glassy carbon rod counter electrode, and a double junction Ag/AgCl reference electrode. Potential control and the resulting current readings were obtained using a μAutolab III potentiostat controlled with NOVA software and connected to a VA663 electrode stand (all Metrohm AG). The NOVA software was programmed to repeat the same CSV procedure for many hours reducing the frequency of analysis as the rate of iron ligand exchange reaction decreased.

UV-digestion was carried out using a home-built system consisting of a 150 W high-pressure mercury vapour lamp in 30 mL quartz tubes with a 2-hour irradiation time.

5.2.3.2. Reagents and materials

Ultrapure Milli-Q water (Millipore, UK) was used for solution preparation and container rinsing. Iron standards were prepared by dilution in acidified ultrapure water (pH ~1.8) of a 1 ppm atomic absorption spectrometry standard solution (BDH, UK). The iron ligand DHN (2,3dihydronaphthalene) (Fluka) was prepared in acidified ultrapure water (pH 1.8) at a concentration of 10 mM. The buffer/catalyst solution was a mixture containing 0.1 M POPSO (piperazine-1,4-bis (2-hydroxypropanesulfonic acid) dehydrate from Sigma Aldrich) and 0.4 M potassium bromate (Sigma Aldrich). The pH of this mixture was raised to 8.2 using ammonia (Ultratrace Fluka). Iron impurities were removed by overnight equilibration with a suspension of MnO2 followed by filtration (0.2 μm cellulose nitrate, Whatman). A solution of NaCl (ultratrace, Fluka) was prepared at a concentration of 0.72 M to reproduce the ionic strength of oceanic seawater.

Suwannee River fulvic acid (SRFA) and humic acid (SRHA) were purchased from the International Humic Substances Society (IHSS) and used as model HS. Stock solutions of 0.2 g L-1 were prepared in Milli-Q water and stored at low temperatures until use. The siderophore desferrrioxamine B (DFOB, (N'-[5-(Acetyl-hydroxy-amino)pentyl]-N-[5-[3-(5-aminopentylhydroxy-carbamoyl) propanoylamino] pentyl]-N-hydroxy-butane diamide) was purchased as mesylate salt (Sigma Aldrich) and dissolved in ultrapure water. An aqueous stock solution of DFOB was diluted to a concentration of 5 μM and kept in the fridge between uses. The tetrapyrrole protoporphyrin IX (PP IX, (3,7,12,17-tetramethyl-8,13-divinyl-2,18- porphinedipropionic acid) was chosen as a typical cell lysis ligand. Due to its poor solubility in water and its tendency to dimerize and polymerize as a function of pH (Scolaro et al., 2002), aqueous PP IX solutions require specific pre-planning (see Section 3.3 and the Supplementary Information file for details). Stock solutions were prepared by dissolving a few mg in 1 M HCl (ultratrace, Merck), subjected to ultrasound to facilitate solubilisation and brought to 1 L volume. This solution was stored at low temperatures in the dark until use.

A 0.1 M EDTA (Ethylenediaminetetraacetic acid, Merck) solution was prepared in ultrapure water. The pH of the solution was raised to 8.2 with ultratrace grade ammonia.

Reagent solutions and seawater mixtures were prepared in low density polyethylene (LDPE) containers (Nalgene) that had been previously sequentially cleaned with detergent (BIO-SEL), 10% HCl and 1 M HCl with ultrapure water rinses in between and before use.

The ligand-free seawater used here was a mixture of leftover filtered (0.2 μm) samples from Polarstern cruise ANT-XXV/3 carried out in waters of the Antarctic Ocean . [Laglera et al., 2017]. The seawater mixture was homogenized in a clean LDPE bottle and UV digested before use to remove any interfering organic matter.

5.2.3.3. Analytical limitations of the use of PP IX and EDTA

We found severe analytical drawbacks using PP IX and EDTA with our analytical scheme. With both ligands, we faced the possibility that the sensitivity of the CSV method changed by a small fraction before and after the addition of the competing ligand, preventing an accurate determination of the initial drop in Fe-SRFA concentrations. Although the kinetics obtained were representative of the ongoing reaction, we could under or overestimate the initial concentration drop and therefore concentration of iron exchanged at equilibrium. We consider these experiments mainly for qualitative purposes.

Both reagents, as it is the case with the SRHS standards, show iron contamination at non-negligible levels for our analytical scheme and interfered with some experiments. Being strong ligands, "cleaning" the ligands by equilibration with MnO2 or resins did not work and, due to their chemical characteristics, reagent recrystallization was not an option. Therefore, since our experiments required to be close to iron saturation without exceeding it, the iron present as an impurity was considered in the iron concentration.

The sensitivity of the Fe-HS method in the presence of bromate is extremely dependent and inversely related to the pH due to the alteration of the kinetics of the catalytic reoxidation of the electrogenerated Fe(II) (Figure **11)**[Laglera et al., 2013]. We found with both reagents small but significant pH changes of a few tenths of pH units that changed our analytical sensitivity before and after reagent addition. This was easily detectable because the anticorrelation between peak potential and pH variations of the method [Laglera et al., 2007].

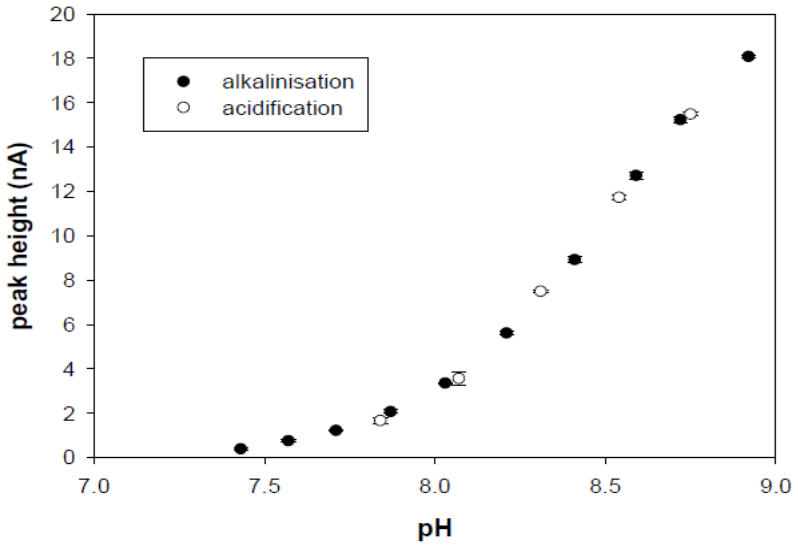

Figure 11. Effect of pH shifting on the analytical response of 1 mg L^{-1} SRFA dissolved in UV-digested seawater in the presence of 19 nM Fe. The solution was 20 mM in BrO_3 and 5 mM in POPSO buffer. The first pH value was increased by NH_4OH additions and, immediate afterwards, decreased by HCl additions.

With respect to PP IX, its solubility is very low in water and its dissolution requires very acidic conditions (pH well below 2) to avoid dimerization at the micromolar concentrations needed to prepare a standard solution [Scolaro et al., 2002]. Only the addition of small PP IX solution volumes at four times the usual buffer concentration (20 mM of POPSO buffer) gave almost stable pH meter readings. Furthermore, we had no method to ensure that nanomolar concentrations of PP IX did not undergo any non-negligible dimerization at pH 8.2.

In the case of EDTA, the drawback came from the strong buffering effect of this ligand at the concentrations needed to compete with strong ligands (millimolar range). Although the pH of the EDTA and bromate/POPSO solutions were precisely adjusted to the same NBS value, the Fe-SRFA peak potential revealed small pH drifts after mixing. We attribute this effect to the strong dependence of the pH electrode readings on the ionic strength that introduces a significant bias in concentrated solutions, so that the same pH readings did not necessarily imply the same proton activities in solution.

Therefore, with both ligands, we were faced with the possibility that the sensitivity of the method changed by a small fraction between the CSV signal before and after the addition

of the competing ligand, preventing an accurate determination of the initial drop in Fe-SRFA concentrations. Although the kinetics obtained were representative of the ongoing reaction, we could under or overestimate the initial concentration drop and the concentration of iron exchanged at equilibrium. Thus, although we performed basic calculations, we consider these experiments mainly for qualitative purposes.

5.2.3.4 . Electrochemical parameters

Since the voltammetric behaviour of Fe-HS and Fe-DHN complexes on the HMDE is similar, both methods share the same electrochemical parameters described in previous publications [Laglera et al., 2007, 2013]. Briefly, prior to analysis, oxygen was removed by purging with water saturated N_2 for 300 s. The iron complexes were deposited on the HMDE by setting the cell potential at -0.1 V for 90 s. After a quiescence period of 7 s, the potential was shifted to -0.7 V using the sampled direct current mode with a scan rate of 50 mV s^{-1}.

5.2 3.5. Total dissolved Fe determinations

Iron concentrations in UV seawater or NaCl solution before or after addition of ligands were determined by AdCSV after overnight acidification at pH 2.0 and neutralization with ammonia in the presence of 1,2 dihydroxynaphtalene (DHN) and bromate according to [Laglera et al., 2013].

Iron contamination in the bromate/POPSO and DHN solutions was measured by repeating the analysis of ultrapure water spiked with 30 μM DHN, 20 mM KBrO3 and 5 mM POPSO (combined solution) before and after tripling the concentration of either DHN or KBrO3 and POPSO and subsequent internal calibration with iron. A typical contamination was below the LOD of 0.005 nM after addition of DHN at a concentration of 30 μM and of 0.07-0.09 nM after the addition of 500 μL of the combined bromate/POPSO solution.

5.2. 3.6 Humic substances binding capacities.

The determination of the iron binding capacity of SRFA and SRHA solutions (BC_{SRFA} and BC_{SRHA}) was carried out according to an established procedure [Laglera & van den Berg, 2009]. Briefly, 1 mg L^{-1} solutions of SRFA or SRHA were titrated in a ligand-free matrix (ultrapure water, 0.72 M NaCl or UV digested seawater) with successive iron additions of a few nanomols L^{-1}. After each iron addition, the solution was purged with N_2 for 5 minutes to allow the formation of Fe-HS complexes. Three to five CSV analyses were then performed to check the stability of the signal before the next iron addition. The Fe-HS peak increases linearly as a function of the concentration of the added iron until the HS binding groups become saturated. Beyond this stage, the CSV peaks fall below the linear trend and decrease with time due to the slow precipitation of excess iron. The iron concentration corresponding to the intersection of the two related sections was used to determine the iron BC_{SRHS}.

5.2.3.7. Iron ligand exchange of Fe-HS complexes

The CSV response of Fe-SRFA complexes was monitored in 20 mL samples (UV seawater or 0.72 M NaCl) spiked with 1 mL of the POPSO/bromate, SRFA or SRHA solution for a cell concentration of 1 mg L-1. Iron concentration was adjusted to ensure that the sum of dissolved iron in the matrix, reagent impurities and the iron spike reached 90-95% of the BCSRHS. Prior to analysis, the quartz cell was conditioned by filling it three times with the same solution described above and then discarded. Several CSV measurements were taken before introducing the competing ligand to confirm the stability of the Fe-HS signal. After the spike, the first scan was obtained with approximately 100 s delay due to the 90 s deposition period. The Fe-HS concentration was monitored until a steady state concentration was observed for at least 20 minutes. It is important to note that this setup was neither suitable for resolving kinetics that completed within seconds nor monitor slow reactions (if any) that would require days to complete. The initial Fe-

HS concentration, used for calibration, was determined as the CSV signal before the addition of the competing ligand, which equated to the total iron concentration in the cell. For fitting purposes and calculation of kinetic rate constants and conditional stability constants, the decrease in Fe-SRHS complex concentration was quantitatively converted into the concentration of the iron complex formed with the competing ligand (Fe-Lad) and the concentration of dissociated iron-free SRHS (Eq. 1).

5.2.3.8. Reversibility. Sequestering of iron bound to FOB and PPIX by HS

We studied the reverse case, i.e., the ligand exchange of Fe-FOB or Fe-PPIX complexes in solution after subsequent addition of HS′. We used only SRFA because SRHA, as purchased, is contaminated with iron and, possibly, after dissolution, their stronger binding groups are saturated with iron. In two separate experiments, we spiked UV seawater with 1 mL of the POPSO/bromate solution and 16 nM of DFOB or PPIX and iron at a concentration sufficient to reach a cell concentration of 16 nM iron. As usual, we conditioned the cell with the same solution twice. For analysis, we previously confirmed the absence of interfering electrolabile iron complexes and after 5 minutes of conditioning we spiked the solution with 2 mg SRFA l-1 for a binding capacity of 29.0 nM Fe and monitored the formation of electroactive Fe-SRFA complexes for several hours. At the end of the data collection, we calibrated the Fe-SRFA with three (DFOB) and four (PPIX) internal additions of 2 nM Fe to determine the sensitivity.

5.2.3.9. Studies of the formation of HS and DFOB adducts.

We investigated whether HS and DFO interact, leading to the formation of HS-DFO and/or HSFe-FO adducts using our voltammetric method. Despite the limitations of non-spectroscopic methods, electrochemical methods offer the advantage of conducting experiments under conditions close to natural concentrations. The iron concentration was kept well in excess of the combined binding capacities of FO and HS to avoid any net

iron ligand exchange. However, organic-organic interactions may introduce deviations from the expected stable CSV signal caused by iron-saturated HS. We conducted a preliminary experiment with immediate monitoring of reagent in-cell additions, which unfortunately was affected by iron precipitation. The interpretation of the results from this experiment was not straightforward, and a detailed account can be found in the Supplementary Information file. This information is provided to prevent other researchers from attempting to use a similar analytical scheme without considering the potential challenges related to iron precipitation.

We prepared two sets of 30 mL LDPE bottles containing 10 mL aliquots of UV-digested seawater. We then sequentially spiked HS (first set with 2 mg L-1 SRFA and the second set with 1 mg L-1 SRHA, for BC_{SRHS} of 29.0 and 32.1 nM Fe, respectively), DFOB (range 0 to 100 for SRFA and 0 to 300 for SRHA with sufficient time to interact) and, finally, 600 nM Fe to saturate all ligands. We allowed the mixture to interact overnight to allow precipitation of excess iron and the next day all aliquots were spiked with bromate/POPSO reagent and analysed by CSV to check whether siderophore-HS interactions could have prevented the equal formation of electrolabile Fe-HS complexes.

5.2.3.10. Modelling of kinetics of iron ligand exchange mechanisms

The Dynafit numerical resolution program [Kuzmič, 1996] was used or the global fitting of the experimental data. This program utilizes the Levenberg-Marquardt algorithm to perform least squares fittings of the kinetic tracer time course. Three iron ligand exchange mechanisms were tested to explore the reaction mechanisms before the accumulation of experimental evidence led us to propose a refined mechanism:

i) homogeneous reversible iron ligand exchange,

ii) reversible heterogeneous iron ligand exchange with two types of departing complexes, $FeSRHA_1$ and $Fe\text{-}SRHA_2$, and

iii) irreversible heterogeneous iron ligand exchange, where we assume the existence of a ternary intermediate in equilibrium with the departing species, but with slow dissociation kinetics (detailed in Section 5.2.4.10).

The mechanism equations, definition of the kinetic rate constants and the number of species fitted for each of the three mechanisms can be found in the Supplementary Information file.

Access to Dynafit scripts and experimental data is detailed in the Data availability statement.

5.2.4. Results and discussion.

5.2.4.1. Binding capacities of different IHSS reference materials in various matrices

Our experimental design required the saturation of the departing ligand and absence of excess inorganic iron in the cell. Therefore, accurate determination of the iron contamination of the reagents and the BC of the IHSS reference FA or HA was essential. Table 3 shows the BC_{SRHS} of different IHSS standards (purchased and analyzed through the years) dissolved in UV digested seawater, ultrapure water, and NaCl 0.72 M.

Table 3. *Binding capacities of different batches of IHSS fulvic acid and humic reference materials determined after titration with iron as described in Laglera et al. [2009]. Uncertainty as the standard deviation of two determinations, three in the case of SRFA 1R101F.*

Matrix	Humic reference	Binding capacity (nmol Fe x mg $SRHS^{-1}$)
Ultrapure water	SRFA 1R101F	31.1 ± 0.2
0.72 M NaCl	SRFA 1R101F	14.9
UV dig. sw	SRFA 1R101F	16.7 ± 2.0
UV dig. sw	SRFA 1S101F	14.6 ± 0.7
UV dig. sw	SRFA 1S101H	14.4 ± 0.5

Ultrapure water	SRHA 1R101F	40.3 ± 0.3
UV dig. sw	SRHA 1R101F	31.9 ± 2.2
NaCl 0.72 M	SRHA 1R101F	28.8
UV dig. sw	SRHA.1S101H	31.8 ± 1.4
0.72 M NaCl	SRHA.1S101H	32.4

Despite the two decades between the first Suwannee River extraction (1R101) and the one currently available from IHSS (1S101), both the iron BC_{SRFA} and BC_{SRHA} have remained constant. This is convenient for the type of study presented here, as it allows comparison of values found in the literature regardless of the batch used in the experiments. The iron BCHS in ultrapure water were much higher than in seawater, indicating a competition of cations for iron binding moieties. Removal of divalent cations (0.72 M NaCl) did not lead to an increase in the BC found in seawater. This indicates that the reduction in iron binding due to the increase of the ionic strength is not due to specific competition with divalent cations.

5.2.4.2. Iron ligand exchange of iron-saturated Fe-SRFA complexes after addition of DFOB

The addition of iron-free DFOB to seawater containing iron-saturated SRFA gave the predicted decrease over time of the CSV signal of the Fe-SRFA complexes (Fig. 12). In all three experiments, the initial concentration of SRFA was 1 mg SRFA L^{-1} (binding capacity of 14.5 ± 0.7 nM Fe) to which Fe was added to have an in-cell concentration of 14.1 nM Fe, approximately 97 % saturation of the SRFA binding sites. After addition of 15, 30 and 50 nM DFOB (equivalent to 1 to 3.5 times the BCSRFA), we observed an immediate sharp decrease in the Fe-SRFA signal followed by slower kinetics until a stable concentration of Fe-SRFA remained in solution (Fig. 12). This type of result indicates a reversible reaction in which the concentrations of both complexes reach a dynamic equilibrium (Eq. 1). The ratio between the iron complexes is controlled by the remaining concentration of iron-free ligands and the ratio of their conditional stability constants (Eq. 4).

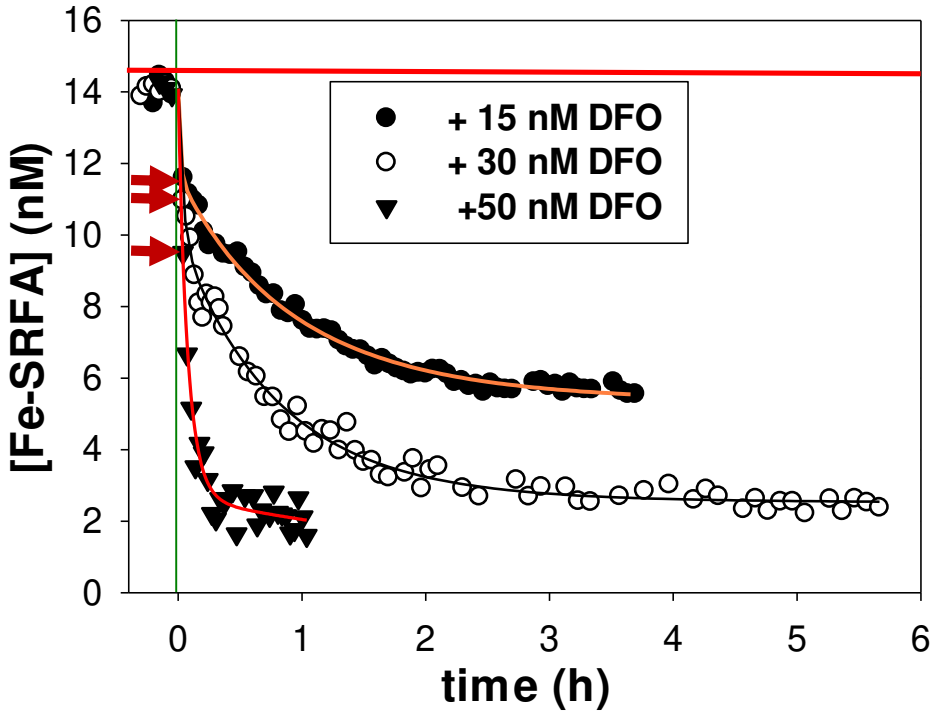

Figure 12. Time course of the concentration of Fe-SRFA complexes in UV-digested seawater in response to different additions of iron-free DFOB. Prior to DFOB addition, SRFA solutions (1 mg L-1, BCSRFA of 14.5 ± 0.7 nM Fe) were spiked with iron to nearly saturate the binding sites. Solid red lines mark the BCSRFA. The red arrows on the left indicate the first measured concentration, approximately 2 minutes after DFOB addition. The lines are the result of fitting the concentration kinetics to the reaction model shown in Section 5.2.4.10**.**

Firstly, we will focus on the pre-equilibrium kinetics. In the first ~100 s required to complete the first measurement after the addition of DFOB, the initial Fe-SRFA signal plummeted as a function of the added DFOB concentration by 18, 22 and 33%, respectively (red arrows in Fig. 12). This immediate exchange of about one third of the iron bound to SRFA could be interpreted as weakly bound iron (binding groups characterized by low K′Fe′-SRFA and high dissociation kinetics), according to a D mechanism. Thereafter, a period of 0.5 to 3 h of slow exchange kinetics started, whereby the higher the DFOB concentration added, the sooner equilibrium was reached. However, this behavior contradicts what is expected according to a D mechanism, where the period before equilibrium depends mainly on the dissociation kinetics of the initial complex and hardly on the nature or concentration of the incoming ligand (Fig. 13).

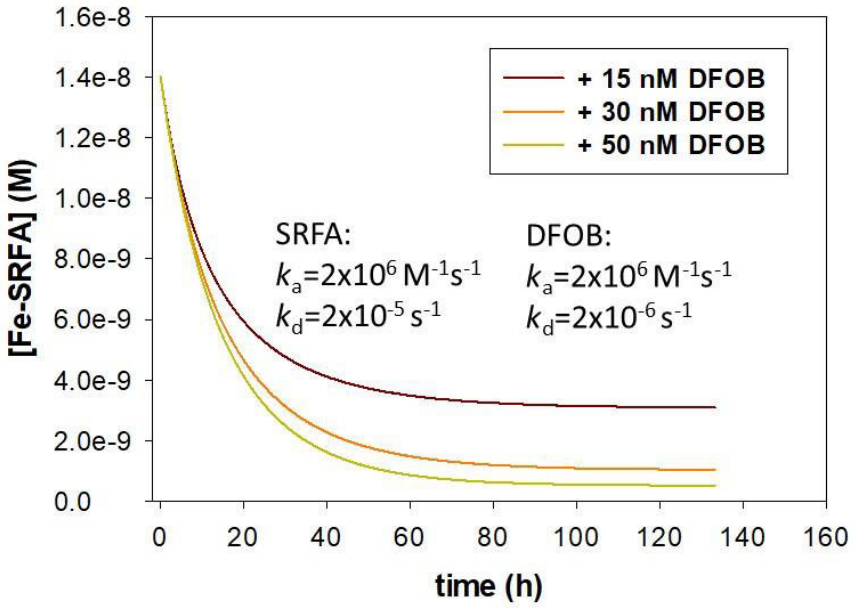

Figure 13. Modelling of the time course of the iron ligand exchange of 14 nM Fe-SRFA complexes in response to different additions of iron-free DFOB. The formation and dissociation constants were approximately those found in (Rose and Waite, 2003; Witter et al., 2000).

Secondly, we will focus on the species partitioning at equilibrium. We found that DFOB additions of 1 to 3.5 times the BCSRFA left 39, 18 and 15% of the initial Fe-SRFA signal at equilibrium, respectively (Fig. 12). Use of Eq. 4 gave K′Fe′-DFOB/K′Fe′-SRFA ratios of 2.0, 3.1 and 2.0 at increasing DFOB concentrations, respectively (average 2.4). Although this result is consistent with a weaker affinity for iron of the SRFA binding groups, the log K′Fe′-FOB was consistently slightly more than twice that of K′Fe′-SRFA.

In the case of the interaction of iron and HS, the common paradigm in aquatic chemistry is that all HS binding sites are weak and can hardly compete against natural ligands of biological origin and higher affinity for iron [Whitby et al., 2020b]. The origin of such a belief is the initial estimation by CLE-AdCSV of logK′Fe′-SRFA at 10.6, using dihydroxynaphtalene as Lad, which was at least one logarithmic unit lower than logK′Fe′-FOB determined at values between 11.6 using 1-nitroso-2-naphtol as Lad and >13 using salycilaldoxime and 2-(2-thiazolylazo)-p-cresol as L_{ad} [Croot & Johansson, 2000; Laglera & van den Berg, 2009; Witter et al., 2000; Rue & Bruland, 1995]. Our low K′Fe′-DFOB/K′Fe′-SRFA ratio is not unique in the sense that it concurs with two previous

works in which the addition of DFOB in large excess of iron to HS-rich samples could only extract a fraction of the HS-bound iron [Kuhn et al., 2014; Laglera et al., 2019] .

5.2.4.3. Iron ligand exchange of iron-partially saturated Fe-SRFA complexes after addition of DFOB

The experiment detailed above was repeated by reducing the concentration of added iron by approximately 3 nM (for 11 nM Fe in cell) (Fig. 14). This roughly corresponds to the concentration of binding groups that interchanged iron with DFOB in less than 100 s in the experiment shown in Fig. 12. The aim was to better characterize the SRFA iron binding groups that experienced slow interchange kinetics in the previous experiment. According to a D mechanism, iron at a concentration below the BCSRFA would be preferentially bound to slower dissociating and higher stability ligands. Thus, by reducing the concentration of iron in solution, the fast-dissociating SRFA binding groups would be left free of iron and, therefore, the iron ligand exchange kinetics would show only the exponential decreasing section without the initial fast drop of ~20% (red arrows in Fig. 12).

However, this was not the observed behavior (Fig. 14). The addition of 10 and 15 nM DFOB also resulted in a rapid drop of the CSV signal in the first 100 s, in this case 3.2 and 5 nM FeSRFA complexes, respectively. This is approximately the same initial Fe-SRFA concentration drop observed at higher iron concentrations (red symbols in Fig. 14). Therefore, the rapid initial iron ligand exchange observed in Fig. 12 does not appear to be caused by a very low stability of one third of the SRFA binding groups.

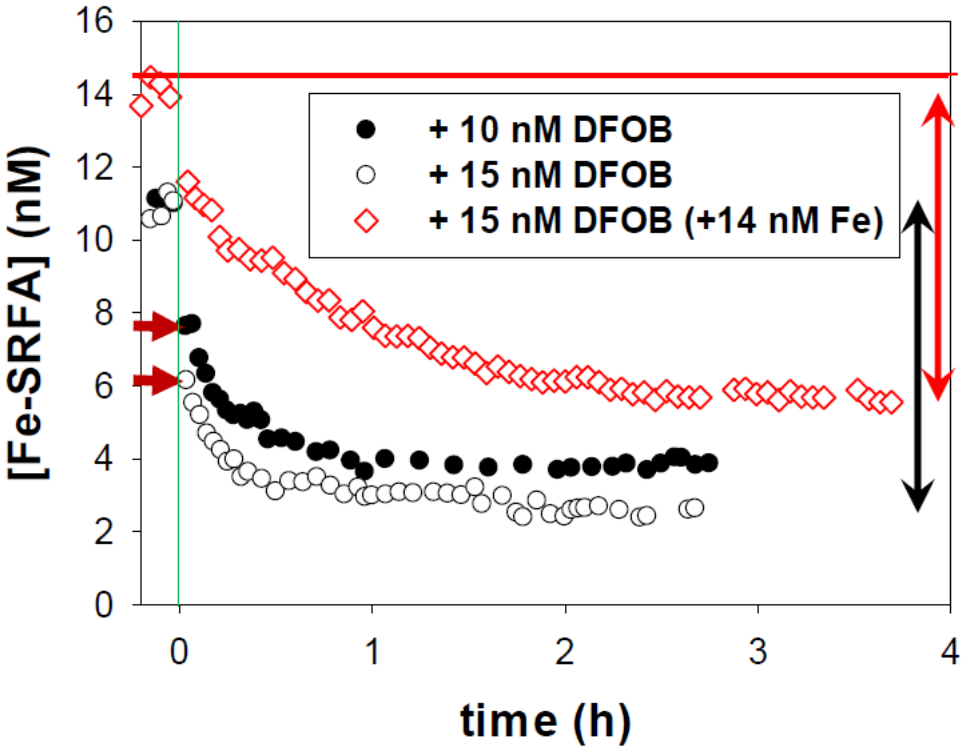

Figure 14. Time course of the concentration of Fe-SRFA complexes (1 mg SRFA L^{-1}) after addition of 10, and 15 nM DFOB. The red line represents the BCSRFA. The red thick arrows indicate the first concentration obtained approximately 100 s after addition of DFOB. The double headed arrows indicate the magnitude of the decrease in Fe-SRFA at equimolar DFOB additions. The red diamonds correspond to the addition of 15 nM DFOB in Fig 10 shown for comparison.

In this case, the iron ligand exchange reached equilibrium in ~1 h, which is approximately three times faster than observed after near full saturation of the SRFA. The concentration of Fe-SRFA complexes that remained at equilibrium were of 3.9 and 2.5 nM, respectively, lower with respect to the experiments under near saturation (open symbols in Fig. 14) but in concurrence the lower iron availability. The decrease in Fe-SRFA concentration was similar to the decrease observed under saturation of the binding groups (black and red double headed arrows in Fig. 14, respectively). This same ability to extract iron despite the presence of more iron-free SRFA binding groups translates into K′Fe′-FOB / K′Fe′-SRFA ratios of 8.1 and 7.4, about three times higher than the values found under near SRFA saturation. Proper interpretation of this result against the common understanding of complexation is discussed in section 5.2.4.9.

5.2.4.4. Labilization effect of seawater major bivalent cations

Seawater cations can interfere with ligand exchange reactions by increasing the lability of the complexes and thus their dissociation [Boiteau & Repeta, 2022; Laglera & Filella, 2015]. The major bivalent cations, Mg2+ and specially Ca2+, are expected to have a great impact [Fujii et al., 2008; Morel F.M. and Hering J.G., 1993; Schijf & Burns, 2016] . Mechanistically, this interaction can be caused by occupation of the iron binding sites (of one or more binding groups in multidentate complexes) or by forcing changes in the spatial arrangement of the complex [Wilkins, 1991].

We repeated the iron ligand exchange kinetic experiment after the addition of 30 nM DFOB to 1 mg SRFA L-1 nearly saturated with iron using now a 0.72 M NaCl matrix to maintain the ionic strength of seawater while eliminating any effect of bivalent cations (Fig. 15). The kinetic section showed two differential features compared to the seawater experiments. First, the immediate drop of the Fe-SRFA signal was absent here (Fig. 15). Thus, matrix effects and not an extremely low affinity of a fraction of the SRFA binding groups for iron controlled the initial fast dissociation of Fe-SRFA complexes in UV seawater shown in Figs. 12 and 13. Second, the time needed to reach equilibrium was much longer, approximately 12 h, implying that Ca^{2+} and Mg^{2+} in solution act as accelerators of iron ligand exchange of Fe-HS complexes in seawater. Our results are in agreement with a previous study that found that additions of Ca^{2+} or Mg^{2+} ions at concentrations similar to those found in seawater substantially retarded the exchange of iron ligands from FA complexes to 5-sulfosalicylic acid in NaCl solutions [Fujii et al., 2008]. Apart of bond perturbation by divalent cations, other phenomena characteristic of HS, such as SRFA conformational changes and alteration of molecule bridging, might have played a role.

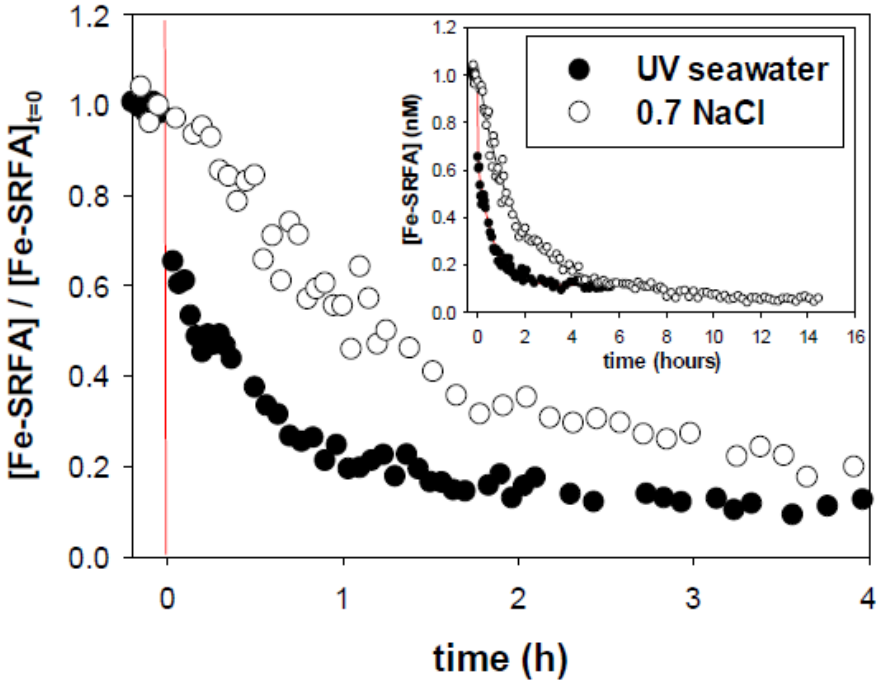

Figure 15. Effect of divalent cations on the kinetics of iron ligand exchange: time course for the first 4 h (to highlight the lack of fast initial signal drop) of the concentration of Fe-SRFA complexes after addition of 30 nM DFOB to 1 mg SRFA L-1 saturated at 90% in UV seawater and in 0.72 M NaCl. Insert plot: the complete experiment.

At equilibrium, DFOB had sequestered more iron, with only 0.7 nM Fe-SRFA remaining in solution (about 5% of the binding capacity) (Fig. 15). Thus, the removal of bivalent cations increased the competing ability of DFOB. As a result, the K′Fe′-FOB /K′Fe′-SRFA ratio was of 13.9, an increase by a factor of ~5 with respect to seawater that could be caused by possible conformational changes and/or by a higher affinity of Ca^{2+} and Mg^{2+} for the iron binding sites of the SRFA than for those of DFOB. The lack of related literature prevents us from confirming or rejecting each hypothesis.

5.2.4.5. Iron ligand exchange of iron saturated Fe-SRHA complexes after addition of DFOB

HA are characterized by higher hydrophobicity, higher average molecular weight, and BC_{SRHA} nearly twice as large than FA extracted from the same source (Table 2). Unfortunately, there is no information in the literature on the kinetics of iron ligand exchange of Fe-SRHA complexes. Previous estimates by CLE-AdCSV using dihydroxynaphtalene, salycilaldoxime and EDTA as L_{ad} have shown that the average stability of Fe-SRHA complexes is slightly higher than that of SRFA with log K′Fe′-SRHA in the range 11.1-11.6, about half a logarithmic unit higher than log K′Fe′-SRFA [Gerringa et al., 2021]. However, in a recent intercalibration exercise, SRFA was found to be stronger or weaker than SRHA depending on Lad [Gerringa et al., 2021]. This discrepancy is possibly due to methodological artefacts caused by the hydrophobicity of HS, which is more pronounced in the HA fraction.

We observed the same plummeting of the Fe-SRHA signals that increased from 10 to 16 nM Fe when the concentration of DFOB increased from equimolar to 7.5 times the iron BC_{SRHA} (Fig. 16). At equilibrium, the Fe-SRHA concentrations were in the range of 52 to 16% of the initial concentration, substantially higher than those found for Fe-SRFA. The K′Fe′-DFOB / K′Fe′SRHA ratios obtained with increasing DFOB additions equal to or higher than the BCSRHA were in a narrow range, 0.73, 0.38, 0.38, 0.74 and 0.69 in order of increasing DFOB concentrations (Fig. 16). Therefore, K′Fe′-SRHA was consistently higher than K′Fe′-FOB.

We added in one experiment only 10 nM DFOB to nearly iron saturated SRHA (Fig. 16). Since the addition of 35 nM DFOB decreased the Fe-SRFA signal in the first 100 s of the experiment by 6.2 nM Fe, according to a D mechanism, we expected a fast decrease of similar magnitude due to the favored dissociation of weak binding groups. However, the addition of 10 nM DFOB reduced the Fe-SRFA signal by only 4.5 nM Fe-SRFA in the initial 100 s and barely more in the following 55 minutes (4.7 nM Fe at the end of the experiment). Thus, approximately 5 nM of DFOB remained iron free at the equilibrium despite the presence of approximately 26 nM of Fe-SRHA complexes. The limited ligand exchange resulted in a K'Fe-FOB / K'Fe-SRFA ratio 0.19, indicating strong complexation by SRHA despite our expectation that only loosely bound iron would be involved.

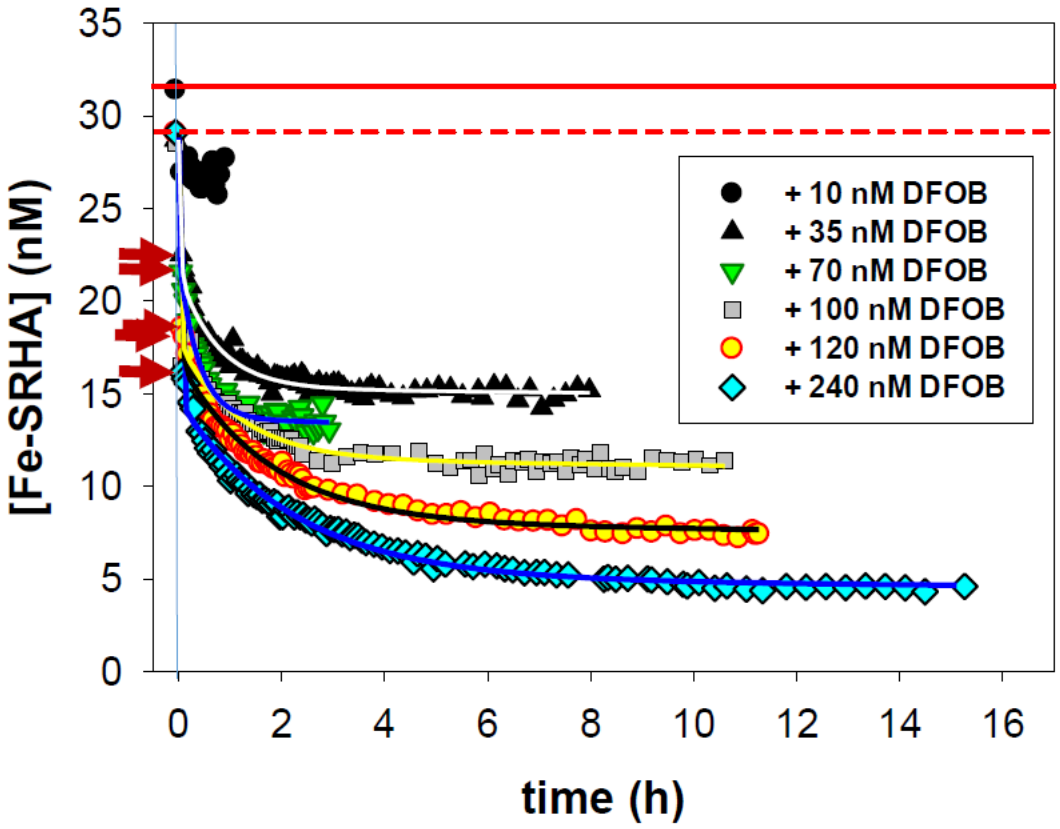

Figure 16. Time course of the concentration of Fe-SRHA complexes when SRHA at a concentration of 1 mg L-1 dissolved in UV-digested seawater and saturated to 90% of its iron binding capacity is spiked with different concentrations of DFOB. The solid red line marks the BC_{SRHA}. The dashed red line marks the initial concentration of Fe-SRHA complexes (except for the addition of 10 nM DFOB, see text for details). The lines are the result of fitting the concentration kinetics to the reaction model shown in Section 5.2 4.10

The experiments with higher DFOB additions showed a period of slow kinetics after the initial rapid decrease of the Fe-SRHA signal that lasted approximately 2 to 11 h until equilibrium was reached (Fig. 16). Contrary to our findings for SRFA, this period before reaching equilibrium was longer with higher additions of DFOB. The behavior could be caused by the higher heterogeneity and overall affinity for iron of SRHA. As the DFOB concentration increases, it mobilizes iron from the HS binding groups with higher affinity for iron and slower dissociation kinetics resulting in a longer time to reach equilibrium. However, this would not coincide with our observation after addition of 10 nM DFOB.

5.2.4.6. Iron ligand exchange of iron saturated Fe-SRHS complexes after addition of other ligands

Since a D mechanism produces similar ligand exchange kinetics regardless of the nature of the competing ligand [Helm & Merbach, 2005; Wilkins, 1991] , we repeated our experiments using two other commonly used ligands in CLE experiments. Specifically, the pigment precursor PP IX, which has shown conditional stability constant and formation and dissociation kinetics similar to those of DFOB in previous CLE-AdCSV [Witter et al., 2000], and EDTA. With both ligands, although the kinetics obtained were representative of the ongoing reaction, we faced the possibility that the sensitivity of the method changed by a small fraction immediately after addition of the competing ligand. This drawback and its consequences are detailed in the Section 5.2.3.3.

Fig. 17 A shows the kinetics of iron ligand exchange after addition of 1.3 mM EDTA to UV seawater spiked with 2 mg SRFA L^{-1} and 1 mg SRHA L^{-1}, respectively. Fig. 17B shows the same experiment with additions of 15 and 30 nM PP IX to 1 mg SRFA L^{-1}. With both ligands, we observed the same rapid initial decrease of the Fe-HS signal, as seen with DFOB in seawater (red arrows in Fig. 17). Thus, the immediate loss of a substantial fraction of Fe-SRFA complexes upon interaction with divalent cations in seawater occurs regardless of the nature of the competing ligand. However, there was an important difference with the results shown in Fig. 10: the period required to reach equilibrium with EDTA was of 18 to 20 h, 2 to 6 times the time required for DFOB while for the addition of 15 nM and 30 nM PP IX it was less than 1 h and about 3 hours, respectively, shorter than for DFOB (see Fig. 12). This is indicative that the iron ligand exchange of Fe-SRHS complexes follows an A route.

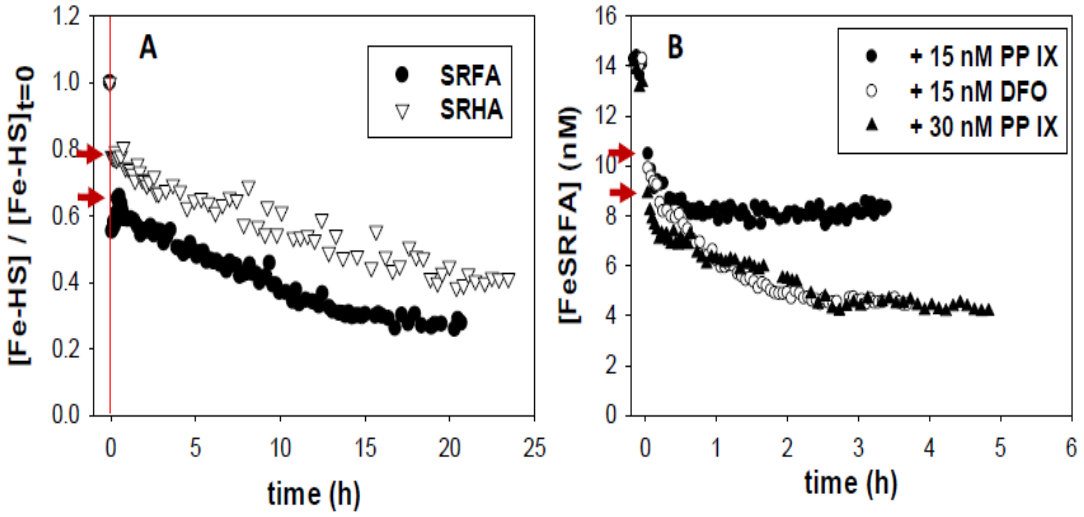

Figure 17. (A) Time course of the normalized concentration of Fe-SRFA and Fe-SRHA complexes in UV-digested seawater in response to the addition of 1.3 mM EDTA. The initial concentrations were 2 mg SRFA L-1 and 1 mg SRHA L-1, respectively (equivalent to iron BC of 29 nM and 32.6 nM Fe, respectively). (B) Same experiment with the addition of 15 and 30 nM PPIX; it was checked that at the end of the experiment the pH drop was less than 0.1 pH units. All solutions were spiked with iron in order to almost saturate (90%) their binding sites. The red arrows indicate the first concentration obtained approximately 100 s after the addition of the competing ligand.

Equilibrium iron partitioning also provides valuable information. In the case of EDTA, there are published stability constants with all major cations in seawater. These constants enable that from KFe′-EDTA, it is possible to estimate that the log K′Fe′-EDTA in a seawater matrix is 7.97 [Croot & Johansson, 2000; Laglera et al., 2011]. From the use in Eq 4 of the mass balances of iron, HS and EDTA (Eq. 2) along with log K′Fe′$_{EDTA}$ of 7.97, and log K′Fe′$_{SRFA}$ =10.6 or log K′Fe′SRHA =11.1 [Laglera & van den Berg, 2009], it can be estimated that only 1 and 3% of the Fe-SRFA and Fe-SRHA complexes, respectively, should have remained in solution at equilibrium. The data presented in Fig. 17A corroborate the prior underestimation of K′$_{Fe'SRHA}$ and K′$_{Fe'SRHA}$. Apparent equilibrium was reached when approximately 30% (2 mg SRFA L^{-1}) or 40% (1 mg SRHA L^{-1}) of the initial Fe-SRHS concentration remained in solution.

A similar result was obtained with PP IX. In a previous CLE-AdCSV experiment the log K′$_{Fe'PPIX}$ was found to be 0.8 logarithmic units higher than log K′$_{Fe'DFOB}$ [Witter et al.,

2000]. The same calculations shown above using Eq. 2 and 4, indicate that after adding 15 and 30 nM PP IX, respectively, the concentration of Fe-SRFA complexes in seawater should have decreased to 8.7 and 1.4 % of the initial concentration. However, Fig. 17B shows again that the concentration of Fe-SRFA binding groups remaining in solution was much higher, at 57 and 32%, respectively. The $K'_{Fe'PP\ IX}/K'_{Fe'SRFA}$ ratios were found to be 0.6 and 1.1 for 15 and 30 nM PP IX, respectively, indicative that in seawater, SRFA and PP IX have similar affinities for iron.

Even when accounting for the uncertainty brought by small pH changes after the introduction of the competing ligand, both experiments again confirm that the stability of Fe-SRHS complexes is substantially higher than previously reported in the literature.

5.2.4.7. Heterogeneity of the SRHS binding sites

While other CLE and spectroscopic methods have been successful in distinguishing between weak and strong SRFA binding groups [Heerah & Reader, 2022; Rose & Waite, 2003], SRFA binding heterogeneity for iron has proven elusive to CLE-AdCSV despite various attempts using different competing ligands[Gerringa et al., 2021; Laglera et al., 2011, 2020]. This was not the case for SRFA and copper which showed clear binding heterogeneity [Kogut & Voelker, 2001; Muller, 2018]

Although strongly influenced by the mobilizing effect of the main bivalent cations, the binding heterogeneity during iron ligand exchange of Fe-SRHS complexes is indicated by the presence of two distinct kinetic periods. The presence of more than one type of binding groups curves the otherwise linear characteristic plot of second order kinetics (Fig. 13) and this curvature is observed in all experiments shown in Figs. 12 to 16 with the exception of the addition of 30 nM DFOB to SRFA and the experiment in 0.7 M NaCl (Fig.18).

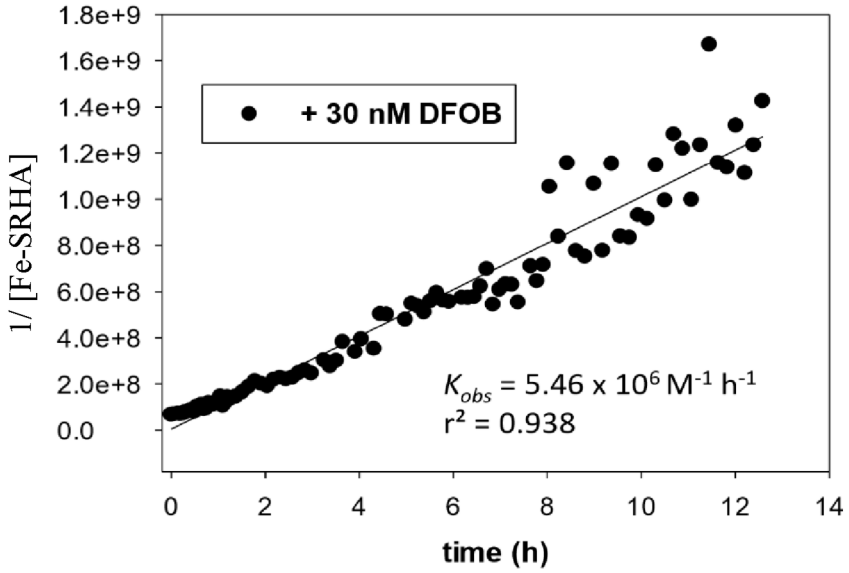

Figure 18.. Kinetic section of the characteristic second-order kinetics plot for all ligand exchange reactions departing from Fe-SRFA complexes shown in Fig.1 3 (0.7 M NaCl).

In Fig. 19, we show two examples of iron ligand exchange and the characteristic plots of second order kinetics. One example involves SRFA complexes, while the other pertains to SRHA complexes. The 1/[Fe-SRHS] vs. time plots from the rest of experiments can be found in Figs. 20 and 21. Deviations from linearity were not limited to the first two points, thus the heterogeneity extends beyond the initial concentration drop. Fig. 18 also shows the substantial improvement resulting from modelling the addition of a second type of SRHS binding groups with different exchange kinetics to the reaction mechanism. In the case of SRFA, there were two pseudolinear segments with different slopes, one for the first 15-20 minutes and a second for the remainder before equilibrium. In the case of SRHA, the curvature is more pronounced, and more sections are apparent upon visual inspection (Fig. 19). We believe that this is due to the presence of more types of binding groups and that reaction models with more types of binding groups could give better fits. We plan to explore the possibilities of this line of work in the future.

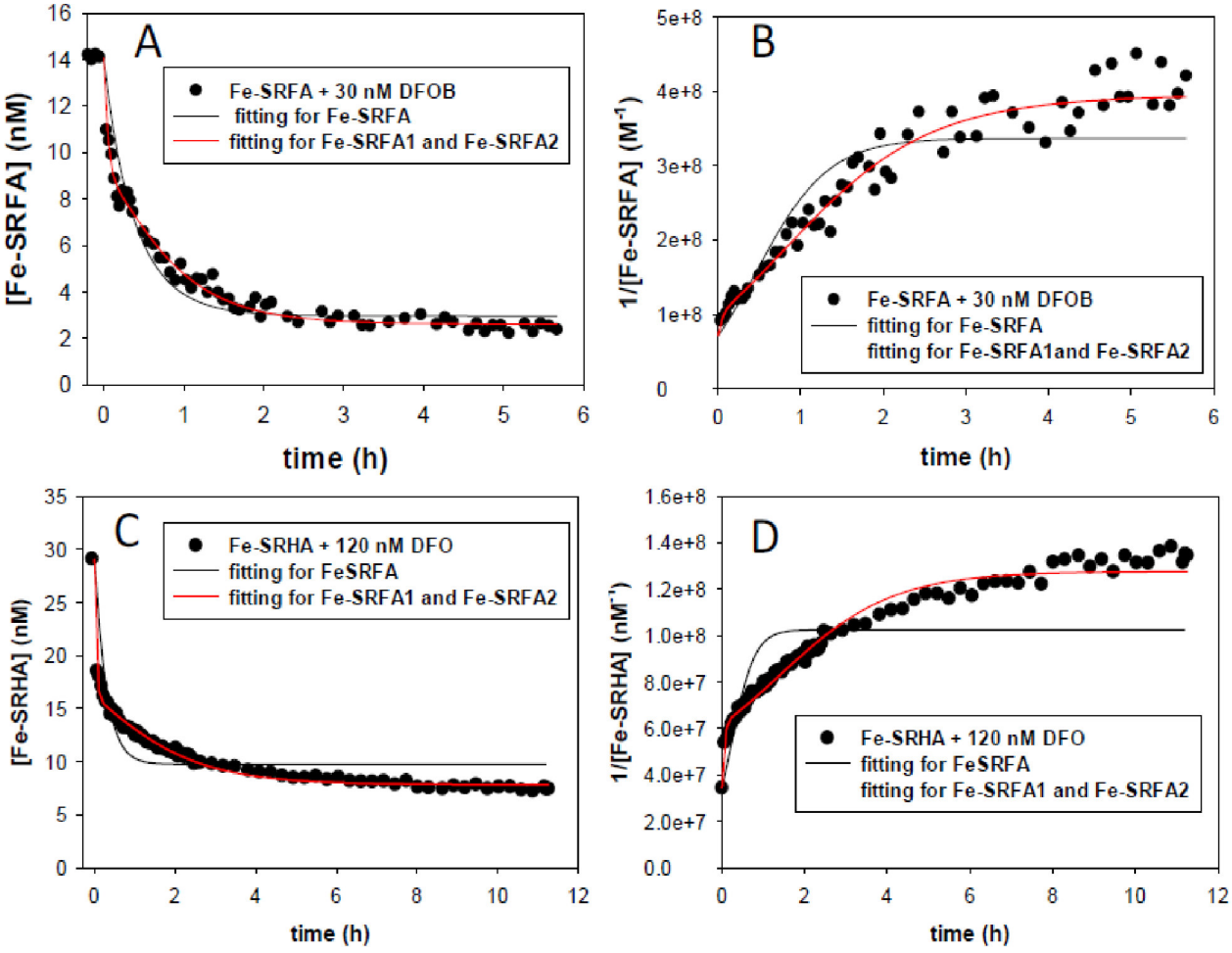

Figure 19. *A and B: A is the experimental results of the addition of 30 nM DFOB to 1 mg SRFA L^{-1} and B is the characteristic plot of second-order kinetics. The lines are non- linear fittings of Eq. 1 (black) and Eq. 1 modified to include two types of binding sites (red). C and D: the same for the addition of 120 nM DFOB to 1 mg SRHA L^{-1}. A: the kinetic rate constants obtained according to a heterogeneous mechanism were k_2=1.58±0.25 and k_{-2}=0.574±0.019 x10^4 $M^{-1}s^{-1}$ for the forward and backward ligand exchange of Fe-$SRFA_1$ complexes and k_1=4.28±0.36 and k_2=59.4±5.8 x10^4 $M^{-1}s^{-1}$ for Fe-$SRFA_2$ complexes. B: for the same model, k_3=0.161±0.003 and k4=0.278±0.007 x10^4 $M^{-1}s^{-1}$ for the forward and backward ligand exchange of Fe-$SRHA_1$ complexes and k_1=1.88±0.09 and k2=21.2±1.1 x10^4 $M^{-1}s^{-1}$ for Fe-$SRHA_2$ complexes.*

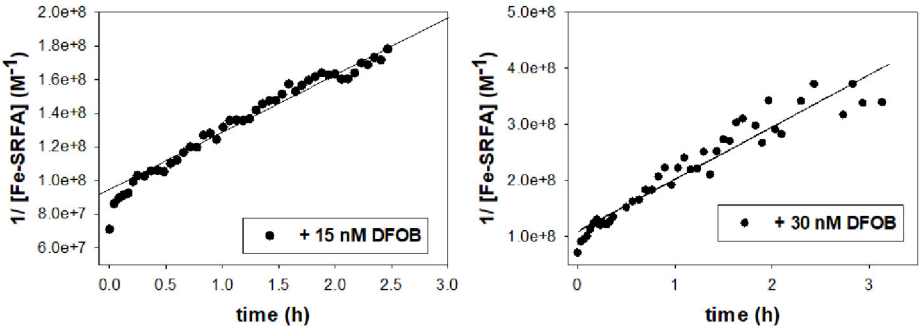

Figure 20.. Kinetic section of the characteristic second-order kinetics plot for all ligand exchange reactions of Fe-SRFA complexes shown in Fig. 10. The lines are linear regressions of the data collected after the initial 20 minutes. They are shown to illustrate the deviations of the initial data from linearity.

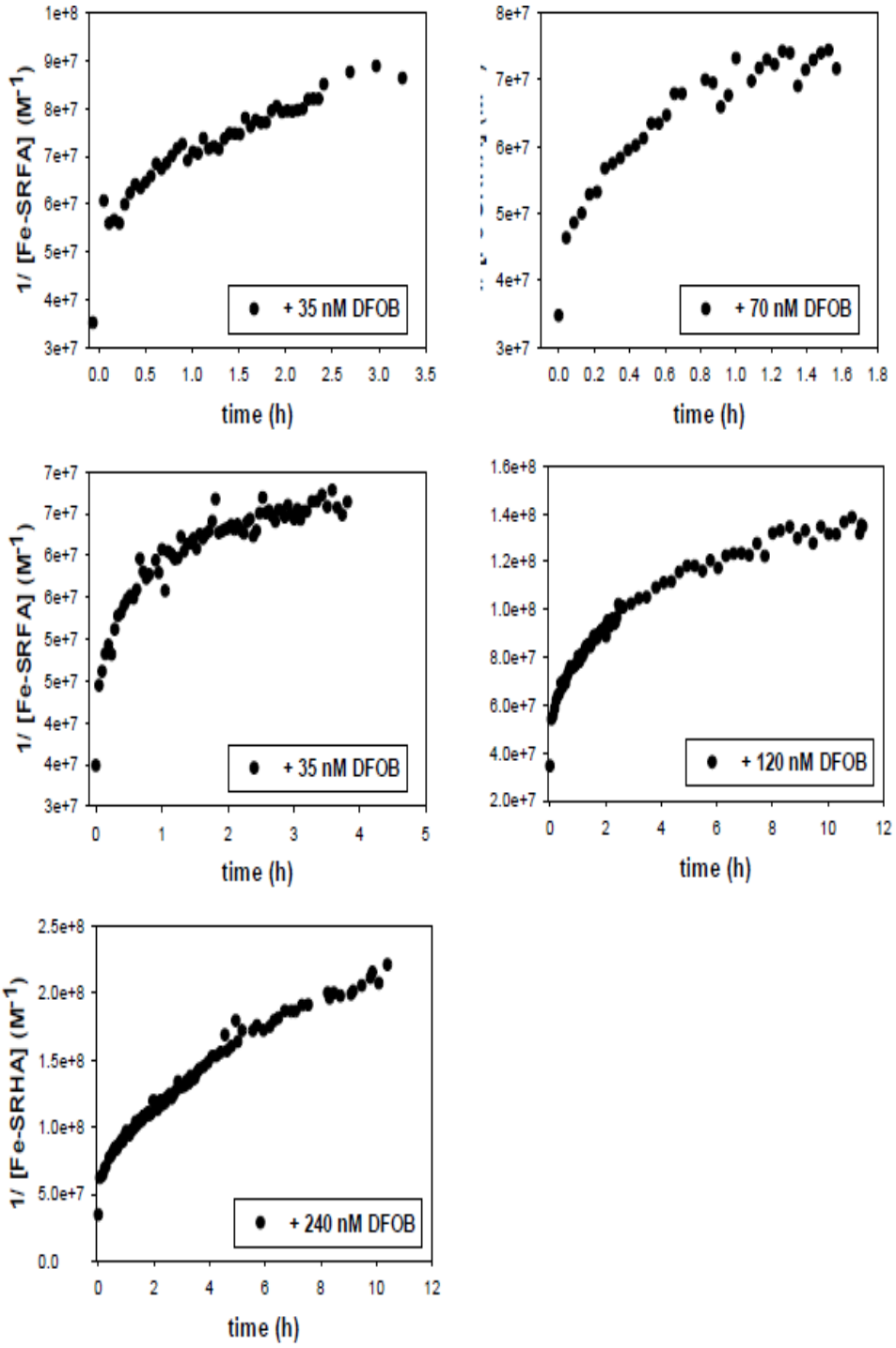

Figure 21. Kinetic section of the characteristic second-order kinetics plot for all ligand exchange reactions departing from Fe-SRHA complexes shown in Fig. 5. The steady-state period at the end has been removed.

Iron binding by DOM has often been described as a combination of "specific" (chelation) and "non-specific" (long range electrostatic attraction) interactions, with the latter being necessarily more susceptible to competition [Morel F.M. and Hering J.G., 1993]. Other authors refer to these two classes as chelated (mostly bidentate) and bridging iron [Boguta et al., 2019]. It is likely that our loosely bound iron is related to the non-chelated fractions referred to in the literature with Ca^{2+} and /or Mg^{2+} disrupting the electrostatic attraction and thereby modulating the initial interaction of SRFA-bound iron and DFOB.

5.2.4.8. Iron ligand exchange of Fe-DFOB and Fe-PP IX complexes in the presence of HS. Reversibility.

We have defined Eq. 1 as reversible, and this seems to be in agreement with the decrease of the initial complex to a steady state observed in all experiments (Figs. 12 to 17). To confirm such reversibility, we repeated our experimental scheme twice using 16.4 nM Fe-FOB and 16 nM Fe-PP IX as the initial complex and SRFA′ as the sequestering ligand. Iron was carefully added for a concentration of 16 nM (including reagent contamination) to fix the concentration of the complex to almost 100% the ligand saturation. The initial ligand saturation prevented the presence of both, significant concentrations of free dissolved iron that could bind to free SRFA and reduce iron ligand exchange or free ligand that could sequester iron impurities form the SRFA reagent. Measurements of reagent impurities gave a concentration of 0.95 nmol Fe mg $SRFA^{-1}$ (batch 1R101F, the one with the lowest contamination, Table 2) implying that approximately 6% of the SRFA binding groups (presumably those with the higher affinity for iron) were not involved in the ligand exchange reaction. In both cases, after cell equilibration, we added 2 mg SRFA L^{-1}, containing 31.45 nM of iron-free SRFA iron binding groups, for a total in-cell iron concentration of 17.9 nM and monitored the formation of Fe-SRFA complexes (Fig. 22).

For a fully reversible system, with our average $K'_{Fe'\text{-}FOB}/K'_{Fe'\text{-}SRFA}$ ratio of 2.37, using Eqs. 2 and 4, the theoretical partitioning of species at the equilibrium was estimated to be 45% of Fe-FOB and 55% of Fe-SRFA complexes. For PP IX, the estimate was 34% as Fe-PP IX and 66% as Fe-SRFA complexes (using our K′Fe′-FOB/K′Fe′-PPIX ratio of 5.2.1.1).

For Fe-PPIX complexes, the formation of Fe-SRFA complexes occurred rapidly within the first 30 minutes (dissociation of approximately one third of the initial Fe-PPIX concentration), followed by a slower kinetic phase that extended for over 4 hours before reaching an apparent equilibrium (Fig. 22). This trend confirmed the reversibility of the reaction and the two-step kinetics observed for the forward ligand exchange kinetics (Fig. 17B). The first value (2.3 nM Fe-SRFA) is a composite of the SRFA contamination (1.9 nM Fe), and the concentration of Fe could be sequestered by the SRFA in the first ~100 s. By the time we stopped the experiment, the Fe-SRFA concentration had apparently stabilized at 10.4 nM Fe-SRFA, equal to 58% of the total in-cell iron concentration, which is close to the predicted value of 55 %. However, the kinetics of ligand exchange were substantially slower than predicted by assuming reversibility of ligand exchange between SRFA and PP IX (Fig 17B). The kinetic rate constants for the addition of 30 nM PP IX to 1 mg L^{-1} of SRFA (Fig. 17B) were k_3=0.679±0.020 and k_4=0.678±0.042 x104 M-1s-1 for the dissociation and formation of Fe-SRHA1 complexes and k_1=13.9 ± 0.78 and k_2=80.3 ± 5.0 x 104 $M^{-1}s^{-1}$ for Fe-SRHA2 complexes. Since we do not know the contribution of SRFA1 and SRFA2 to Fe-SRFA, we modelled in Fig. 22 the formation of FeSRFA twice. Firstly, we assumed that all SRFA binding sites were fast dissociation sites and secondly, we assumed that all of them were slow dissociation sites. In both cases, the dissociation of Fe-PP IX complexes or the formation of Fe-SRFA complexes is clearly slower, indicating that the nature of the incoming ligand dictates the kinetics of ligand exchange and thus points to an A mechanism.

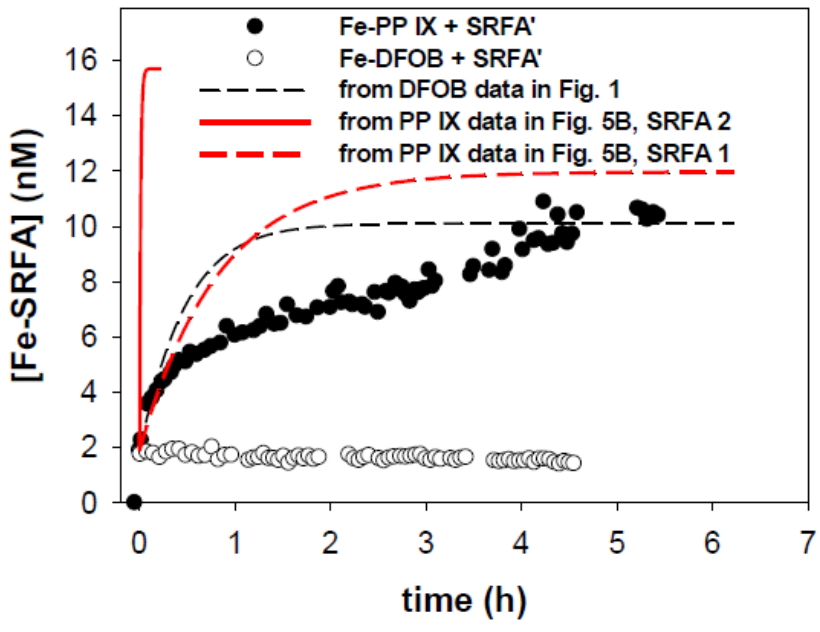

Figure 22. Time course of Fe-SRFA complex formation when 2 mg SRFA L-1 are added to two aliquots of UV seawater previously spiked with 16 nM of PP IX and DFOB, respectively. The maximum value on the Y-axis is equal to the total concentration of iron in the cell (17.9 nM).

The black solid line is the result of calculating Fe-SRFA formation from the kinetic rate constants obtained according to Eq. 1 for the addition to 1 mg SRFA L^{-1} of 30 nM DFOB (Fig. 10, k_1=0.0727 $M^{-1}s^{-1}$ and k_{-1}=0.0317 M^{-1}s-1). Red lines are the result of using data fitted for the addition of 30 nM PP IX to 1 mg SRFA L-1 (Fig. 22). The solid line models Fe-SRFA concentrations calculated assuming that all the SRFA binding sites are fast dissociation sites. The dashed line models Fe-SRFA concentrations calculated assuming that all the SRFA binding sites are slow dissociation sites. See Section 5.2.4.8 for details.

In the other experiment, these identical SRFA iron binding sites were unable to sequester any iron that had been previously complexed with DFOB. We even observed a small slow signal decrease, equivalent to nearly 1 nM Fe-SRFA. We interpret this trend as the slow removal of the 1.9 nM Fe present as an impurity in the SRFA by the small initial concentration of iron-free DFOB (about 0.4 nM). Fe-FOB complexation in seawater is thus irreversible upon competition with SRFA.

The partial dissociation of the Fe-DFOB complexes within few hours after addition of small sized Lad was confirmed in several prior publications [Croot & Johansson, 2000; Witter et al., 2000]. The striking difference shown here must be related to the tridimensional conformation of both iron complexes and the size of HS. The four nitrogen bases of the tetrapyrrole core of PP IX that bind iron form a square plane. This spatial arrangement allows interactions of solvent molecules and matrix components located perpendicular to the plane. Ligands and accelerators can interact with the iron atom even before dissociation of any of the aforementioned bonds, thus labilizing the Fe-N bonds. On the other hand, the spatial conformation of the Fe-DFOB complex at pH 8.2 is hexadentate with the oxygen and nitrogen bases of three hydroxamate groups completely surrounding the iron ion free of coordinated water molecules. This implies that there is no physical space left to allow direct interaction of matrix components that could labilize the Fe-FOB bonds, at least above a certain size. In our context, the molecular sizes of the HS are substantially larger compared to the average size of the electrolabile ligands used in CLE-AdCSV and in particular for the case presented here, the siderophores. It is

evident that size hinders the physical approach of HS to a distance that could provoke the destabilization of one of the Fe-DFOB complex bonds.

5.2.4.9. Mechanism of iron ligand exchange of Fe-HS complexes with DFOB

According to the evidence we have gathered in this study, the intimate mechanism of iron ligand exchange from SRHS complexes to DFOB in seawater must take into account the following facts:

- the reaction pathway is A because the kinetics of iron ligand exchange is a function of the nature of the competing ligand.

- Iron binding SRHS cannot be described by a single type of binding group. Although this is strongly modulated by matrix effects (which we do not include in our mechanism), it is necessary to define (at least) two different groups of binding sites according to their exchange kinetics (SRFA1 and SRFA2). The difference here with respect to the traditional L1/L2 ligand classification is that we adopt a kinetic rather than an affinity criterion.

- the overall reaction is irreversible.

The following reaction mechanism fulfils all three premises:

$$\text{Fe-SRFA}_1 + \text{DFOB} \xleftrightarrow{k1,-k2} \text{Fe-SRFA}_1\text{-DFOB} \xrightarrow{k5} \text{Fe-FOB} + \text{SRFA}_1 \quad (8)$$

$$\text{Fe-SRFA}_2 + \text{DFOB} \xleftrightarrow{k3,-k4} \text{Fe-SRFA}_2\text{-DFOB} \xrightarrow{k6} \text{Fe-FOB} + \text{SRFA}_2 \quad (9)$$

where k1 and k3 are the kinetic rate constant of the association of DFOB to the pre-existing FeSRFA1 and Fe-SRFA2 complexes to form a ternary complex, k2 and k4 are the kinetic rate constants of the release of the DFOB complex from the ternary complex and k5 and k6 are the kinetic rate constant of the release of SRFA from the ternary complex to yield the Fe-FOB binary complex. Irreversibility over a time period of many hours implies very slow dissociation of the ternary complex, i.e.: small k_5 and k_6. We fixed k_5 and k_6 to the published value of 1.5 x10-6 s^{-1} for the dissociation of Fe-DFOB complexes [Witter et al., 2000].

The mechanism explains the same decrease of the Fe-SRFA concentration found when the SRFA binding groups are fully or partially saturated (Figs. 12 and 14 and section 5.2.4.3) as the iron free SRFA lacks the ability to compete with the irreversibly bound Fe-DFOB complexes.

Table 4. Kinetic rate constants obtained from fitting the data shown in Figs. 1 and 4 according to the reaction mechanism described by Eqs. 8 and 9. Irreversibility in the time scale of the study was achieved by setting k3 and k6 to a value of 1.5 10-6 s-1. *Value 3 orders of magnitude lower than the other two k4, **value had to be fixed to achieve convergence.

1 mg SRFA L^{-1}				
[DFOB]	k1 (104 $M^{-1}\cdot s^{-1}$)	k2 (10-4 s^{-1})	k3 (104 $M^{-1}\cdot s^{-1}$)	k4 (10-4 s-1)
+15	18.10 ± 4.70	117.00 ± 31.00	1.85 ± 0.03	0.772 ± 0.027
+ 30	6.50 ± 0.89	50.00 ± 7.50	1.56 ± 0.04	0.686 ± 0.031
+50	5.56±5.28	6.39±5.56	0.94±5.28	~0*
1 mg SRHA L^{-1}				
+35	0.627 ± 0.025	2.10 ± 0.08	5.94 ± 0.61	54.4 ± 6.4
+70	0.625 ± 0.025	3.86 ± 0.14	7.22 ± 3.89	169 ± 94
+100	0.168 ± 0.007	1.46 ± 0.06	4.17**	64.4 ± 1.7
+120	0.142 ± 0.003	0.639 ± 0.018	2.56 ± 0.14	39.6 ± 2.4
+240	0.075 ± 0.001	0.406 ± 0.011	18.44 ± 0.11	43.9 ± 2.8

The kinetic rates and conditional equilibrium constants produced by fitting the data in Figs. 12 and 16 to the model described in Eqs. 8 and 9 can be found in Table 4. The quality of fitting of the selected mechanism and kinetic rate constants in Table 4 to the

experimental data can be examined in Fig. 23. Overall, the dissociation and formation kinetic rate constants of the slowly dissociating Fe-SRHS1 complexes tend to decrease as the concentration of DFOB increases, presumably due to the labilization of higher iron affinity moieties, while the kinetic rate constants of the fast-dissociating Fe-$SRHS_2$ complexes did not show any significant trend.

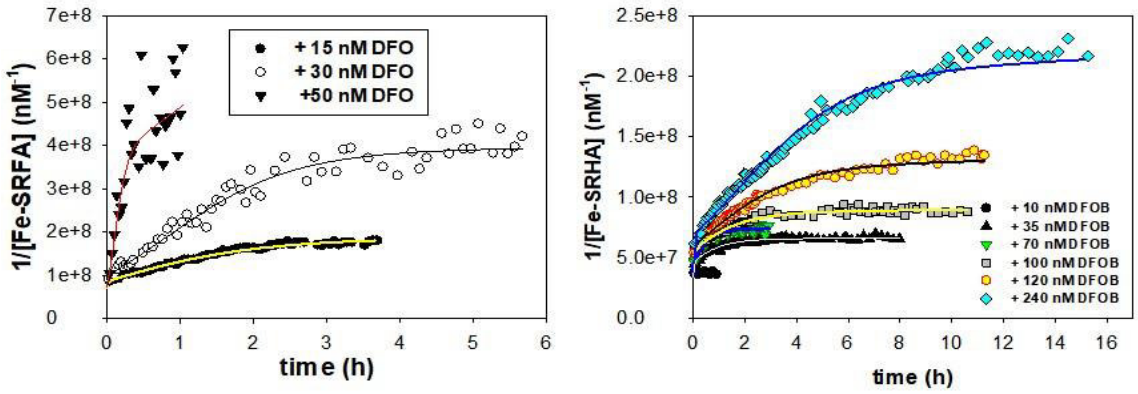

Figure 23. Characteristic plot of second-order kinetics for all data shown in Figs. 12 and 16. Lines are the result of modelling the kinetic data according to the associative irreversible mechanism with two types of SRHS binding sites shown in Eqs. 8 and 9.

5.2.4.10. Formation of organic-organic bonds or ternary species

A further source of deviation from the D and A mechanisms shown in Eqs. 5 to 7 can be introduced through the formation of complexes in which both ligands are present. This could occur by formation of ternary complexes (A mechanism) that do not dissociate at the equilibrium, direct L-L binding or binding of a ligand to non-binding components of the DOM (L-DOM). Consequently, the binding ability of a fraction of the binding moieties of one or both ligands could be modified or even compromised. Unfortunately for the sake of simplicity, organic-organic interactions in the environment are common. HS, characterized by their hydrophobicity, form adducts with many other hydrophobic ligands via π–π interactions, hydrophobic effect and hydrogen bonding [Chianese et al., 2020]. DFOB-organic interactions involving hydroxamate and non-binding functional

groups are common in nature as a strategy to facilitate membrane transport (see [Higashi et al., 1998] and references therein).

The binding of HS to DFOB has been verified by NMR spectroscopy and pyrolysis-GC-MS techniques [Stewart et al., 2013] and by using FTIR spectroscopy in the presence of iron at pH 6.5 [Stewart et al., 2013]. However, NMR and FTIR spectroscopy techniques require concentrations many orders of magnitude higher than those found in seawater. It cannot be concluded that at natural concentrations, ligand-ligand complexes will form at concentrations enough to significantly interfere with our calculations.

Despite knowing in advance that our CSV method could not produce unambiguous evidence for ternary complex formation, we explored the presence or absence of deviations from the known behavior of binary systems in an experiment with iron in excess of the combined concentration of SRFA and DFOB. Important considerations are that:

- the CSV signal is exclusively created by the adsorption of the Fe-HS complex on the HMDE and electrochemical reduction of Fe(III) [Laglera et al. 2007], without contribution from Fe-DFOB complexes [Spasojević et al., 1999],

- iron-free HS can adsorb onto the HMDE but do not give any CSV signal [Laglera et al. 2007],

- under iron in excess, all ligands are saturated and changes in the CSV signal cannot be caused by net ligand exchange but formation of adducts.

However, there are three possible sources of uncertainty for our experimental design that could impede a correct interpretation of the CSV signals:

- if SRHS-Fe-DFOB complexes are formed, retaining the hydrophobicity of HS and adsorb on the HMDE, hypothetically, they could produce a CSV signal. Fe-DFOB electrolabilization could involve SRFA binding (stability or decrease of the CSV signal) or not binding (CSV signal increase) functional groups. Our reverse ligand exchange experiment (Fig. 20) showed that an electrolabile ternary compound is definitely not formed in a time scale of many hours if DFOB is saturated with iron prior to iron-free SRFA′ additions. The experimental exploration of the existence of electrolabile ternary complexes requires that DFOB interacts with SRFA in its iron-free form.

For this experiment, 10 mL aliquots of UV seawater were sequentially spiked first with 2 mg SRFA L-1 or 1 mg SRHA L-1, then with DFOB for a concentration in the range of 0 to 100 nM DFOB for SRFA, or 0 to 300 nM DFOB for SRHA and finally 600 nM Fe. All samples were equilibrated overnight at room temperature before the first measurement with the aim to complete the precipitation of iron before analysis. We did not observe any changes in the CSV peak within the 30 minutes period required to complete five analyses, indicating that the overnight period was sufficient to complete the precipitation of excess iron. The Fe-SRFA signal increased by a factor of about 1.2 with the added concentration of DFOB until it reached an apparent maximum after the addition of 30 nM DFOB (Fig. 24). This result would support the possible electrolabilization of the Fe-FOB complexes through the formation of ternary FeFOB-SRFA complexes. In the case of SRHA, the CSV signal decreased with the DFOB concentration reaching 80% of the initial signal at DFOB concentrations between 100 and 200 nM. At a DFOB addition of 300 nM, the Fe-SRHA signal increased, although we would need better resolution to confirm such recovery at higher DFOB concentrations.

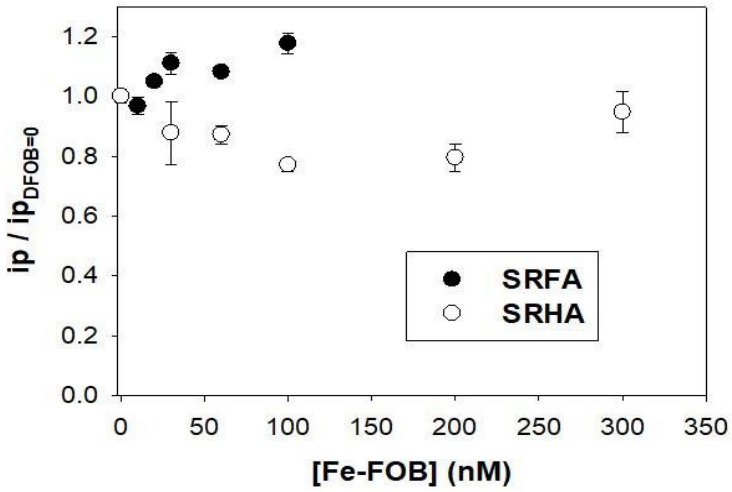

Figure 24. CSV signal obtained in seawater after the addition of 2 mg L^{-1} SRFA and 1 mg L1 SRHA, different concentrations of DFOB and Fe in excess of the combined ligand concentrations, allowing equilibration overnight before analysis.

In the absence of spectroscopic evidence, we can only hypothesize about the processes that could explain this behavior. Firstly, the higher iron contamination of the SRHA standard could have prevented the interaction of DFOB with the key iron complexing moieties of the SRHA. Secondly, co-precipitation of iron and Fe-SRHA complexes could partially explain the decrease of the CSV signal. HA molecules are larger and more

hydrophobic than FA molecules and should be more prone to processes such as flocculation. This preferential precipitation of higher molecules has been observed in salinity gradients [Aftab & Hur, 2017; Linkhorst et al., 2017]. Thirdly, we cannot rule out that DFOB may cause conformational changes in SRHA molecules or decrease the hydrophobicity of ternary complexes by reducing their affinity to adsorb onto the HMDE during the analytical accumulation step.

If any of the hypothesis presented above is confirmed on a significant scale, it is possible that the estimation of HS binding affinity, including this study, may have been biased in CLE experiments (sections 5.2.4.2 to 5.2.4.5). Firstly, if the binding ability of any of the DFOB hydroxamate groups was compromised by non-binding SRHS or iron-free binding SRHS generated during the kinetic phase, we could have overestimated the K′Fe′-SRHS. Secondly, direct interactions between SRHS and DFOB could have altered or impeded binding by SRHS resulting in either over- or underestimation of K′Fe′-SRHS, depending on whether the hydroxamate groups, the terminal non-iron binding terminal amine of the siderophore, or both were involved. To shed more light on the interactions between the components of the Fe/SRHS/DFOB system, further experiments with spectroscopic techniques at lower concentrations are necessary.

5.2.5. Implications for the study of iron cycling in seawater

5.2.5.1 Contribution of humic iron to the iron cycle

Humic iron is possibly the main source of iron in estuarine and coastal waters [Krachler et al., 2015] and probably contributes decisively to the iron pool in vast areas of the open ocean [Laglera et al., 2019; Muller, 2018]. Our electrochemical method is currently unique in allowing the calculation of HS concentrations after calibration with SRFA and their contribution to the iron ligand pool prior to knowledge of their iron BC. The range of published HS concentrations in open ocean waters expands from near the detection limit (0.005 mg SRFA L^{-1}) to many tenths of mg SRFA L^{-1}, equivalent to humic ligand concentrations of tens of pM to around 1 nM Fe [Dulaquais et al., 2018; Laglera & van

den Berg, 2009; Mellett & Buck, 2020; Slagter et al., 2019]. This is below or close to the ligand concentrations found in the ocean, which would make HS the main contributor to the pool of organic ligands in some water masses. The limited iron ligand exchange of Fe-HS complexes with other ligands predicted from our K′Fe′-FOB/K′Fe′SRHS ratios, it is not just a change of paradigm, it is also important in terms of iron bioavailability. The formation of HS complexes increases iron bioavailability [Chen et al., 2009]not only because of iron exchange with cell membrane functional group, but also because HS chromophores in the euphotic layer are prone to participate in the reduction of Fe(III) into the more bioavailable Fe(II) [Fujii et al., 2010]. The high stability of Fe-HS complexes concurs with the prevalence of humic iron (~80% of DFe) found in HS-rich surface waters of the Arctic Transpolar Drift despite months to years of residence under ice [Laglera et al., 2019; Slagter et al., 2019] and the residual humic iron (0-20% DFe) concentrations found in HS-poor waters of blooming surface waters over the Brazilian coast shelf [Sukekava et al., 2023].

5.2.5.2 Understanding the partitioning of iron between different ligands.

The low concentration and large heterogeneity of oceanic DOM have prevented the identification of individual contributors to the pool of iron ligands in the ocean. Our results provide a biochemical and ecological sense of the relative concentrations of the different ligands found so far in ocean waters.

Recent advances in HPLC-MS techniques have allowed for the detection of combined siderophore concentrations ranging from units to tens of pmol L-1 across various marine regions. These concentrations are found to be one to two orders of magnitude lower than those reported for L and HS ligand concentrations in oceanic waters. [Boiteau et al., 2016; Boiteau et al., 2019; Bundy et al., 2018; Gledhill et al., 2022] The low concentrations imply that siderophore consumption processes such as photodegradation [Barbeau et al., 2003], prokaryotic uptake [Hopkinson and Barbeau, 2012] and scavenging [Hogle et al., 2022] shorten their half-life in the ocean sufficiently to prevent their accumulation. The involvement of Fe-siderophore complexes in chemical reactions with time scales significantly longer than their residence time in the ocean would be of negligible

environmental significance. Ligand exchange rates such as those obtained in this study and dissociation rate constants leading to half-lives of the order of months such as those found for the hydroxamate siderophores desferrioxamine E and ferrichrome and extracted amphibactins by iron isotope exchange in seawater [Boiteau & Repeta, 2022]could be considered irreversible from an ecological perspective.

The K′Fe′-FOB/K′Fe′-SRHS ratios we report here, and the use of Eq. 4 indicate that at natural HS:siderophore concentration ratios, the contribution of siderophores to iron complexation at equilibrium would be residual. However, the irreversibility of iron-siderophore complexation in competition with HS describes a situation where iron speciation closely adheres to a "first come, first served" principle: siderophore concentrations one to two orders of magnitude lower than HS concentrations would struggle to effectively sequestering significant concentrations of iron bound to HS; conversely, iron bound to a siderophore would not be sequestered by HS.

It is crucial to understand that, in the light of our results, small concentrations of exuded siderophores can satisfy the iron requirements of the prokaryotic fraction assimilating Fe-siderophore complexes. Accumulating siderophores in the water column at nanomolar concentrations to compete with other ligands is not feasible because prokaryotes would need to bear the high cost of synthesizing and exuding energy-consuming siderophores [Völker & Wolf-Gladrow, 1999] . According to our K′Fe′-FOB/K′Fe′-SRHS ratios, picomolar concentrations of Fe-siderophore complexes would be over competed by HS failing to hold any significant iron concentration. However, the lack of reversibility of Fe-siderophore complexes by HS implies that small concentrations of siderophores in the water column maintain the Fe-siderophore requirements of prokaryote communities.

Our K′Fe′-FOB/K′Fe′-SRHS ratios also explain the recent discovery using clean HPLC-MS techniques of iron saturated siderophores in coastal waters that in open ocean waters were approximately 40% iron-free despite DFe concentrations two orders of magnitude above the combined concentration of siderophores. [Boiteau et al., 2016a] Coastal waters contain iron saturated siderophores from freshwater supplies [Maknun et al., 2023]and autochthonous siderophores can compete with the iron oxyhydroxide forms common in riverine and upwelling sources. However, fresh iron-free siderophores released in open ocean waters have to sequester iron from DOM complexes (including HS), which are present in much higher concentrations.

However, in deep waters, the lack of capacity of HS to sequester iron bound to other natural ligands (such as hexadentate siderophores) could be behind the low iron saturation of HS (1520%) found at a deep Arctic Ocean station [Laglera et al., 2019]. Siderophores in deep waters are released during microbial remineralization of POC (and thus iron), which would facilitate the direct binding of iron to siderophores. The strong correlation observed between the vertical profiles of DFe and fluorescent DOM in deep ocean waters gave rise to the hypothesis that HS may regulate iron solubility at depth [Kitayama et al., 2009]. Recent developments that allow the estimation of the concentration of iron bound to HS [Sukekava et al., 2018] warrant further studies to verify or challenge the controlling role of HS in deep-sea iron speciation.

Our description of the competition between siderophores and HS closely aligns with the modeling based on field measurements of siderophores recently published by Gledhill and coauthors [Gledhill et al., 2022].

From an analytical point of view, it can be expected that in a "first come, first served" complexation scenario, the reversibility of iron complexes, the order of reagent addition and the presence of accelerators prior to analysis could impact the results of CLE-CSV analysis. Moreover, if the presence of ternary siderophore-Fe-HS complexes in seawater is confirmed, the conventional use of three terms mass balances (Eq. 2) would introduce significant bias for the estimation of K′F′eL. The implications for the reliability of speciation models could be serious. The existence of ternary and ligand-ligand complexes could also affect HPLC extraction and MS analysis as adducts may exhibit different chemical reactivity on the column, and the m/z ratio of an undetermined fraction of siderophores could be substantially altered.

5.2.6. Conclusions

We are beginning to understand the real role of HS in the solubility and transport of iron from terrestrial sources. The chemical characteristics of HS present a drawback for their analysis by HPLC-MS and the determination of their complexing parameters by CLE-AdCVS, although they allow their direct determination at natural concentrations by AdCSV of their iron complexes. We took advantage of this electrolability to monitor the kinetics of iron ligand exchange up to equilibrium when iron from Fe-HS complexes is sequestered by the siderophore DFOB and other complexes in the nanomolar range. We

established that the segmented kinetics we observed is evidence of the heterogeneity of the HS binding groups although a fraction of the ligand exchange is severely accelerated by the effect of the major divalent cations in seawater. Partitioning at the equilibrium showed that, contrary to the current paradigm, HS have, on average, a similar affinity for iron as DFOB, corroborating previous observations showing that the affinity of HA for iron is higher than that of FA. However, when iron is bound to hexadentate ligands, this complexation is inert to competition from the large molecules of HS. This irreversibility, in combination with the different ligand exchange kinetics we observed using PP IX and EDTA as competing ligands, indicates that iron exchange between HS and DFOB is associative. Our experiments suggest that a small but significant concentration of the ternary complex or a ligand-ligand complex could be stable at equilibrium.

Our findings explain the discovery of a significant fraction of ocean siderophores found in their iron-free form, the high concentrations of strong ligands found in HS-rich waters, or the problems encountered with the study of HS complexation of iron by CLE-AdCSV techniques.

Studies under saturation of all ligands point to the presence of small but significant concentrations of complexes where ligand to ligand interactions could change the physicochemical and or binding (log K′) characteristics of the iron complexes when mixed in seawater. Consequently, the ratios of reagents in CLE studies and the sequential order of reagent addition are essential in CLE experiments.

Data Availability

Experimental data and Dynafit software scripts are available through Zenodo. At https://doi.org/ 10.5281/zenodo.8047795

5.2. 7. Supplementary Material

The Supplementary Information file includes i) some experimental and modelled kinetics that support the text but are not essential to its understanding, ii) a description of the analytical problems we found during our experimental, their source and the limitations

that suppose for interpretation and iii) a brief description of the mechanistic models of iron ligand exchange used in this work with the definition of the kinetic rate constants and the number of chemical species used to fit kinetic data for each mechanism.

5.2.7.1 Conceptual framework of the study of ligand exchange reactions

The iron ligand exchange of the departing complexes (Fe-HS here) caused by competition with an added ligand (L_{ad}), a situation similar to the arrival of DOM and Fe rich riverine waters to estuaries, is defined according to Eq. S1:

$$Fe - HS + L'ad \leftrightarrow HS' + Fe - Lad \qquad \mathrm{Fe - HS + L'ad} \overset{kobs}{\longleftrightarrow} \mathrm{HS' + Fe - Lad} \qquad (S1)$$

where HS′ and L'_{ad} are the concentrations of HS and the added competing ligand that are not bound to iron. Therefore, any proton, hydroxyl ion and other ions that may be incorporated into the molecules are omitted. If the products are not completely consumed and reach a steady concentration, this is indicative of a dynamic equilibrium and therefore k_{obs} is the composite of the kinetic rates of the direct (k_1, $M^{-1}s^{-1}$) and reverse (k_{-1}, $M^{-1}s^{-1}$) second order reactions that make up Eq. S1:

$$\frac{d[Fe-SRHS]}{dt} = -k_1[Fe - HS][L'_{ad}] + k_{-1}[HS'][Fe - L_{ad}] \qquad (S2)$$

Mass balances for both ligands are defined as follows where the prime superscript combines all the non-ferric forms:

$$[HS]_{TOT} = [HS'] + [FeHS] \qquad [L_{ad}]_{TOT} = [L'_{ad}] + [FeL_{ad}] \qquad (S3)$$

This simplification implies the conditionality to the matrix composition of all stability constants:

$$K'_{Fe'HS} = \frac{[Fe'-HS]}{[Fe'][HS']} \qquad K'_{Fe'L_{ad}} = \frac{[Fe'-L_{ad}]}{[Fe'][L'_{ad}]} \tag{S4}$$

where Fe′ is the total concentration of iron inorganic species.

At the equilibrium, we can calculate the ratio between the conditional stability constants of both ligands as (Luther et al., 2021):

$$\frac{K'_{Fe\prime-L_{ad}}}{K'_{Fe\prime-HS}} = \frac{[Fe\prime-L_{ad}]\cdot[HS']}{[Fe\prime-HS]\cdot[L'_{ad}]} \tag{S5}$$

There are two major routes for ligand exchange to happen, depending on whether intermediate chemical species have a lower or higher coordination number.

Dissociative mechanism (D): it is characterized by the complete dissociation of the departing ligand (Fe-HS) before iron establishes any interaction with the incoming ligand. Eq. 1 can be divided into two consecutive reactions:

$$Fe' - HS \rightleftharpoons Fe' + HS' \qquad k_{a,Fe'HS},\ k_{d,Fe'HS} \tag{S6}$$

$$Fe' + L'_{ad} \rightleftharpoons Fe' - L_{ad} \qquad \text{fast},\ k_{a,Fe'L_{ad}},\ k_{d,Fe'L_{ad}} \tag{S7}$$

where k_a ($M^{-1}s^{-1}$) and k_d (s^{-1}) are the formation and dissociation kinetic rates of both complexes.

The formation and dissociation rates of both complexes in Eq. 1 are given by:

$$\frac{d[Fe-HS]}{dt} = -k_{d,Fe'HS}[Fe - HS] + k_{a,Fe'HS}[Fe'][HS'] \tag{S8}$$

$$\frac{d[Fe-L_{ad}]}{dt} = -k_{d,Fe'L_{ad}}[Fe - L_{ad}] + k_{a,Fe'L_{ad}}[Fe'][L_{ad}'] \tag{S9}$$

Scientists favour this mechanism because both equations are linked by Fe′ and therefore the relationship between the (also conditional) kinetic rates and the conditional equilibrium constants is straightforward:

$$K'_{Fe'HS} = \frac{k'_{a,Fe'L}}{k'_{d,Fe'L}} \qquad K'_{Fe'Lad} = \frac{k'_{a,Fe'Lad}}{k'_{d,Fe'Lad}} \tag{S10}$$

If the values of the kinetics constants in Eq. S6 and S7 are available from previous iron CLE experiments, equations S8 and S9 allow simple modelling of the kinetics of the dissociation of the initial complex and formation of the complex with the competing ligand. In order to illustrate the expected shape of the kinetic curve of case of a reversible second order kinetic reaction, Fig S1 (black lines) shows the kinetics of iron ligand exchange when 15 nM iron free DFOB is added to seawater containing 1 mg SRFA L^{-1} 95% saturated with iron using the kinetic rate constants of Fe-SRFA and Fe-DFOB formation and dissociation found in the literature (Rose and Waite, 2003b; Witter et al., 2000). We can observe in Fig S1 that, in this case, the characteristic 1/[Fe-SRFA] vs. time plot is linear in the kinetic section with a curved transition section before the flat line marking the equilibrium.

Associative mechanism (A): in this case the incoming ligand forms a chemical bound with the departing complex resulting in a ternary complex of higher coordination. The breaking of the initial bond occurs in a secondary reaction.

$$\mathrm{Fe'-HS} + \mathrm{L_{ad}} \overset{A1}{\leftrightarrow} \mathrm{HS-Fe'-L_{ad}} \overset{A2}{\leftrightarrow} \mathrm{Fe'-L_{ad}} + \mathrm{HS'} \qquad \text{(S11)}$$

A ligand exchange mechanism is common in multidentate ligands, including siderophores [Crumbliss and Harrington, 2009].

The associative mechanism makes the calculations extremely complicated. Firstly, iron is distributed in three organic species, which adds extra species to all the mass balance equations. Secondly, the obtained k'_a and k'_d for the binary complexes are not applicable because they do not describe the kinetics of formation and dissociation of the ternary complex, which has its own stability constant and association and dissociation kinetics. Thirdly, the ternary complex may not necessarily involve the simultaneous bonding of Fe to both ligands; ligand-ligand interactions can modulate the affinities of the iron binding moieties of one or both ligands.

From an analytical point of view, it is unusual to have the analytical capability to monitor the concentration of all three complexes simultaneously. At the nanomolar to picomolar concentrations found in seawater, the number of suited analytical methods is dramatically reduced, and analysis of the ternary complex may become unattainable. For our specific

experimental design, there is also uncertainty about the electrolability of the ternary complex (see details below).

It is important to note that route D (spontaneous dissociation of the departing complex) is always possible, but that A route, which requires some affinity of the incoming ligand for the dissociating complex, is not. Therefore, the observation of an A mechanism necessarily accelerates the ligand exchange kinetics with respect to the D case.

Most ligand exchange reactions do not fully conform to the above mechanisms and their kinetics are referred to as *interchange mechanisms (I)* covering a wide spectrum of interactions. The incoming ligand can interact with the bound iron or the departing ligand, reducing the complex's stability without chemically binding. In the dissociative interchange mechanisms (I_d), the incoming ligand creates electrostatic interferences that labilize the departing complex and trigger its dissociation prior to before the interaction of the binding group of L_{ad} and Fe′. In associative exchange mechanisms (I_a), the incoming ligand occupies a place in the inner sphere of iron either by breaking one of the bonds with the departing complex or by substituting one of the remaining waters in the inner solvation sphere of the iron atom.

From a kinetic point of view, the tendency of the initial complex to exchange iron by a given pathway can be studied simply by comparing the ligand exchange kinetics with different incoming ligands (Helm and Merbach, 2005). Since the D mechanism requires “spontaneous” (as free of interaction from the incoming ligand) dissociation of the departing complex, the ligand exchange kinetics hardly depend on the nature of the incoming ligand. In contrast, the A mechanisms involves the chemical attachment of the incoming ligand to the initial complex, thus, the ligand exchange kinetics vary significantly with the chemical nature of the metal and both ligands. In this case, different combinations of metal and ligand will show very different ligand exchange kinetics.

When reactions are studied at natural concentrations in real matrices, the situation can be further altered by the action of accelerators, which are mainly cations or sometimes other third-party ligands known as synergistic ligands Accelerators present the ability to weaken the bond of the initial iron complex, thus labilizing the complex and reducing its stability.

From an experimental point of view, it is unusual to have evidence of whether ternary species are in equilibrium, especially if the experimental design tries to reproduce low natural concentrations and complex matrices. If the ternary complex according to Eq. S8 is simply a necessary short-lived transient, reaction A2 of Eq. S8 can be considered irreversible. If the A2 reaction of Eq. S6 is reversible, there could be a permanent dynamic concentration of the ternary complex at equilibrium.

From a practical point of view, it is not possible to deduce the presence of a ternary intermediate solely based on changes observed in the 1/[Fe-SRFA] vs. time plot (Fig. S1) when dealing with humic substances (HS). This limitation is due to another important chemical characteristic of HS: the heterogeneity of HS binding groups. Fig, S1 models the impact of two distinct types of iron binding ligands within SRFA, each with different dissociation rate constants (and thus conditional stability constants), on the dissociation kinetics of Fe-SRFA complexes. Since each binding group reaches equilibrium after a different period, the 1/[Fe-SRFA] vs. time plot lacks linear sections.

5.2.7.2 Fitting of kinetic data to iron ligand exchange mechanisms

- Mechanism homogeneous reversible iron ligand exchange as in Eq. 1:

$A + B \rightarrow C + D$ *k1*

$C + D \rightarrow A + B$ *k2*

where A, B, C and D are the concentrations of Fe-SRHS, L_{ad}', Fe-L_{ad} and SRHS'. All four species were calculated at each time from the CSV signal (Fe-SRHS) and the mass balances of DFe, SRHS and L_{ad} and adjusted by the algorithm.

- Mechanism heterogeneous reversible iron ligand exchange where we assume that there are two types of departing complexes, Fe-$SRHA_1$ and Fe-$SRHA_2$, as a function of their dissociation kinetics:

$A + B \rightarrow C + D$ *k1*

$C + D \rightarrow A + B$ *k2*

$A + B \rightarrow C + E$ *k3*

$C + E \rightarrow A + B$ *k4*

where D and E are the concentrations of $SRHA_1'$ and $SRHA_2'$, respectively. Here D and E were not adjusted since the concentrations of $SRFA_1$ and $SRFA_2$ are not known.

- Mechanism heterogeneous irreversible iron ligand exchange, detailed in Section 5.2.4.10:

$A + B \rightarrow AB$ *k1*

$AB \rightarrow A + B$ k_2

$AB \rightarrow D$ *k5*

$A + B \rightarrow AC$ *k3*

$AC \rightarrow A + B$ *k4*

$AC \rightarrow E$ *k6*

In this case the concentrations of $SRHA_1'$ and $SRHA_2'$ are D and E. Only the concentrations of Fe-SRHS and L_{ad}' were adjusted. The values of the kinetic rate constants k_3 and k_6 values were set to 1.5 x 10^{-5} $M^{-1}s^{-1}$.

5.2.7.3. Preliminary studies on the formation of HS and DFOB adducts affected by iron precipitation.

In a preliminary study, we added 2 mg SRFA L^{-1}, 300 nM iron and finally DFOB at concentrations in the range 5 to 100 nM to a series of UV seawater aliquots sequentially in the voltammetric cell (allowing 15 min periods for equilibration between them), and immediately started monitoring the CSV signal. This experimental design has the major drawback that free Fe(III) in excess of the combined ligands concentration will

progressively precipitate. During the analysis, the Fe(III) electrochemical reduction to Fe(II) on the surface of the HMDE leads to the subsequent breaking of the Fe-SRHS complex [Laglera & van den Berg, 2009]. The formation and adsorption of fresh Fe(III)SRFA complexes on the HMDE during the potential scan is accelerated if excess Fe(III) accumulates in the vicinity of the HMDE. The result is an increase of the CSV signal. However, free Fe(III) is not stable and slowly aggregates and precipitates in the cell reducing its concentration in solution and therefore reducing the CSV signal. Therefore, if Fe(III) is spiked in the cell iron in excess of the sum of the iron BC_{HS}, the Fe-SRFA signal decrease is only partially related to ligand exchange. Eventually, as free Fe(III) completely precipitates, the CSV signal stabilises at the iron BC_{HS} [Laglera & van den Berg, 2009; Sukekava et al., 2018]. The in-cell precipitation of tens of nanomols per litre of excess inorganic iron in the presence of HS takes between 2 and 15 h depending on the iron and HS concentrations [Laglera & van den Berg, 2009], but in the presence of more ligands this period could be significantly extended [Rose & Waite, 2003]. Figure 25 shows the time course of the Fe-SRFA CSV peak in response to the addition of different concentrations of DFOB. Two unexpected features were observed:

. i) the first CSV signal collected after the addition of iron increased with the DFOB concentration in solution from 5 nM DFOB to reach a maximum at 20 nM DFOB with no further increases at higher DFOB additions. This result was counter intuitive, as at a constant concentration of Fe-SRFA complexes, the CSV signal increased as higher DFOB concentrations left less inorganic Fe(III) in solution.

ii) the kinetics of the CSV signal also varied with the magnitude of the DFOB addition. Low DFOB additions gave the expected decrease of the CSV signal to a constant value in agreement with previous experiments [Laglera & van den Berg, 2009; Sukekava et al., 2018] At DFOB additions of 30 nM (approximately the binding capacity of 2 mg SRFA L^{-1}) and higher, there was an initial increase in the CSV signal from half an hour to 2 h, followed by a slow decrease over tens of hours. We never observed such increase in the many experiments we performed in binary SRFA and iron in excess systems or ternary systems with iron fully complexed prior to the addition of the second ligand (Figs. 10 to 16).

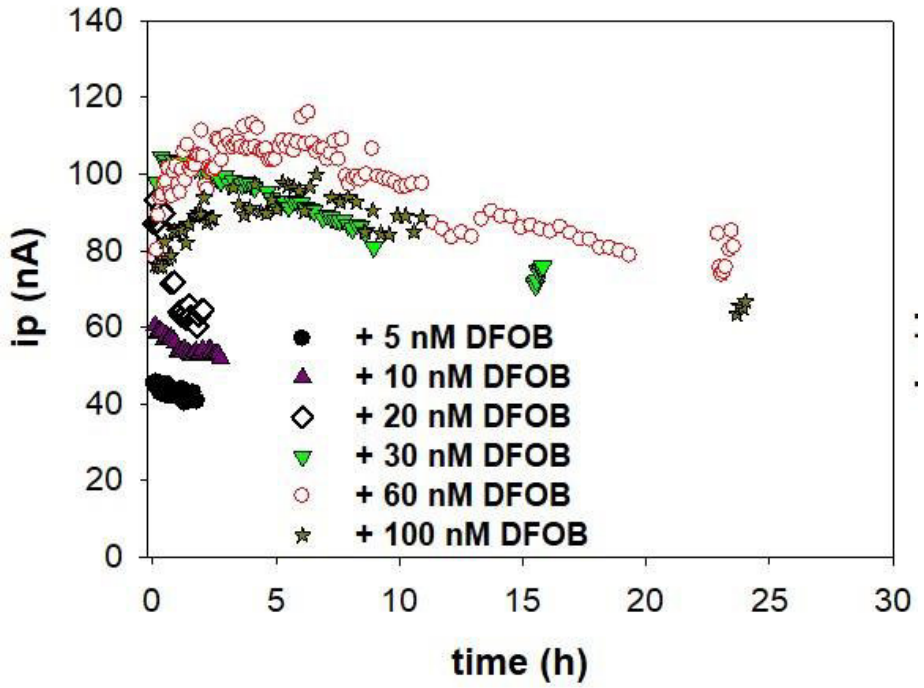

Figure 25. Time course of the CSV signal obtained in seawater after the addition of 2 mg L^{-1} SRFA, different concentrations of DFOB and Fe in excess of the combined ligand concentrations. After sequential addition of all reagents with 15 minutes equilibration between them, the concentration of Fe-SRFA complexes was monitored.

We propose that two processes could explain the unexpected trends. First, the initial increase of the CSV signal could be caused by the electrolabilization of the Fe-FOB complexes through the formation of ternary Fe-FOB-SRFA complexes. Second, the slower than expected decrease of the CSV signal was caused by a slowing down of the precipitation of inorganic Fe(III) due to the presence of DFOB as previously reported (Rose and Waite, 2003a). The 2.5-fold increment of the initial CSV signal caused by DFOB additions up to 20 nM, the existence of periods of signal increment, and the fact that the CSV signal never dropped to the values registered at low DFOB concentrations (Fig. 23) point to the formation of electrolabile Fe-FOB-HS complexes, although we stress that these trends do not constitute direct evidence. The huge increase of the first CSV signal as a function of the concentration of Fe-FOB complexes would suggest that the hypothetical electrolabile ternary complex would include fractions of the SRFA that do not bind iron. Therefore, the explanation behind the observed deviations lies either in the prevention of iron precipitation caused by DFOB or that the SRFA and DFOB

molecules bind efficiently in the absence of iron generating after addition of iron, an electrolabile ternary complex or a combination of both.

Capítulo VI- Síntese dos resultados e conclusões

Desde a publicação do primeiro artigo relacionando substâncias húmicas como um

importante ligante do ferro em zonas oceânicas [Laglera & van den Berg, 2009] até a implementação do nosso método analítico publicado nove anos mais tarde [Sukekava, 2018] inúmeros trabalhos já demonstraram a forte capacidade de complexação das substâncias húmicas sua inegável importância no meio oceânico para o ciclo biogeoquímico do ferro. Com isso, essa tese teve como principal intuito aplicar um método analítico onde pode ser detectada a capacidade complexante do ferro e comprova-se quão importante as substâncias húmicas podem ser para este processo.

Em suma o primeiro artigo obteve inúmeras referências sobre como o ferro, embora em baixa concentração no meio em questão pode exercer um papel importante para a biota. Sendo assim: os resultados reforçaram a importância dos complexos substâncias húmicas - ferro como um mantenedor de ferro no talude, impulsionando esse elemento para regiões mais afastadas das áreas fontes. Essa hipótese foi comprovada na quebra do talude na região de Santa Marta, onde a ressuspensão de sedimento, durante o processo de

“downwelling” poderia garantir a manutenção biológica nessa zona, com a inserção de complexos Fe-HS na coluna d’água.

Assim como, o segundo artigo em que foi observado uma grande heterogeneidade de HS e alta capacidade de complexação de ferro impedindo a quebra da dissolução de Fe-HS. Esses resultados inferem que Fe-HS possuem alta capacidade de manutenção em meio oceânico, embora quando o ferro é complexado com outros ligantes, principalmente sideróforos, o resultado pode ser distinto, reforçando a ideia de quem “obtém o item quem chegar primeiro”. Os testes usados nesse capítulo indicaram que HS pode ser um forte candidato a ligante, mesmo em áreas oceânicas, e estar sendo subvalorizado devido as técnicas empregadas ou mesmo ignorado devido a poucos estudos relacionados a sua complexidade.

Em resumo, embora os resultados do primeiro artigo não demonstraram uma predominância de HS no meio, seu papel é inegável quando se trata de manutenção do ferro na coluna de água. Já no segundo capítulo fica claro o quão esse ligante, quando complexado com ferro pode ser importante, uma vez que sua complexidade demonstra alta capacidade de manutenção de ferro, mesmo quando esteja sob influência de outros ligantes, reforçando a segunda hipótese de que esse ligante pode competir com os demais.

Esses dois artigos reforçam a ideia de que essas substâncias húmicas devem ser mais estudadas ao longo da costa e zonas oceânicas, embora esteja invalidando a hipóteses de que HS é o principal complexante em Santa Marta Grande, mas reforçando uma inegável função no ciclo biogeoquímico do ferro.

Espera-se que os resultados do segundo artigo possam ser uteis para uma reformulação da metodologia de especiação orgânica do ferro, podendo valorizar os dados que até em estão mascarados junto aos demais ligantes. Assim como trabalhos ao longo da costa Brasileira devem ter continuidade principalmente em regiões aonde a existe alta descarga de rios, principalmente ao sul da Plataforma.

Capítulo VII – Referências bibliográficas

Acha EM, Mianzan HW, Guerrero RA, Favero M, Bava J (2004). Marine fronts at the continental shelves of austral South America: Physical and ecological processes. Journal of Marine Systems. 44:83–105. doi:10.1016/j.jmarsys.2003.09.005.

Aftab B, Hur J (2017). Fast tracking the molecular weight changes of humic substances in coagulation/flocculation processes via fluorescence EEM-PARAFAC. Chemosphere. 178:317–324. doi:10.1016/j.chemosphere.2017.03.068.

Batchelli S, Muller FLL, Chang KC, Lee CL (2010). Evidence for strong but dynamic iron-humic colloidal associations in humic-rich coastal waters. Environ Sci Technol. 44:8485–8490. doi:10.1021/es101081c.

Bif MB, Yunes JS (2016). Distribution of the marine cyanobacteria Trichodesmium and their association with iron-rich particles in the South Atlantic ocean. Aquatic Microbial Ecology. 78:107–119. doi:10.3354/ame01810.

Biller D V., Bruland KW (2014). The central California Current transition zone: A broad region exhibiting evidence for iron limitation. Prog Oceanogr. 120:370–382. doi:10.1016/j.pocean.2013.11.002.

Boguta P, D'Orazio V, Senesi N, Sokołowska Z, Szewczuk-Karpisz K (2019). Insight into the interaction mechanism of iron ions with soil humic acids. The effect of the pH and chemical properties of humic acids. J Environ Manage. 245:367–374. doi:10.1016/j.jenvman.2019.05.098.

Boiteau RM, Mende DR, Hawco NJ, McIlvin MR, Fitzsimmons JN, Saito MA, Sedwick PN, Delong EF, Repeta DJ (2016a). Siderophore-based microbial adaptations to iron scarcity across the eastern Pacific Ocean. Proc Natl Acad Sci U S A. 113:14237–14242. doi:10.1073/pnas.1608594113.

Boiteau RM, Mende DR, Hawco NJ, McIlvin MR, Fitzsimmons JN, Saito MA, Sedwick PN, Delong EF, Repeta DJ (2016b). Siderophore-based microbial adaptations to iron scarcity across the eastern Pacific Ocean. Proc Natl Acad Sci U S A. 113:14237–14242. doi:10.1073/PNAS.1608594113/SUPPL_FILE/PNAS.201608594SI.PDF.

Boiteau RM, Repeta DJ (2022). Slow Kinetics of Iron Binding to Marine Ligands in Seawater Measured by Isotope Exchange Liquid Chromatography-Inductively Coupled Plasma Mass Spectrometry. Environ Sci Technol. 56:3770–3779. doi:10.1021/ACS.EST.1C06922/SUPPL_FILE/ES1C06922_SI_001.PDF.

Braga ES, Chiozzini VC, ucia Berbel GB, Maluf JC, Aguiar VM, Charo M, Molina D, Romero SI, Eichler BB (2008). Nutrient distributions over the Southwestern South Atlantic continental shelf from Mar del Plata (Argentina) to Itajaí (Brazil): Winter-summer aspects. doi:10.1016/j.csr.2007.06.018.

Brandini FP, Nogueira M, Simião M, Carlos Ugaz Codina J, Almeida Noernberg M (2014). Deep chlorophyll maximum and plankton community response to oceanic bottom intrusions on the continental shelf in the South Brazilian Bight. Cont Shelf Res. 89:61–75. doi:10.1016/j.csr.2013.08.002.

Breitbarth E, Achterberg EP, Ardelan MV, Baker AR, Bucciarelli E, Chever F, Croot PL, Duggen S, Gledhill M, Hassellov M, Hassler C, Hoffmann LJ, Hunter K a., Hutchins D a., Ingri J, Jickells T, Lohan MC, Nielsdottir MC, Sarthou G, Schoemann V, Trapp JM, Turner DR, Ye Y (2010). Iron biogeochemistry across marine systems - progress from the past decade. Biogeosciences. 7:1075–1097. doi:10.5194/bg-7-1075-2010.

Bruland KW, Rue EL, Smith GJ (2001). Iron and macronutrients in California coastal upwelling regimes: Implications for diatom blooms. Limnol Oceanogr. 46:1661–1674. doi:10.4319/LO.2001.46.7.1661.

Buffle J, Cominoli A (1981). Voltammetric Study of Humic and Fulvic Substances .4. Behavior of Fulvic Substances at the Mercury-Water Interface. Journal of Electroanalytical Chemistry. 121:273-299 ST-Voltammetric Study of Humic and Fulv.

Bundy RM, Abdulla HAN, Hatcher PG, Biller D V, Buck KN, Barbeau KA, Bay N (2015). Iron-binding ligands and humic substances in the San Francisco Bay estuary and

estuarine-in fl uenced shelf regions of coastal California. Mar Chem. 173:183–194. doi:10.1016/j.marchem.2014.11.005.

Bundy RM, Boiteau RM, McLean C, Turk-Kubo KA, McIlvin MR, Saito MA, Mooy BA Van, Repeta DJ (2018). Distinct Siderophores Contribute to Iron Cycling in the Mesopelagic at Station ALOHA. Front Mar Sci. in press:1–15. doi:10.3389/fmars.2018.00061.

Campos EJD, Miller JL, Müller TJ, Peterson RG (1995). Physical Oceanography of the Southwest Atlantic Ocean. Source: Oceanography. 8:87–91.

Campos EJD, Velhote D, Da Silveira ICA (2000). Shelf break upwelling driven by Brazil current cyclonic meanders. Geophys Res Lett. 27:751–754. doi:10.1029/1999GL010502.

Campos PC, Möller OO, Piola AR, Palma ED (2013). Seasonal variability and coastal upwelling near Cape Santa Marta (Brazil). J Geophys Res Oceans. 118:1420–1433. doi:10.1002/JGRC.20131.

Capone DG, Hutchins DA (2013). Microbial biogeochemistry of coastal upwelling regimes in a changing ocean. Nat Geosci. 6:711–717. doi:10.1038/ngeo1916.

Caprara S, Laglera LM, Monticelli D (2015). Ultrasensitive and Fast Voltammetric Determination of Iron in Seawater by Atmospheric Oxygen Catalysis in 500 µL Samples. Anal Chem. 87:6357–6363. doi:10.1021/acs.analchem.5b01239.

Chen M, Wang WX, Crumbliss AL, Harrington JM (2009). Iron sequestration by small molecules: Thermodynamic and kinetic studies of natural siderophores and synthetic model compounds. Elsevier. 179–250 p.

Chianese S, Fenti A, Iovino P, Musmarra D, Salvestrini S (2020). Sorption of organic pollutants by humic acids: A review. Molecules. 25:1–17. doi:10.3390/molecules25040918.

Ciotti ÁM, de Mahiques M, Möller OO (2014). The meridional gradients of the S-SE Brazilian continental shelf: Introduction to the special volume. Cont Shelf Res. 89:1–4. doi:10.1016/j.csr.2014.08.008.

Ciotti ÁM, Odebrecht C, Fillmann G, Moller OO (1995). Freshwater outflow and Subtropical Convergence influence on phytoplankton biomass on the southern Brazilian continental shelf. Cont Shelf Res. 15:1737–1756. doi:10.1016/0278-4343(94)00091-Z.

Croot PL, Johansson M (2000). Determination of Iron Speciation by Cathodic Stripping Voltammetry in Seawater Using the Competing Ligand 2-(2-Thiazolylazo)-p-cresol (TAC). Electroanalysis. 12:565–576. doi:10.1002/(SICI)1521-4109(200005)12:8<565::AID-ELAN565>3.0.CO;2-L.

Cullen JJ, Stewart E, Renger E, Eppley RW, Winant CD (1983). Vertical motion of the thermocline, nitracline and chlorophyll maximum layers in relation to currents on the Southern California Shelf (Ceratium). J Mar Res. 41:239–262. doi:10.1357/002224083788520171.

Cutter GA, Casciotti K, Croot PL, Geibert W, Heimbürger L-E, Lohan M, Planquette H, van de Flierdt T (2017). Sampling and Sample-handling Protocols for GEOTRACES Cruises, version 3. 139pp. & Appendices p.

Dittmar T (2004). Evidence for terrigenous dissolved organic nitrogen in the Arctic deep sea. Limnol Oceanogr. 49:148–156.

Dulaquais G, Waeles M, Gerringa LJA, Middag R, Rijkenberg MJA, Riso R (2018). The biogeochemistry of electroactive humic substances and its connection to iron chemistry in the North East Atlantic and the Western Mediterranean Sea. J Geophys Res Oceans.1–19. doi:10.1029/2018JC014211.

Franco BC, Defeo O, Piola AR, Barreiro M, Yang H, Ortega L, Gianelli I, Castello JP, Vera C, Buratti C, Pájaro M, Pezzi LP, Möller OO (2020). Climate change impacts on the atmospheric circulation, ocean, and fisheries in the southwest South Atlantic Ocean: a review. Clim Change. 162:2359–2377. doi:10.1007/S10584-020-02783-6/FIGURES/5.

Fujii M, Rose AL, Waite TD, Omura T (2008). Effect of divalent cations on the kinetics of Fe(III) complexation by organic ligands in natural waters. Geochim Cosmochim Acta. 72:1335–1349. doi:10.1016/j.gca.2007.12.017.

Geider RJ, La Roche J (1994). The role of iron in phytoplankton photosynthesis, and the potential for iron-limitation of primary productivity in the sea. Photosynth Res. 39:275–301. doi:10.1007/BF00014588.

Gerringa LJ a, Rijkenberg MJ a, Thuróczy CE, Maas LRM (2014). A critical look at the calculation of the binding characteristics and concentration of iron complexing ligands in seawater with suggested improvements. Environmental Chemistry. 11:114–136. doi:10.1071/EN13072.

Gerringa LJA, Gledhill M, Ardiningsih I, Muntjewerf N, Laglera LM (2021). Comparing CLE-AdCSV applications using SA and TAC to determine the Fe-binding characteristics of model ligands in seawater. Biogeosciences. 18:5265–5289. doi:10.5194/bg-18-5265-2021.

Gerringa LJA, Rijkenberg MJA, Schoemann V, Laan P, de Baar HJW (2015). Organic complexation of iron in the West Atlantic Ocean. Mar Chem. doi:10.1016/j.marchem.2015.04.007.

Gledhill M (2007). The determination of heme b in marine phyto- and bacterioplankton. Mar Chem. 103:393–403. doi:10.1016/j.marchem.2006.10.008.

Gledhill M, Achterberg EP, Honey DJ, Nielsdottir MC, Rijkenberg MJA (2013). Distributions of particulate Heme b in the Atlantic and Southern Oceans - Implications for electron transport in phytoplankton. Global Biogeochem Cycles. 27:1072–1082. doi:10.1002/2013GB004639.

Gledhill M, van den Berg CMG (1995). Measurement of the redox speciation of iron in seawater by catalytic cathodic stripping voltammetry. Mar Chem. 50:51–61. doi:10.1016/0304-4203(95)00026-N.

Gledhill, M, Buck KN (2012). The organic complexation of iron in the marine environment: A review. Front Microbiol. 3. doi:10.3389/fmicb.2012.00069.

Hassler CS, Schoemann V, Nichols CM, Butler ECV, Boyd PW (2011). Saccharides enhance iron bioavailability to southern ocean phytoplankton. Proc Natl Acad Sci U S A. 108:1076–1081. doi:10.1073/pnas.1010963108.

Heerah KM, Reader HE (2022). Towards the identification of humic ligands associated with iron transport through a salinity gradient. Sci Rep. 12:1–11. doi:10.1038/s41598-022-19618-2.

Helm L, Merbach AE (2005). Inorganic and bioinorganic solvent exchange mechanisms. Chem Rev. 105:1923–1959. doi:10.1021/CR030726O/ASSET/CR030726O.FP.PNG_V03.

Higashi RM, Fan TWM, Lane AN (1998). Association of desferrioxamine with humic substances and their interaction with cadmium(II) as studied by pyrolysis-gas chromatography-mass spectrometry and nuclear magnetic resonance spectroscopy. Analyst. 123:911–918. doi:10.1039/a708177d.

Hogle SLS, Barbeau K a, Gledhill M (2014). Heme in the marine environment: from cells to the iron cycle. Metallomics. 6:1107–20. doi:10.1039/C4MT00031E.

Ito RG, Garcia CAE, Tavano VM (2016). Net sea-air CO2 fluxes and modelled pCO2 in the southwestern subtropical Atlantic continental shelf during spring 2010 and summer 2011. Cont Shelf Res. 119:68–84. doi:10.1016/j.csr.2016.03.013.

Kogut MB, Voelker BM (2001). Strong Copper-Binding Behavior of Terrestrial Humic Substances in Seawater. Environ Sci Technol. 35:1149–1156. doi:10.1021/ES0014584.

Krachler R, Krachler R, Valda A, Keppler BK (2019). Natural iron fertilization of the coastal ocean by “blackwater rivers.” Science of the Total Environment. 656:952–958. doi:10.1016/j.scitotenv.2018.11.423.

Krachler R, Krachler RF (2021). Northern High-Latitude Organic Soils As a Vital Source of River-Borne Dissolved Iron to the Ocean. Environ Sci Technol. 55:9672–9690. doi:10.1021/acs.est.1c01439.

Krachler RRRF, Krachler RRRF, Valda A, Keppler BK, Wallner G, Hann S, Laux M, Cervantes Recalde MF, Jirsa F, Neubauer E, von der Kammer F, Hofmann T, Keppler BK, Kuzmič P, Luther GW, Mullaugh KM, Hauser EJ, Rader KJ, Di Toro DM, Völker C, Wolf-Gladrow DA (2015). Natural iron fertilization of the coastal ocean by “blackwater rivers.” Mar Chem. 65:103998. doi:10.1016/j.scitotenv.2018.11.423.

Kuhn KM, Maurice PA, Neubauer E, Hofmann T, Von Der Kammer F (2014). Accessibility of humic-associated Fe to a microbial siderophore: Implications for bioavailability. Environ Sci Technol. 48:1015–1022. doi:10.1021/ES404186V/SUPPL_FILE/ES404186V_SI_001.PDF.

Kustka AB, Jones BM, Hatta M, Field MP, Milligan AJ (2015). The influence of iron and siderophores on eukaryotic phytoplankton growth rates and community composition in the Ross Sea. Mar Chem. 173:195–207. doi:10.1016/j.marchem.2014.12.002.

Kuzmič P (1996). Program DYNAFIT for the analysis of enzyme kinetic data: Application to HIV proteinase. Anal Biochem. 237:260–273. doi:10.1006/abio.1996.0238.

Laglera LM, Battaglia G, van den Berg CMG (2011). Effect of humic substances on the iron speciation in natural waters by CLE/CSV. Mar Chem. 127:134–143. doi:10.1016/j.marchem.2011.09.003.

Laglera LM, Filella M (2015). The relevance of ligand exchange kinetics in the measurement of iron speciation by CLE–AdCSV in seawater. Mar Chem. 173:100–113. doi:10.1016/j.marchem.2014.09.005.

Laglera LM, Santos-Echeandía J, Caprara S, Monticelli D (2013). Quantification of Iron in Seawater at the Low Picomolar Range Based on Optimization of Bromate/Ammonia/Dihydroxynaphtalene System by Catalytic Adsorptive Cathodic Stripping Voltammetry. Anal Chem. 85:2486–2492. doi:10.1021/ac303621q.

Laglera LM, Sukekava C, Slagter HA, Downes J, Aparicio-Gonzalez A, Gerringa LJA (2019). First Quantification of the Controlling Role of Humic Substances in the Transport of Iron across the Surface of the Arctic Ocean. Environ Sci Technol. doi:10.1021/acs.est.9b04240.

Laglera LM, Tovar-Sánchez A, Iversen MH, González HE, Naik H, Mangesh G, Assmy P, Klaas C, Mazzocchi MG, Montresor M, Naqvi SWA, Smetacek V, Wolf-Gladrow DA (2017). Iron partitioning during LOHAFEX: Copepod grazing as a major driver for iron recycling in the Southern Ocean. Mar Chem. 196:148–161. doi:10.1016/j.marchem.2017.08.011.

Laglera LM, Tovar-Sanchez A, Sukekava CF, Naik H, Naqvi SWA, Wolf-Gladrow DA (2020). Iron organic speciation during the LOHAFEX experiment: Iron ligands release under biomass control by copepod grazing. Journal of Marine Systems. 207:103151. doi:10.1016/j.jmarsys.2019.02.002.

Laglera LM, van den Berg CMG (2009). Evidence for geochemical control of iron by humic substances in seawater. Limnol Oceanogr. 54:610–619. doi:10.4319/lo.2009.54.2.0610.

Laglera LM;, Battaglia G, Van den Berg CMG (2007). Determination of humic substances in natural waters by cathodic stripping voltammetry of their complexes with iron. Anal Chim Acta. 599:58–66. doi:10.1016/j.aca.2007.07.059.

Linkhorst A, Dittmar T, Waska H (2017). Molecular Fractionation of Dissolved Organic Matter in a Shallow Subterranean Estuary: The Role of the Iron Curtain. Environ Sci Technol. 51:1312–1320. doi:10.1021/ACS.EST.6B03608/ASSET/IMAGES/LARGE/ES-2016-03608R_0003.JPEG.

Liu X, Millero FJ (2002a). The solubility of iron in seawater. Mar Chem. 77:43–54. doi:10.1016/S0304-4203(01)00074-3.

Liu X, Millero FJ (2002b). The solubility of iron in seawater. Mar Chem. 77:43–54. doi:10.1016/S0304-4203(01)00074-3.

Longhini CM, Mahieu L, Fabian S, van den Berg CMG, Salaün P, Neto RR (2021). Coastal waters contamination by mining tailings: What triggers the stability of iron in the dissolved and soluble fractions? Limnol Oceanogr. 66:171–187. doi:10.1002/lno.11595.

Lorenzzetti JA, Dias FG (2013). Internal Solitary Waves in the Brazilian SE Continental Shelf: Observations by Synthetic Aperture Radar. International Journal of Oceanography. 2013:1–11. doi:10.1155/2013/403259.

Luther GW, Mullaugh KM, Hauser EJ, Rader KJ, Di Toro DM (2021). Determination of ambient dissolved metal ligand complexation parameters via kinetics and pseudo-

voltammetry experiments. Mar Chem. 234:103998. doi:10.1016/j.marchem.2021.103998.

Maknun L, Kińska K, González-Álvarez I, Ouerdane L, Lauga B, Siripinyanond A, Szpunar J, Lobinski R (2023). Quantitative Determination of Iron–Siderophore Complexes in Peat by Isotope-Exchange Size-Exclusion UPLC–Electrospray Ionization High-Resolution Accurate Mass (HRAM) Mass Spectrometry. Anal Chem. 95:9182–9190.
doi:10.1021/ACS.ANALCHEM.3C00122/SUPPL_FILE/AC3C00122_SI_001.PDF.

Martin JH, Coale KH, Johnson KS, Fitzwater SE, Gordon RM, Tanner SJ, Hunter CN, Elrod VA, Nowicki JL, Coley TL, Barber RT, Lindley S, Watson AJ, Van Scoy K, Law CS, Liddicoat MI, Ling R, Stanton T, Stockel J, Collins C, Anderson A, Bidigare R, Ondrusek M, Latasa M, Millero FJ, Lee K, Yao W, Zhang JZ, Friederich G, Sakamoto C, Chavez F, Buck K, Kolber Z, Greene R, Falkowski P, Chisholm SW, Hoge F, Swift R, Yungel J, Turner S, Nightingale P, Hatton A, Liss P, Tindale NW (1994). Testing the iron hypothesis in ecosystems of the equatorial Pacific Ocean. Nature. 371:123–129. doi:10.1038/371123a0.

Martin JH, Gordon RM, Fitzwater SE (1990). Iron in Antarctic waters. Nature. 345:156–158. doi:10.1038/345156a0.

Martins LR, Coutinho PN (1981). The Brazilian continental margin. Earth Sci Rev. 17:87–107. doi:10.1016/0012-8252(81)90007-6.

Mawji E, Gledhill M, Milton JA, Tarran GA, Ussher S, Thompson A, Wolff GA, Worsfold PJ, Achterberg EP (2008). Hydroxamate siderophores: Occurrence and importance in the Atlantic Ocean. Environ Sci Technol. 42:8675–8680. doi:10.1021/es801884r.

Mellett T, Brown MT, Chappell PD, Duckham C, Fitzsimmons JN, Till CP, Sherrell RM, Maldonado MT, Buck KN (2018). The biogeochemical cycling of iron, copper, nickel, cadmium, manganese, cobalt, lead, and scandium in a California Current experimental study. Limnol Oceanogr. 63:S425–S447. doi:10.1002/LNO.10751.

Mellett T, Buck KN (2020). Spatial and temporal variability of trace metals (Fe, Cu, Mn, Zn, Co, Ni, Cd, Pb), iron and copper speciation, and electroactive Fe-binding humic

substances in surface waters of the eastern Gulf of Mexico. Mar Chem. 227:103891. doi:10.1016/J.MARCHEM.2020.103891.

Möller OOJr a, Piola AR, Cristina A, Campos EJD (2008). The effects of river discharge and seasonal winds on the shelf off southeastern South America. 28:1607–1624. doi:10.1016/j.csr.2008.03.012.

Morel F.M. and Hering J.G. (1993). Principles and applications of aquatic chemistry.

Muelbert JH, Acha M, Mianzan H, Guerrero R, Reta R, Braga ES, Garcia VM, Berasategui A, nica Gomez-Erache M, Ramírez F (2008). Biological, physical and chemical properties at the Subtropical Shelf Front Zone in the SW Atlantic Continental Shelf. doi:10.1016/j.csr.2007.08.011.

Muller FLL (2018). Exploring the potential role of terrestrially derived humic substances in the marine biogeochemistry of iron. Front Earth Sci (Lausanne). 6:159. doi:10.3389/FEART.2018.00159/XML/NLM.

Muller FLL, Cuscov M (2017). Alteration of the Copper-Binding Capacity of Iron-Rich Humic Colloids during Transport from Peatland to Marine Waters. Environ Sci Technol. 51:3214–3222. doi:10.1021/acs.est.6b05303.

Niencheski LF, Windom HL, Moore WS (2014). Controls on water column chemistry of the southern Brazilian continental shelf. Cont Shelf Res. 88:126–139. doi:10.1016/j.csr.2014.07.007.

Norman L, Worms IAM, Angles E, Bowie AR, Nichols CM, Ninh Pham A, Slaveykova VI, Townsend AT, David Waite T, Hassler CS (2015). The role of bacterial and algal exopolymeric substances in iron chemistry. Mar Chem. 173:148–161. doi:10.1016/j.marchem.2015.03.015.

Obernosterer I, Herndl GJ (2000). Differences in the optical and biological reactivity of the humic and nonhumic dissolved organic carbon component in two contrasting coastal marine environments. Limnol Oceanogr. 45:1120–1129. doi:10.4319/lo.2000.45.5.1120.

Oldham VE, Miller MT, Jensen LT, Luther GW (2017). Revisiting Mn and Fe removal in humic rich estuaries. Geochim Cosmochim Acta. 209:267–283. doi:10.1016/j.gca.2017.04.001.

Piola AR, Campos EJD, Möller OO, Charo M, Martinez C (2000). Subtropical Shelf Front off eastern South America. J Geophys Res Oceans. 105:6565–6578. doi:10.1029/1999JC000300.

Piola AR, Matano RP, Palma ED, Möller OO, Campos EJD (2005). The influence of the Plata River discharge on the western South Atlantic shelf. Geophys Res Lett. 32:1–4. doi:10.1029/2004GL021638.

Pižeta I, Sander SG, Hudson RJM, Omanović D, Baars O, Barbeau KA, Buck KN, Bundy RM, Carrasco G, Croot PL, Garnier C, Gerringa LJA, Gledhill M, Hirose K, Kondo Y, Laglera LM, Nuester J, Rijkenberg MJA, Takeda S, Twining BS, Wells M (2015). Interpretation of complexometric titration data: An intercomparison of methods for estimating models of trace metal complexation by natural organic ligands. Mar Chem. 173:3–24. doi:10.1016/j.marchem.2015.03.006.

Resgalla C, de La Rocha C, Montú M (2001). The Influence of Ekman Transport on Zooplankton Biomass Variability off Southern Brazil. J Plankton Res. 23:641–650. doi:10.1093/PLANKT/23.6.641.

Rose AL, Waite TD (2003). Kinetics of iron complexation by dissolved natural organic matter in coastal waters. Mar Chem. 84:85–103. doi:10.1016/S0304-4203(03)00113-0.

Rue EL, Bruland KW (1995). Complexation of iron(III) by natural organic ligands in the Central North Pacific as determined by a new competitive ligand equilibration/adsorptive cathodic stripping voltammetric method. Mar Chem. 50:117–138. doi:10.1016/0304-4203(95)00031-L.

Ružić I (1982). Theoretical aspects of the direct titration of natural waters and its information yield for trace metal speciation. Anal Chim Acta. 140:99–113. doi:10.1016/S0003-2670(01)95456-X.

Sato M, Wakuta Y, Takeda S (2022). Distribution and chemical speciation of iron on the outer edge of the Changjiang diluted water plume of the East China Sea. Cont Shelf Res. 234. doi:10.1016/j.csr.2022.104646.

Schijf J, Burns SM (2016). Determination of the side-reaction coefficient of desferrioxamine B in trace-metal-free seawater. Front Mar Sci. 3:1–15. doi:10.3389/fmars.2016.00117.

Scolaro LM, Castriciano M, Romeo A, Patanè S, Cefalì E, Allegrini M (2002). Aggregation behavior of protoporphyrin IX in aqueous solutions: Clear evidence of vesicle formation. Journal of Physical Chemistry B. 106:2453–2459. doi:10.1021/jp013155h.

Sholkovitz ER (1978). The flocculation of dissolved Fe, Mn, Al, Cu, Ni, Co and Cd during estuarine mixing. Earth Planet Sci Lett. 41:77–86. doi:10.1016/0012-821X(78)90043-2.

Slagter HA, Laglera LM, Sukekava C, Gerringa LJA (2019). Fe-Binding Organic Ligands in the Humic-Rich TransPolar Drift in the Surface Arctic Ocean Using Multiple Voltammetric Methods. J Geophys Res Oceans. 124:1491–1508. doi:10.1029/2018JC014576.

Spasojević I, Armstrong SK, Brickman TJ, Crumbliss AL (1999). Electrochemical Behavior of the Fe(III) Complexes of the Cyclic Hydroxamate Siderophores Alcaligin and Desferrioxamine E. Inorg Chem. 38:449–454. doi:10.1021/ic980635n.

Stewart AG, Hudson-Edwards KA, Dubbin WE (2013). Mechanisms of goethite dissolution in the presence of desferrioxamine B and Suwannee River fulvic acid at pH 6.5. Geochim Cosmochim Acta. 115:1–14. doi:10.1016/j.gca.2013.04.006.

Stockdale A, Tipping E, Hamilton-Taylor J, Lofts S (2011). Trace metals in the open oceans: speciation modelling based on humic-type ligands. Environmental Chemistry. 8:304–319. doi:10.1071/EN11004.

Stramma L, Ikeda Y, Peterson RG (1990). Geostrophic transport in the Brazil current region north of 20°S. Deep Sea Research Part A, Oceanographic Research Papers. 37. doi:10.1016/0198-0149(90)90083-8.

Strickland JDH, Parsons TR (1972). A practical handbook of seawater analysis, 2nd editio. J.C. Stevenson PHD, editor. Ottawa, Canada. 328 p.

Su H, Yang R, Li Y, Wang X (2018). Influence of humic substances on iron distribution in the East China Sea. Chemosphere. 204:450–462. doi:10.1016/j.chemosphere.2018.04.018.

Su H, Yang R, Pižeta I, Omanovic D, Wang S, Li Y (2016). Distribution and speciation of dissolved iron in Jiaozhou Bay (Yellow Sea, China). Front Mar Sci. 3. doi:10.3389/fmars.2016.00099.

Su H, Yang R, Zhang A, Li Y (2015). Dissolved iron distribution and organic complexation in the coastal waters of the East China Sea. Mar Chem. 173:208–221. doi:10.1016/j.marchem.2015.03.007.

Sukekava C, Downes J, Slagter HA, Gerringa LJA, Laglera LM (2018). Determination of the contribution of humic substances to iron complexation in seawater by catalytic cathodic stripping voltammetry. Talanta. 189:359–364. doi:10.1016/j.talanta.2018.07.021.

Sukekava CF (2018). A new voltammetric method for the measurement of the effect of humic substances in iron speciation. Application to Surface Arctic waters. Master's thesis.37.

Sukekava CF, Andrade CFF De, Niencheski LFH, Souza MS De, Laglera LM (2023). Macronutrients , iron and humic substances summer cycling over the extended continental shelf of the South Brazil Bight. Science of the Total Environment. 865:161182. doi:10.1016/j.scitotenv.2022.161182.

Tagliabue A, Bopp L, Aumont O, Arrigo KR (2009). Influence of light and temperature on the marine iron cycle: From theoretical to global modeling. Global Biogeochem Cycles. 23:1–12. doi:10.1029/2008GB003214.

Tagliabue A, Bowie AR, Philip W, Buck KN, Johnson KS, Saito MA (2017). The integral role of iron in ocean biogeochemistry. Nature. 543:In Press. doi:10.1038/nature21058.

Till CP, Solomon JR, Cohen NR, Lampe RH, Marchetti A, Coale TH, Bruland KW (2019). The iron limitation mosaic in the California Current System: Factors governing Fe availability in the shelf/near-shelf region. Limnol Oceanogr. 64:109–123. doi:10.1002/LNO.11022.

Tipping E, Hurley MA (1992). A unifying model of cation binding by humic substances. Geochim Cosmochim Acta. 56:3627–3641. doi:10.1016/0016-7037(92)90158-F.

van Den Berg CMG (1982). Determination of copper complexation with natural organic ligands in seawater by equilibration with MnO2 II. Experimental procedures and application to surface seawater. Mar Chem. 11:323–342. doi:10.1016/0304-4203(82)90029-9.

van den Berg CMG (1995). Evidence for organic complexation of iron in seawater. Mar Chem. 50:139–157. doi:10.1016/0304-4203(95)00032-M.

van den Berg CMG (2006). Chemical speciation of iron in seawater by cathodic stripping voltammetry with dihydroxynaphthalene. Anal Chem. 78:156–163. doi:10.1021/ac051441+.

Völker C, Wolf-Gladrow DA (1999). Physical limits on iron uptake mediated by siderophores or surface reductases. Mar Chem. 65:227–244. doi:10.1016/S0304-4203(99)00004-3.

Vraspir JM, Butler A (2009). Chemistry of Marine Ligands and Siderophores. Ann Rev Mar Sci. 1:43–63. doi:10.1146/annurev.marine.010908.163712.

Whitby H, Bressac M, Sarthou G, Ellwood MJ, Guieu C, Boyd PW (2020b). Contribution of Electroactive Humic Substances to the Iron-Binding Ligands Released During Microbial Remineralization of Sinking Particles. Geophys Res Lett. 47:1–11. doi:10.1029/2019GL086685.

Whitby H, Planquette H, Cassar N, Bucciarelli E, Osburn CL, Janssen DJ, Cullen JT, González AG, Völker C, Sarthou G (2020a). A call for refining the role of humic-like substances in the oceanic iron cycle. Sci Rep. 10:1–12. doi:10.1038/s41598-020-62266-7.

Whitby H, van den Berg CMG (2015). Evidence for copper-binding humic substances in seawater. Mar Chem. 173:282–290. doi:10.1016/j.marchem.2014.09.011.

Wilkins RG (1991). Kinetics and Mechanism of Reactions of Transition Metal Complexes. Kinetics and Mechanism of Reactions of Transition Metal Complexes. doi:10.1002/3527600825.

Windom HL, Moore WS, Niencheski LFH, Jahnke R a. (2006). Submarine groundwater discharge: A large, previously unrecognized source of dissolved iron to the South Atlantic Ocean. Mar Chem. 102:252–266. doi:10.1016/j.marchem.2006.06.016.

Witter AE, Hutchins DA, Butler A, Luther GW (2000). Determination of conditional stability constants and kinetic constants for strong model Fe-binding ligands in seawater. Mar Chem. 69:1–17. doi:10.1016/S0304-4203(99)00087-0.

Wu J, Luther GW (1995). Complexation of Fe(III) by natural organic ligands in the Northwest Atlantic Ocean by a competitive ligand equilibration method and a kinetic approach. Mar Chem. 50:159–177. doi:10.1016/0304-4203(95)00033-N.

Yang R, Su H, Qu S, Wang X (2017). Capacity of humic substances to complex with iron at different salinities in the Yangtze River estuary and East China Sea. Sci Rep. 7:1–9. doi:10.1038/s41598-017-01533-6.